DIAGNOSTICS

J. Borer and R. Jung
CERN, Geneva, Switzerland

1. NON-INTERCEPTING BEAM MONITORS OR PICKUPS

1.1 The particle beam and its induced image current in the chamber wall

All the non interacting monitors used for the p-$\bar{p}$ instrumentation can be related to the use of the wall image current as induced by relativistic charged particle bunches circulating in a metallic pipe or vacuum chamber. The monitors are then classified by their type of beam coupling impedance. This allows a more generalized approach of the design of the so-called pickups. (orig. /HSI)

Let us assume:

- A beam of relativistic particles with $\gamma > 10$.
- A cylindrical metallic chamber either perfectly conducting or with a skin depth $\ll$ wall thickness for the considered frequency domain.

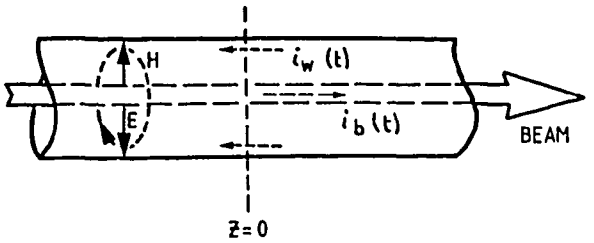

The beam is accompanied by an electromagnetic field of TEM type, i.e. radial electrical field E and circular magnetic field H. Since there are no other sources (charges) in the chamber, the continuity equation $\frac{\delta \rho}{\delta t} + \nabla J = 0$

and hence

$$i_w (t) = -i_b (t) \text{ at } z$$

z being the longitudinal coordinate (Ref. 52, 114, 115).

In addition the electrical field has no longitudinal component within a chamber of constant cross-section. The electrical field E has the same configuration as in the electrostatic case for a frozen charge distribution at the instant t. Therefore, both the longitudinal and azimuthal distributions of the wall current density have the same configuration as the ones of the influenced charge distribution in the static case. Both distributions are functions of the transverse position of the beams "centre of mass" (Ref. 52, 58, 3, 114, 115).

- Therefore this image wall current and its azimuthal distribution can be used to monitor the beam intensity and position.

At low frequencies this is no longer valid once the skin depth is larger than the wall thickness and the beam induced magnetic fields exist outside the metallic chamber. The

electrical field however, is still shielded by the conductive wall and does not penetrate outside the chamber.

The skin depth is an important factor in the design of a beam monitor or pickup. It is given in the following formula and the table as a function of frequency and relative to the copper resistivity ρ_{Cu} (Ref. 115):

$$\delta = 66{,}1\sqrt{\frac{1}{f} \cdot \frac{1}{\mu_r} \cdot \frac{\rho}{\rho_{Cu}}} \quad (mm)$$

The skin depth δ is defined as the depth at which the induced current has diminished by $^1/_e$. A depth of 3 δ corresponds to an attenuation of about 20 dB.

f	Cu	Inox	Al
10 KH_z	0,66	4,75	0,844
100	0,209	1,506	0,267
1 MH_z	0,066	0,475	0,0844
10	0,0209	0,1506	0,0267
100	0,0066	0,0475	0,00844
1 GH_z	0,00209	0,0150	0,00267

δ (mm) for $\mu_r = 1$

1.2 Electromagnetic monitors

1.2.1 Longitudinal or intensity response in both time and frequency domains

Let us assume such a monitor to be built from the vacuum chamber interrupted by two gaps separated by length ℓ. The gaps are shunted by two distributed resistors of value R. The two gaps and the central tube are covered by an external tube forming with the central one a coaxial line of characteristic impedance Z_0.

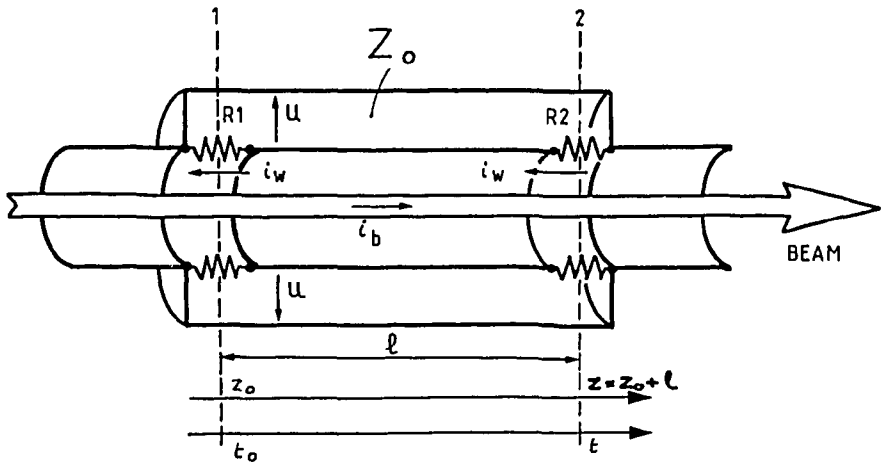

Let us assume that the beam current is a step function with magnitude I_b at t_0 at position z_0. The same step will appear at z after the length ℓ with a delay t.

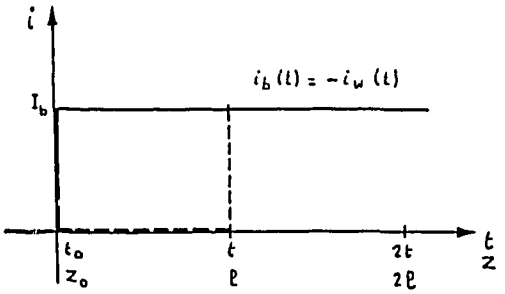

If in addition $R = Z_0$ then the induced voltage U in position z_0 at time t_0 is:

$$U = \frac{I_b \cdot Z_0}{2}$$

since $i_w = -i_b$ and i_w is split in two half currents flowing in both R_1 and in the coaxial outer line of impedance Z_0. The beam continues to propagate along the pipe at almost the speed of light and in parallel, at the same speed ($\varepsilon_r = 1$), a forward wave along the outer line. When both beam and forward outer wave (u_{fo}, i_{fo}) arrive after the length ℓ at the second gap where resistor R_2 is connected with the reversed polarity, the voltage produced by i_w is canceled by the outer forward wave. For the outer line the voltage being zero, it represents a short circuit and the outer wave is totally reflected. A backward wave (u_{ba}, i_{ba}) of null voltage and reversed current is now propagating toward z_0 in the outer line. After time 2t it arrives in R_1 where it cancels the wall current $i_w/2$ and the voltage becomes zero. This propagation of signals in both time and space along the pipe and line of length ℓ can be represented in the following diagram:

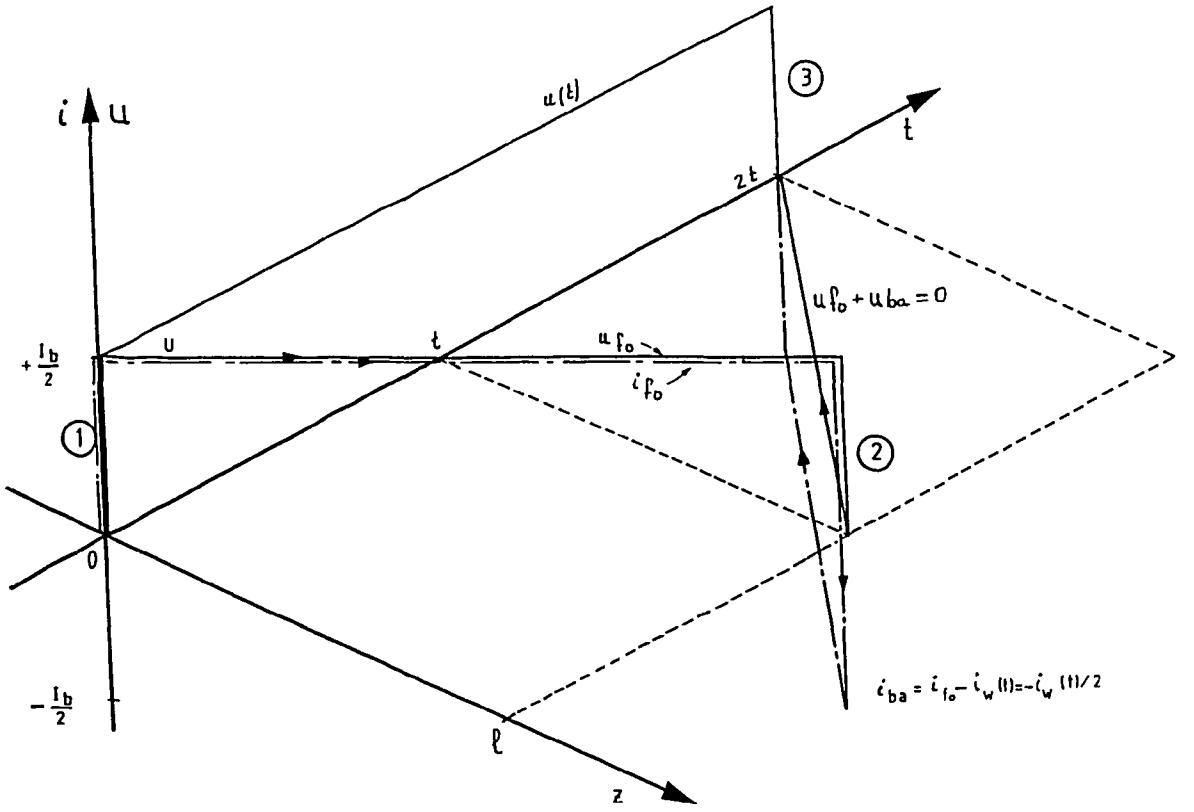

The voltages produced by $i_w(t)$ can now be described:

Case 1. $t = t_0$, $z = z_0$:

The wall current is a current source flowing in both R_1 producing u_1 and in the coax line producing the forward wave.

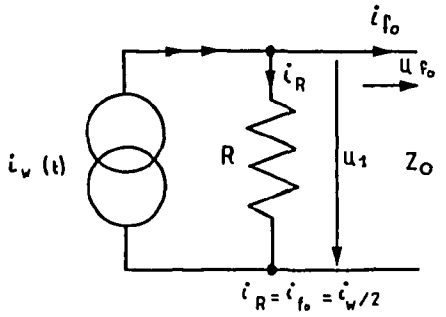

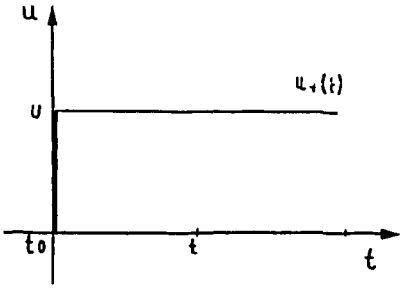

Case 2. $t = t$, $z = \ell + z_0$:

R_2 being connected in reversed polarity (terminating resistor for the outer line) the equivalent circuit is as follows:

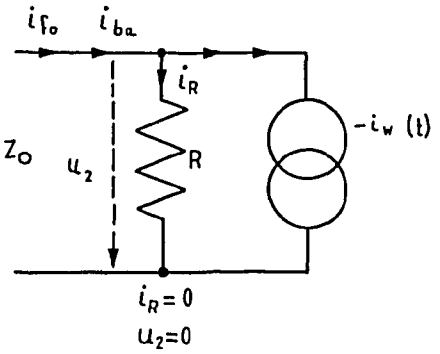

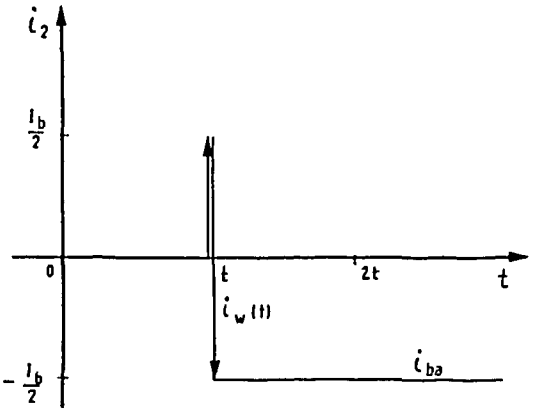

Case 3. $t = 2t$, $z = z_0$

The backward wave has now cancelled the beam induced signal and the voltage is zero in R_1 at $t = 2t$.

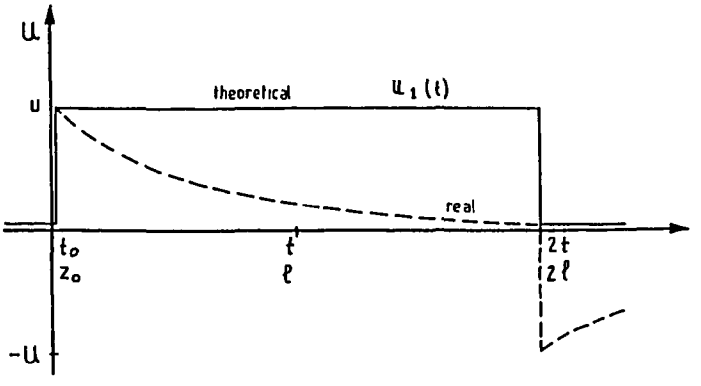

Such a response is identical to the one of a short-circuited line if the beam has only one direction. This configuration is a directional coupler for the total intensity of the beam if R_1 represents the connected load to the device. The square response is theoretical and would apply to a superconducting metal or no magnetic field penetrating outside the outer conductor. In reality, at low frequencies, the voltage is shunted by the device inductance and the voltage will decay with the time constant L/R. The resulting voltage is then as represented by the dashed line. In practice the time constant can be increased by adding magnetic materials for frequencies below the skin depth equal to the tube wall thickness.

A coupling impedance Z_{co} can now be defined for this monitor in order to relate it to the beam intensity, but since this directionnal coupler has a response equivalent to the one of a short-circuited line of length ℓ, Z_{co} is also a function of frequency:

$$Z_{co} = Z_o \cdot \frac{1}{2} \cdot \sin \frac{2\pi f \ell}{c} \qquad c = \text{speed of light}$$

$$\text{and } u(f) = i_b(f) \cdot Z_{co}$$

Ref.: 16, 45, 46, 114.

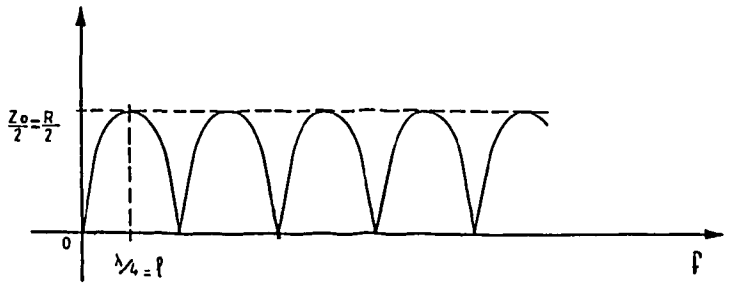

It is a quarter wave length device, with $f_o = c/4\ell$.

This basic directional coupler configuration has also related configurations which are known under different denominations.

This device having a short-circuited line characteristic, R_2 can be suppressed and replaced by a short-circuit. This eliminates the directivity characteristic but the device becomes a tuned cavity.

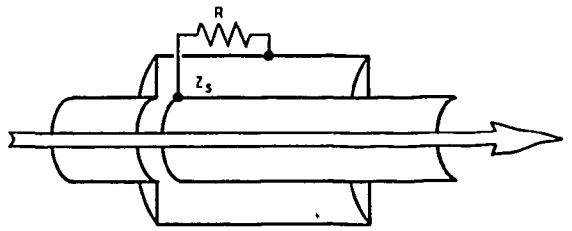

$$Z_s = j\,60 \ln \frac{D}{d} \operatorname{tg} 2\pi \frac{\ell f}{c} \; [\Omega]$$

Ref.: 51, 46, 23, 29.

The directional coupler can also be modified in a different way by suppressing the coupling of R_2 with the beam. R_2 is then the external loading resistor. Such a device has lost the directivity but has very wide band-width. Such devices are usually called gap monitors or "Resistor Bugs":

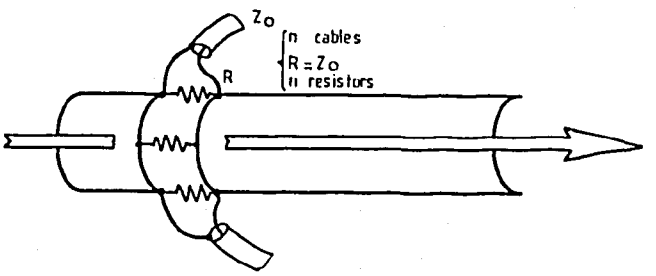

n cables

$R = Z_0$

n resistors

$$Z_{co} = \frac{R}{2 \cdot n}$$

Ref. 67, 68, 69, 46, 63, 33, 114.

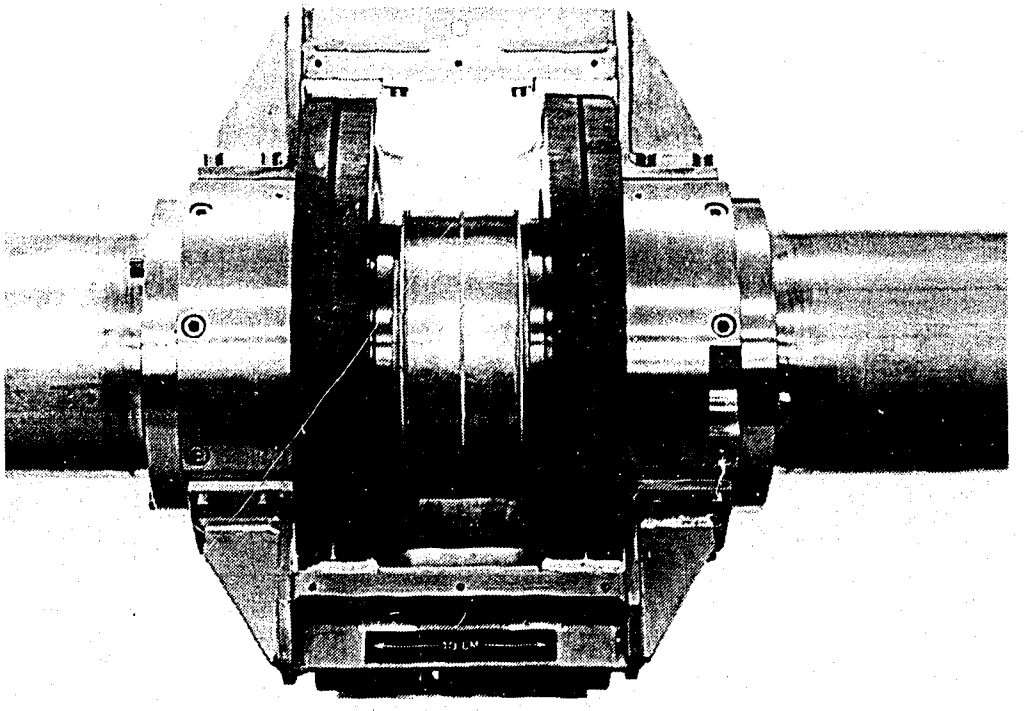

Gap of the wall current monitor
or broad band coaxial current transformer (ISR).

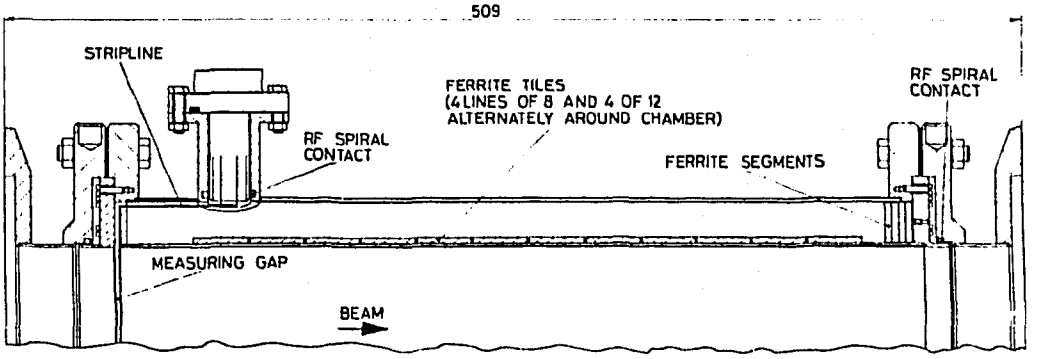

Wall current monitor with eight 50 Ω outputs (SPS)

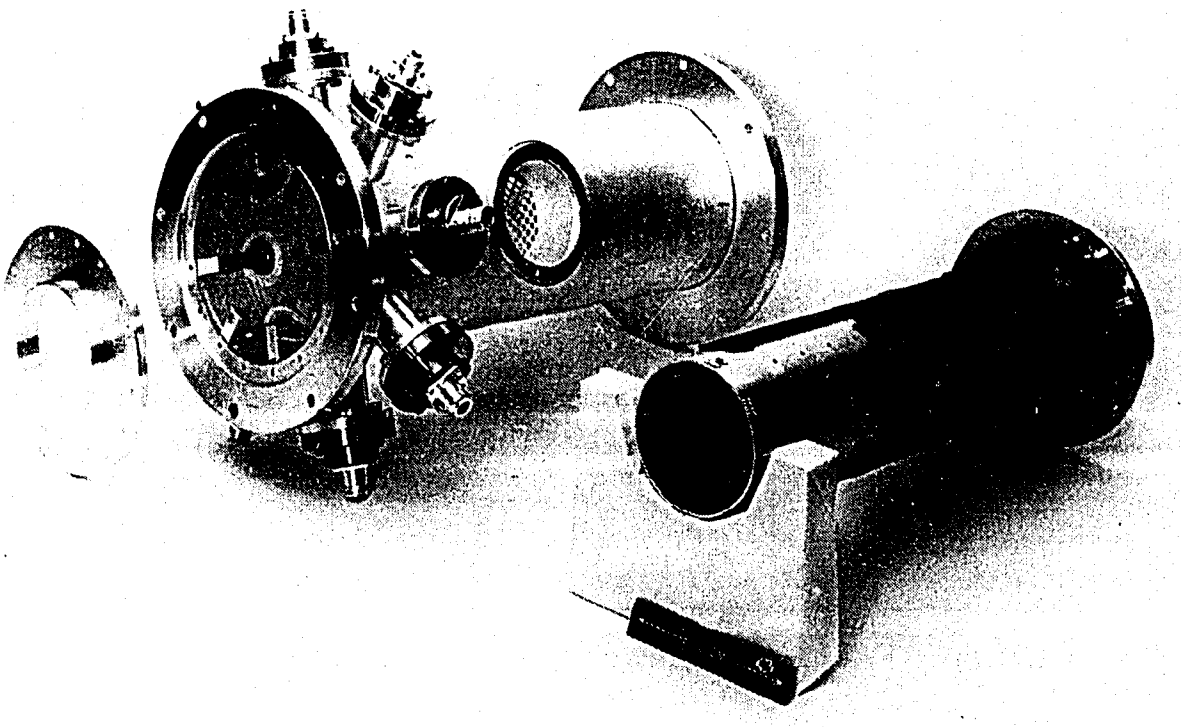

Wall current monitor with eight 50 Ω outputs (SPS)

Another version is the wide-band intensity monitor or coaxial transformer:
(See also § 1.4.1).

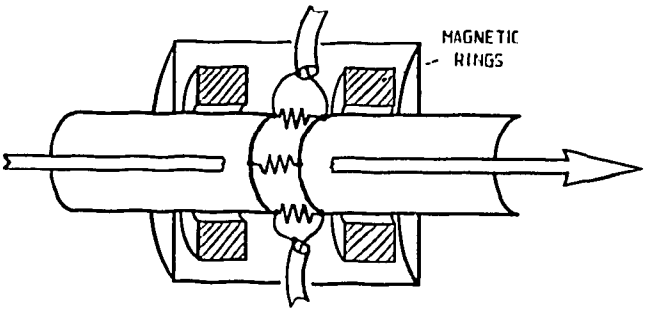

Ref.: 105, 63, 33

1.2.2 Azimuthal wall current density distribution:

- This distribution is a function of ' transverse position of the beam
- It is identical to the induced charge ' stribution of the static case

Circular case:

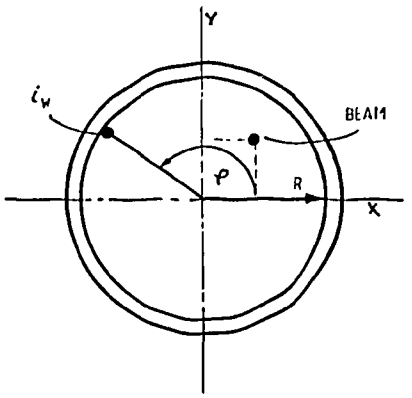

$$I_w = - I_b = \int_0^{2\pi} i_w d\phi$$

$$= - \frac{I_b}{2\pi} \int_0^{2\pi} F(\phi)\, d\phi$$

$$F(\phi) = \frac{1 - x^2 - y^2}{1 + x^2 + y^2 - 2x \cos\phi - 2y \sin\phi}$$

Both circular and elliptical cases have been calculated by conformal mapping. (Ref.: 52, 3, 42). Finite elements method and simulation method (Rheography) can also be used.

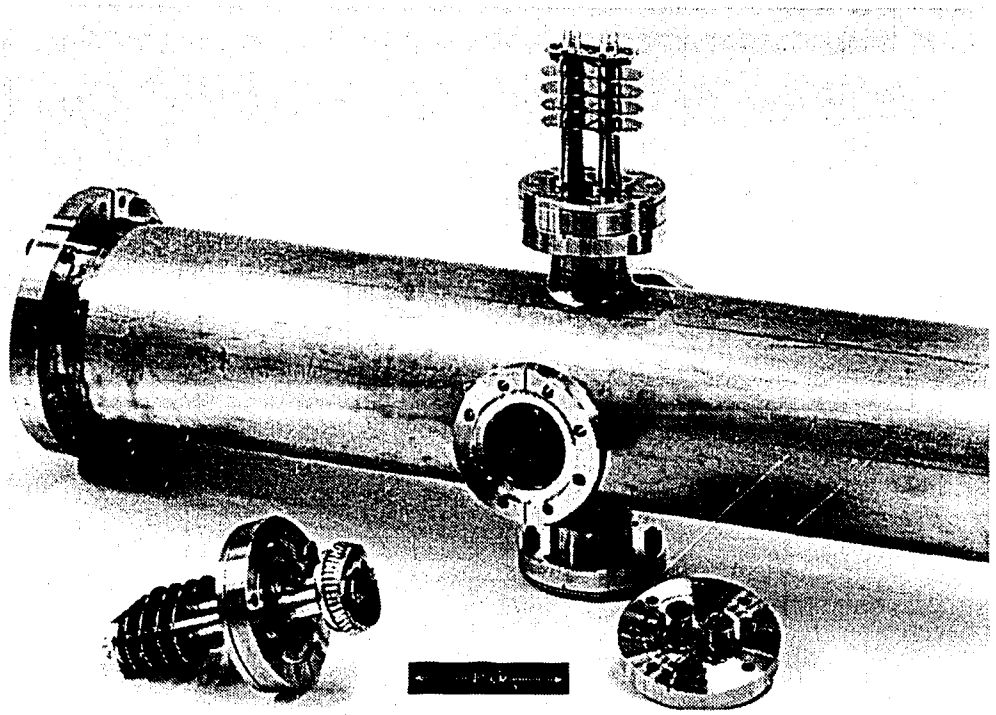

Directional and transversal
strip-line HF (2 GHz) monitor (ISR).

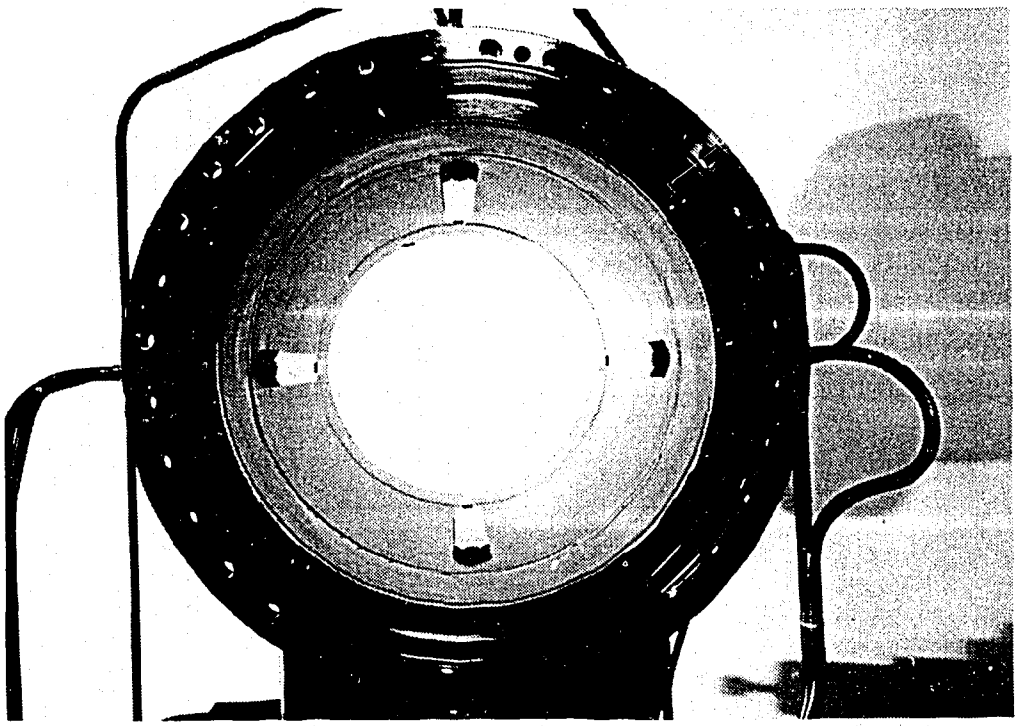

Directional position monitor for $p\bar{p}$ in SPS.

If the active part of the monitor integrates i_w over only a part of the chamber circumference, Z_{co} will be reduced by the factor $\frac{W}{2\pi R}$

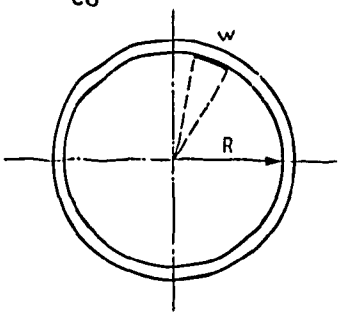

$$Z_{co} = Z_{cotot} \cdot \frac{W}{2\pi R}$$

or the image current in the active strip is:

$$i_s(t) = - i_b(t) \frac{W}{2\pi R}$$

(beam centered)

Such monitors are called <u>strip-line</u> or <u>directional coupler</u> monitors.

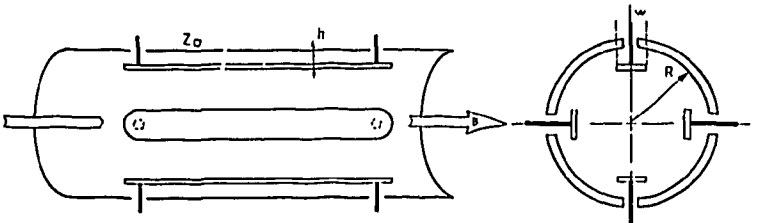

$$Z_{co} = \underbrace{60\ \Omega\ \ln \frac{R}{R-h}}_{Z_0} \sin \frac{2\pi f \ell}{c}$$

for the strip-line $Z_0 = 50\ \Omega$

if $h = 0.1\ R$ $W = 5h$ Ref.: 45, 16.

Such monitor has a non-linear transfer function for the beam position, but has the advantage of directivity for accelerators and colliders with the presence of two beams, i.e. p and $\bar{p}$, circulating in opposite directions. The isolation between up-stream and down-stream parts is about 40 dB. The position transfer function is then both proportional to Z_{co} for a centred beam and to the current or azimuthal charge distribution integrated over the width W of the strip. (See the circular case).

Other related configurations have been developed, such as:

<u>Strip-line with variable coupling</u>:

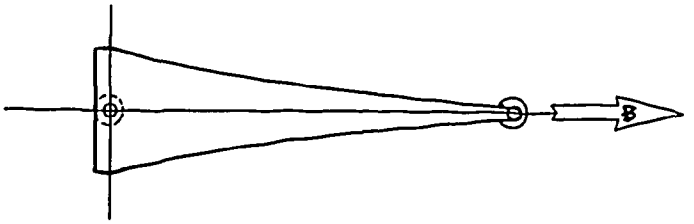

Purpose: to avoid the beam coupling at the down-stream end in order to increase the frequency bandwidth. Ref.: 46.

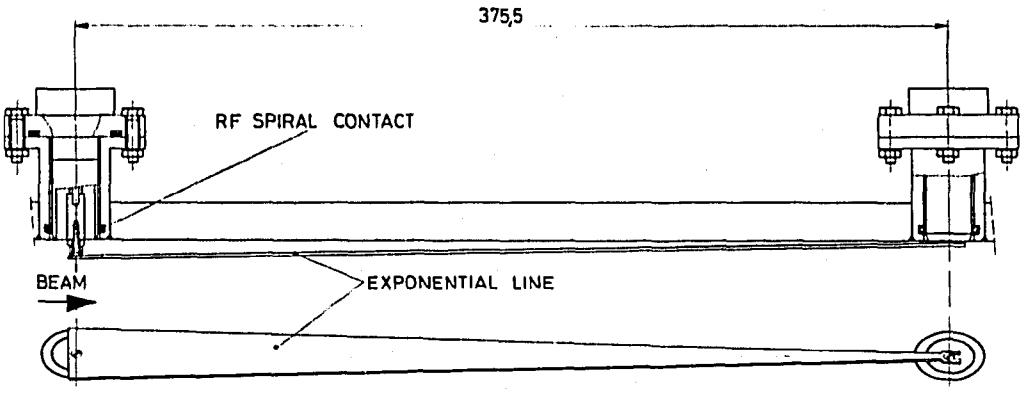

Broad band tapered strip-line monitor (SPS)

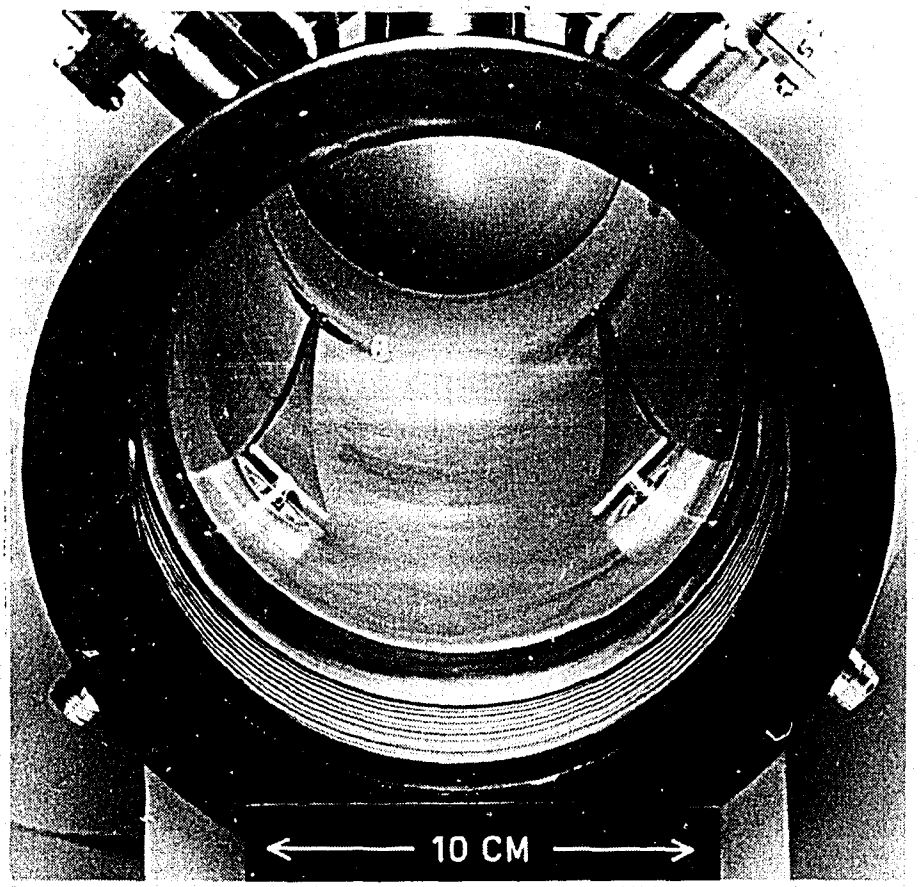

Tuned cavity or gap monitor with four coupling points:

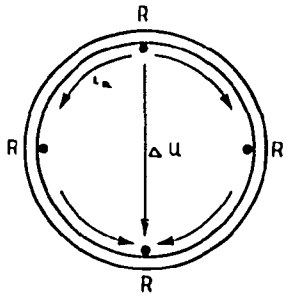

Purpose: high sensitivity or large bandwidth.
Difficulty: the azimuthal parallel impedance of the gap is shunting Δ u

The gap with four or more coupling points has also been used for multipolar motions observation. Ref.: 51, 58, 69.

For damping or cooling applications, maximum transverse sensitivity and linearity are required. The preferred and most usually used configuration is the one of separate horizontal and vertical functions, which is called:

Full coupling directional coupler with linear transverse characteristics

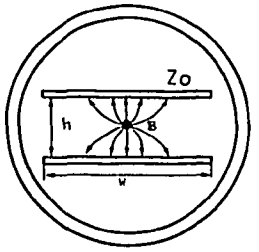

Each strip sees:
i_b (t) / 2
if w ≫ h

Ref.: 112, 88

It presents a linear transverse function if :

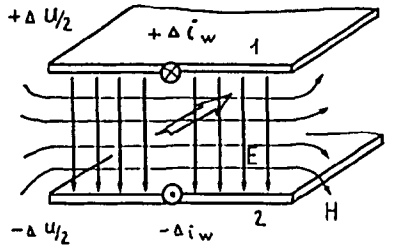

- Both E and H fields homogeneous
- and hence

$$\left.\begin{aligned} \Delta\, i_w &= i_{w1} - i_{w2} \\ \Delta\, u &= u_1 - u_2 \end{aligned}\right\} = 0 \text{ at } Y = 0$$

To be compared to the window-frame magnetic monitor used at low frequencies (§ 1.4.2)

This is a very important device used as the pickup for transverse cooling and momentum cooling with Palmer's method. The same device can be used as a broad-band transverse feed-back kicker when powered in push-pull mode. Ref.: 112, 108.

1.3 Electrostatic Monitors:

1.3.1 Longitudinal or intensity response:

Coming back to the original coaxial pipe structure of § 1.2, the terminating resistors R_1 and R_2 can be suppressed and the inner pipe can be connected to the outside via a feed-through, without loading resistor, to a high impedance preamplifier.

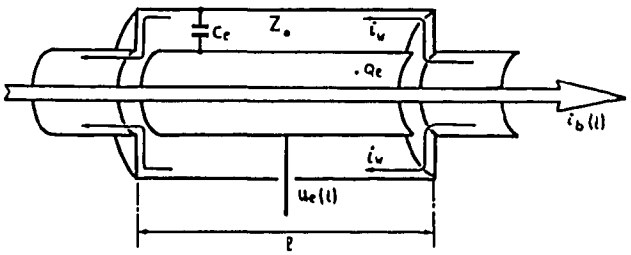

Such a structure is equivalent to an inner-electrode with capacity C_e to the outer wall and on which a charge Q_e (t) is influenced by the presence of the charged particles of the beam. The device "sees" or integrates the beam charges over the length ℓ, Q_e (t) being the instantaneous influenced charge:

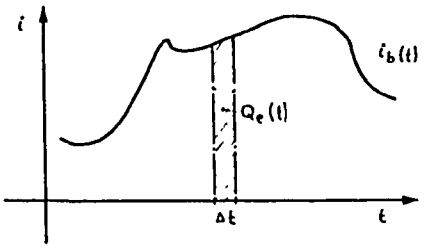

If $\Delta t = \frac{\ell}{c}$

with c = speed of light

then

$$Q_e(t) = \int_t^{t+\Delta t} i_b(t)dt \approx i_b(t)\cdot\Delta t$$

and from electrostatics , Faraday's law:

$$u_e(t) = \frac{Q_e(t)}{C_e} = \frac{i_b(t)\cdot\ell}{C_e\cdot c}$$

This is valid if $\ell \ll$ bunch length, which is mostly the case for the capacitive monitor. The coupling impedance becomes:

$$Z_{co} = \frac{\ell}{C_e\cdot c}$$

But in a coaxial line:

$$C_e = \ell \cdot C'$$

and $$c = \frac{1}{\sqrt{L' \cdot C'}}$$

C' being the capacity of unit length of line

L' being the inductance of unit length of line

$$Z_0 = \sqrt{\frac{L'}{C'}}$$

therefore, $Z_{CO} = Z_0$

It is interesting to note that the coupling impedance Z_{CO} is defined by the characteristic impedance of the structure Z_0 which in turn depends only on the ratio of the outer to inner diameter and not on the length ℓ.

Comment: For bunch lengths $< \ell$ the electrode structure may resonate at higher modes or with parasitic reactive elements. By careful construction (see button electrodes example) these resonances may be pushed above the useful frequency range.

A more precise calculation of the influenced charge as function of time is then needed:

$$Q_e(t) = \underbrace{\int_{-t}^{t} i_b(t)\,dt}_{\text{total charge of the bunch} = N \cdot q \text{ at the input of device.}} - \underbrace{\int_{-t}^{t} i_b(t + \Delta t)\,dt}_{\text{total charge at the output of the device}}$$

with: $\Delta t = \frac{\ell}{c}$

N = Nb. of particles

q = electron charge

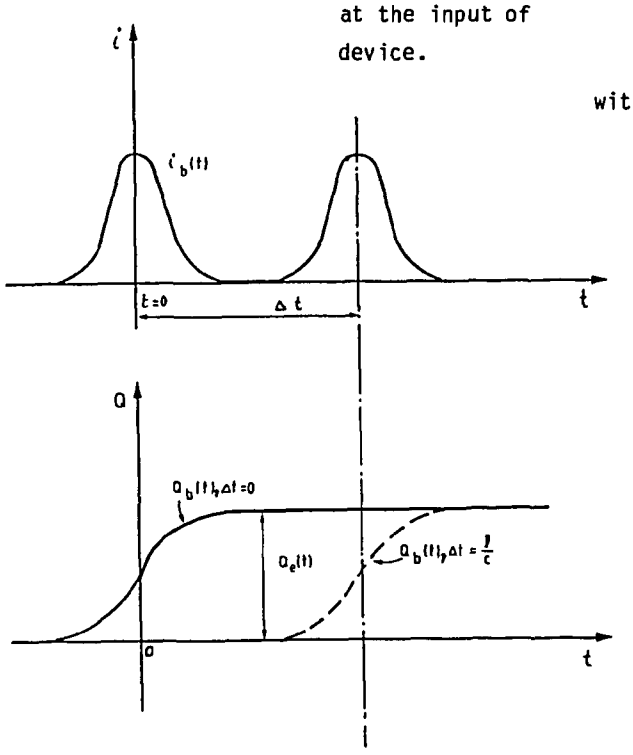

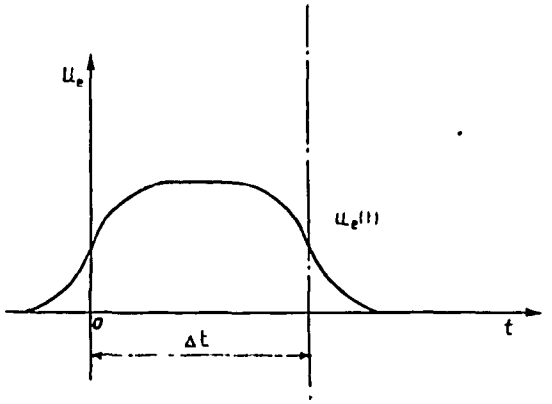

$$u_e(t) = \frac{Q_e(t)}{C_e}$$

This case corresponds to the electromagnetic coupler of § 1.2 where the influenced or wall current at the beginning and at the end of the device are inverted and the resulting voltage, after the passage of the bunch, is zero. Ref.: 2, 114.

1.3.2 Transverse response:

If the cross-section of the internal plates has $w \gg h$, it corresponds to the case of a capacitor with parallel plates of large width.

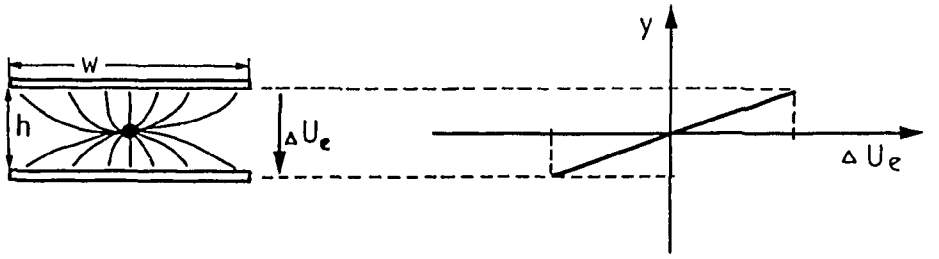

This well known case has a linear voltage function ΔU_e versus the position Y of the charge between the plates.

In the case of a limited width w, an identical function of position is obtained if the electrode tube, of any cross-section, is separated by a cut presenting a linear function of y in the projection on the y-z plane:

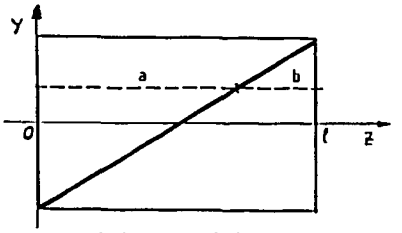

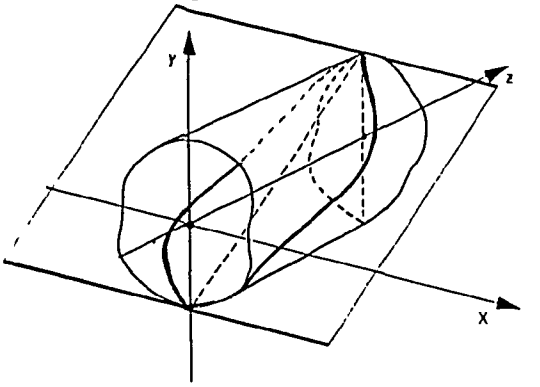

At any y, a(y) and b(y) are linear and a(y) + b(y) = ℓ

The difference signal of such linear cut electrode is a linear function of the position. Ref.: 80, 76, 79, 65

Position function:

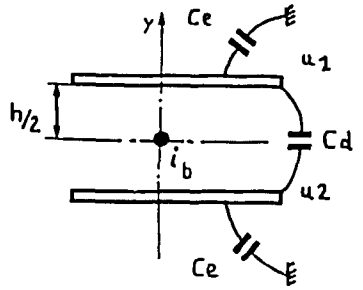

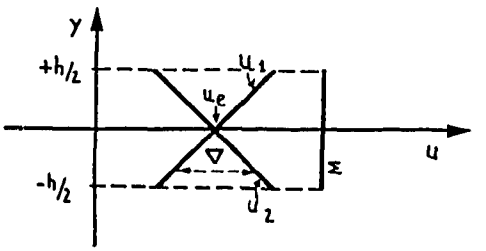

$$\frac{\Delta}{\Sigma} = \frac{2}{h} \cdot y \cdot \frac{1 - \frac{C_d}{C_e + C_d}}{1 + \frac{C_d}{C_e + C_d}}$$

with : $u_e = i_b \cdot Z_{co}$

$$u_{1max} = 2u_e \cdot \frac{1}{1 + \frac{C_d}{C_e + C_d}}$$

$$u_{1min} = 2u_e \cdot \frac{\frac{C_d}{C_e + C_d}}{1 + \frac{C_d}{C_e + C_d}}$$

Other linear-cut configurations have been developed which allow the combination of both vertical and horizontal plane with compensated cross-talk by balanced dispositon. If tuned electrodes and amplifiers are used, vertical and horizontal electrodes sets should be separated by a guard ring or fully separated. Ref.: 65, 64, 66, 57, 76, 32, 21, 18, 79, 34.

- Case whereby the intensity information is obtained from the sum of the four electrodes:

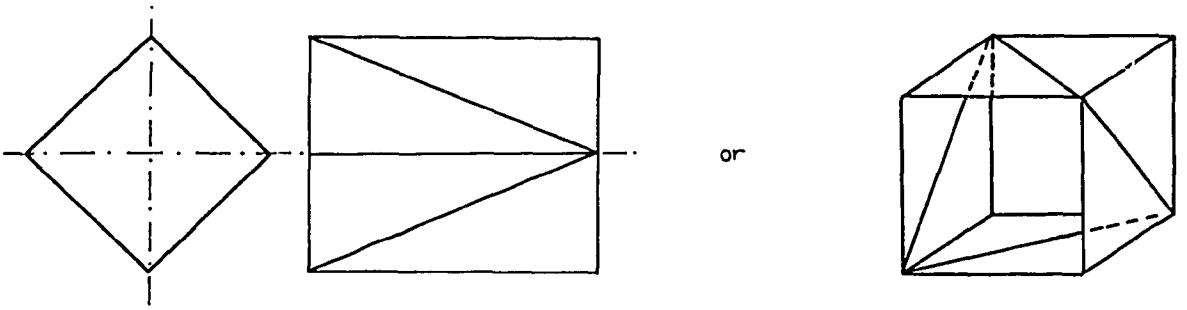

- Case whereby the intensity information can be derived from the sum of two plates of x or y plane:

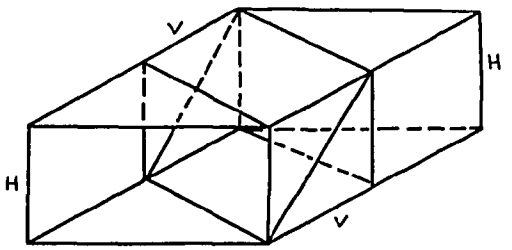

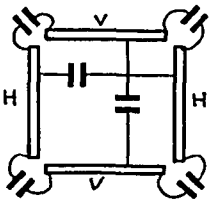

This is also a balanced structure.

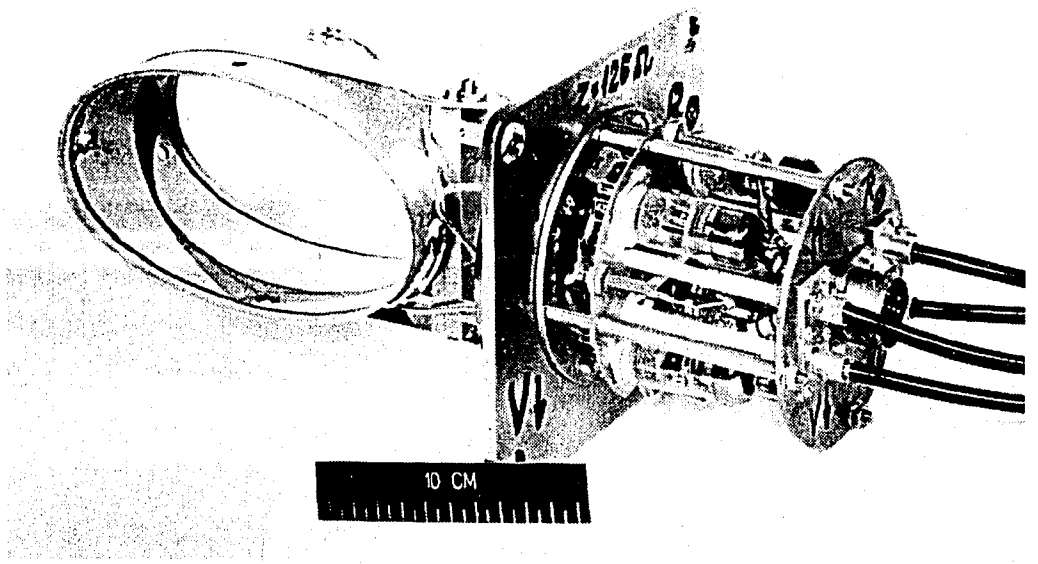

Elliptical electrostatic position monitor
with electrodes deposited on a ceramic tube (PS).

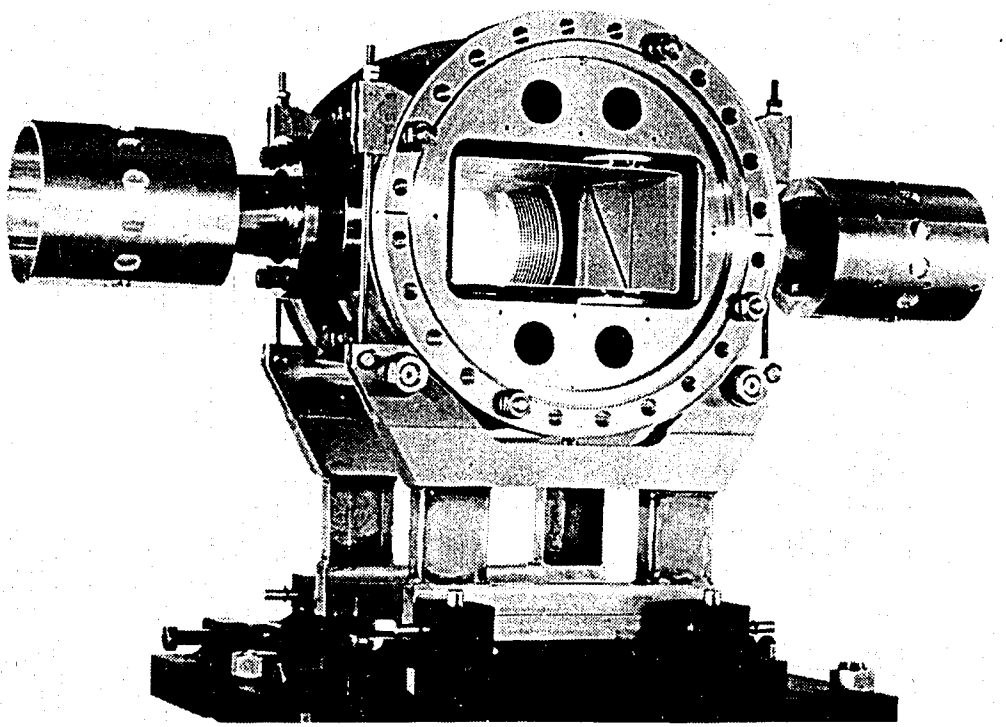

Ultra-high vacuum electrostatic position monitor
(backable to 350°C) for ISR.

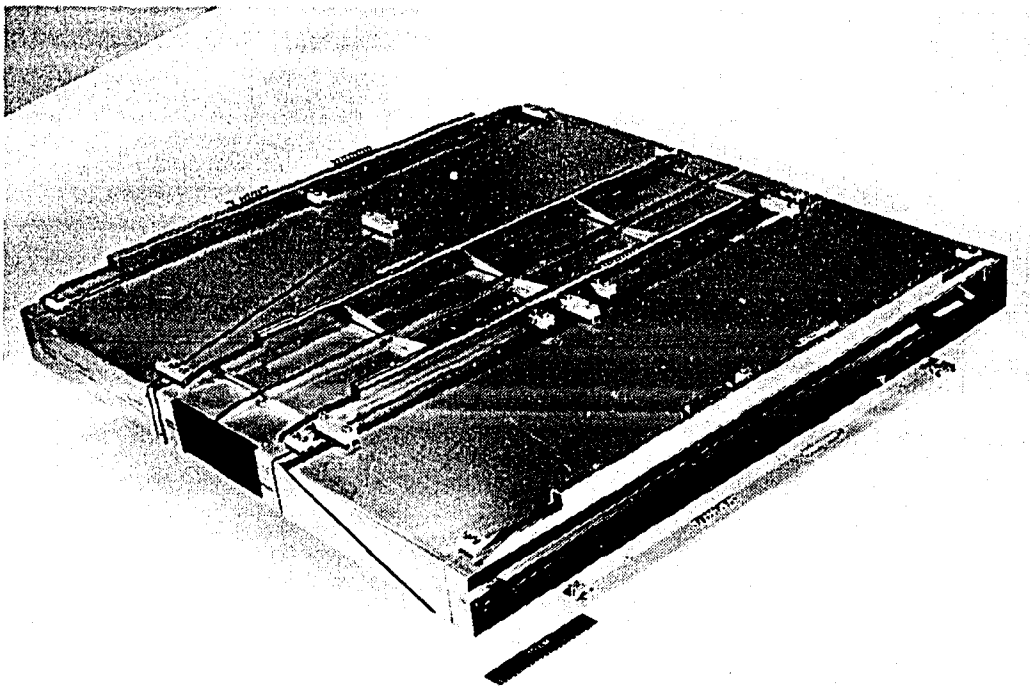

Very broad aperture electrodes assembly
of the LEAR electrostatic position monitor.

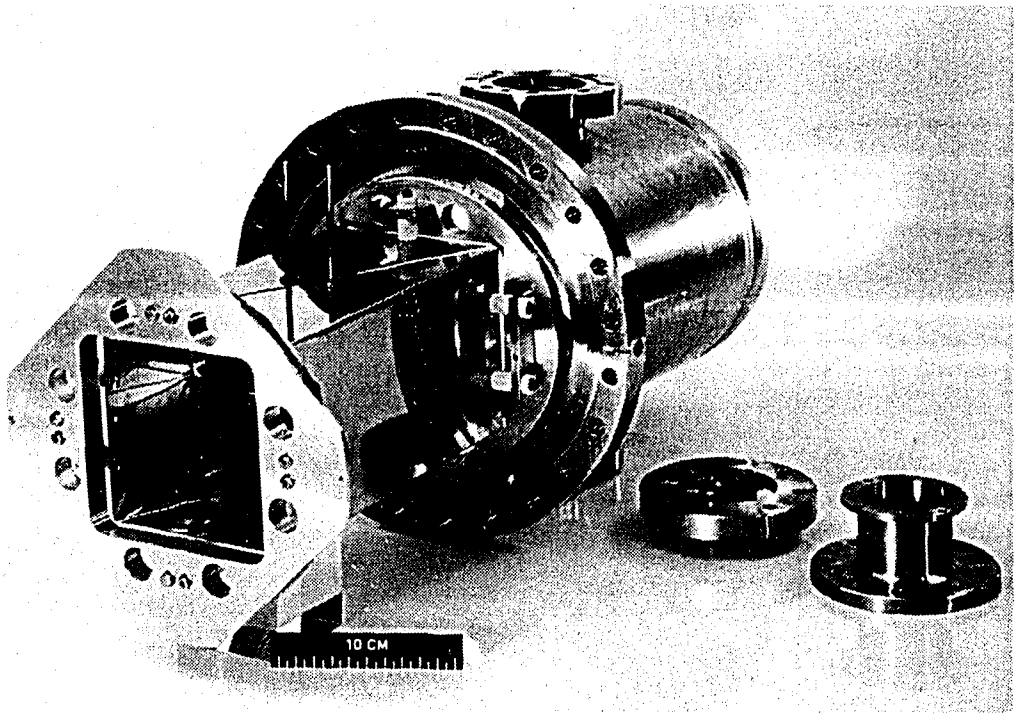

Very simple electrode assembly (horizontal)
of the $\bar{p}$ transfer line monitors (TT6).

Many other cuts can be invented:

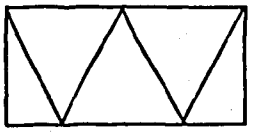

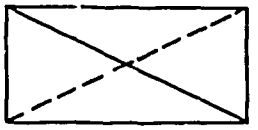

Remarks:

- The linearity of the transverse position function is assured only if the tube cross-section is maintained at both ends of the electrode structure and this at least for a length equal to the largest transverse dimension. If the chamber cannot fulfil this condition, grounded guard rings of the same cross-section should be used.

- Electrostatic monitors have a large impedance at low frequency and they are therefore very good collectors of charge. They should not be used in places where ionized molecules or secondary particles are present in large quantities as they produce perturbing low frequency signals. A small DC bias can help to avoid these spurious collection effects. In some cases such signals can be turned to good use and can be used to detect a localized beam loss.

For electron machines, the most frequently used electrostatic solution is the button electrode. Ref.: 3.

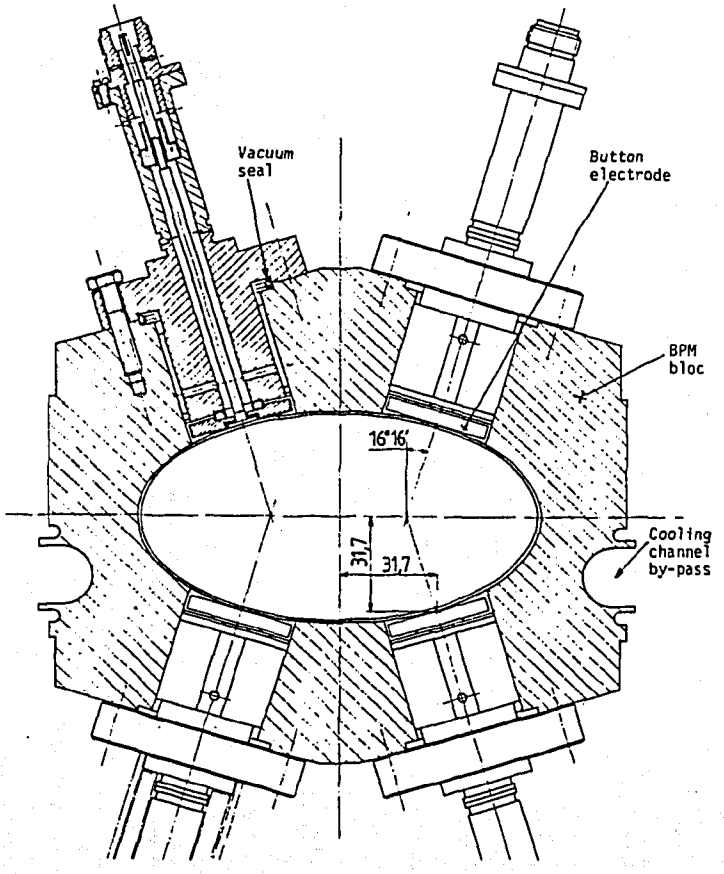

This configuration is imposed by the emission of the synchrotron light in the horizontal mid-plane, which should not hit the button electrodes directly.
Such a monitor has a non-linear position transfer-function.

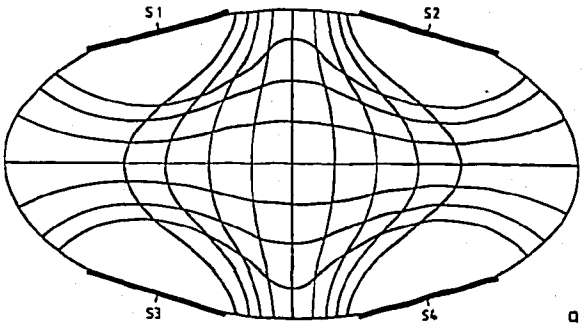

a

Isolevel curves for $\Delta H/\Sigma$ and $\Delta V/\Sigma$

This function has been calculated by conformal maping and the result is given in the form of isolevel curves.

Curves a:

$$\frac{\Delta V}{\Sigma} = \frac{(S_1 + S_2) - (S_3 + S_4)}{\Sigma_{tot}}$$

$$\frac{\Delta H}{\Sigma} = \frac{(S_2 + S_4) - (S_1 + S_3)}{\Sigma_{tot}}$$

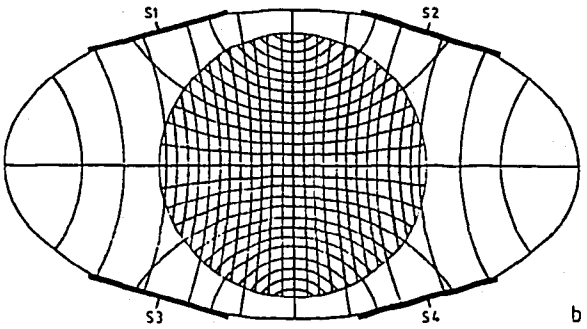

b

Isolevel curves for δ_H and δ_V

Curves b: diagonal treatment

$$\delta V = \frac{S_1 - S_4}{S_1 + S_4} + \frac{S_2 - S_3}{S_2 + S_3}$$

$$\delta H = -\frac{S_1 - S_4}{S_1 + S_4} + \frac{S_2 - S_3}{S_2 + S_3}$$

Multipolar electrostatic monitors:

Such monitors have been proposed but not yet applied.

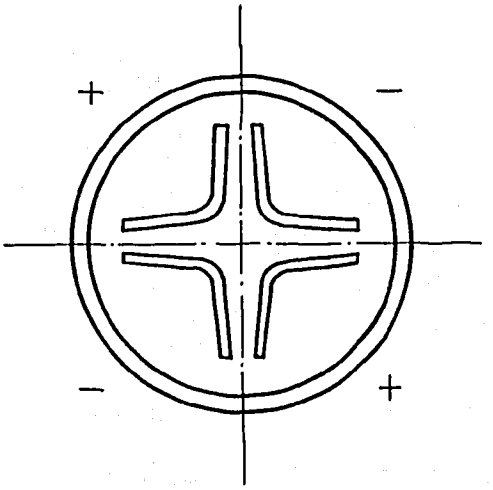

quadrupolar (tilted)
hyperbolic shape Ref.: 79, 66

1.4 Magnetic monitors

1.4.1 Intensity response

Returning to the original coaxial pipe structure of § 1.2, the terminating resistors can be replaced; R_1 by an external very low impedance to measure the current and R_2 by a short circuit.

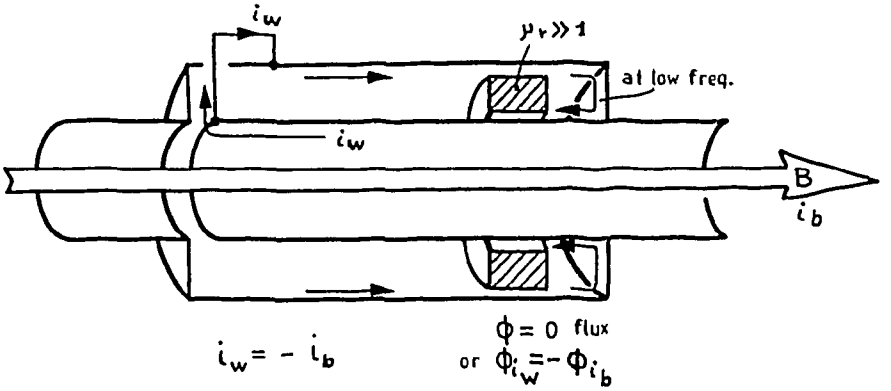

This monitor is then a coaxial current transformer with a turns ratio of 1:1. This turns ratio can be changed by adding windings around the magnetic core. The secondary loading resistor must also be low in order to have negligeable voltage across the gap. This loading resistor R_L is shunted by the parallel cavity inductance which is:

$$L_T = \frac{Z_o^2}{C_e}$$

related to the characteristic impedance of the coaxial structure:

$$L_T = \frac{\lambda \mu_0}{2\pi} \ln \frac{b}{a} \qquad \begin{array}{l} b = \text{outer radius} \\ a = \text{inner radius} \end{array}$$

The device is then also a high-pass filter with a cut-off frequency $\frac{R_L}{2\pi L_T}$.

The usual way to lower the cut-off frequency is to increase L_T by adding a magnetic ring which also increases the coupling to the beam for frequencies below the point where the skin depth $\delta >$ wall thickness.

The device's lower cut-off frequency can be pushed down to DC in order to obtain a DC transformer. Active feed-back and DC beam flux detector has then to be added.

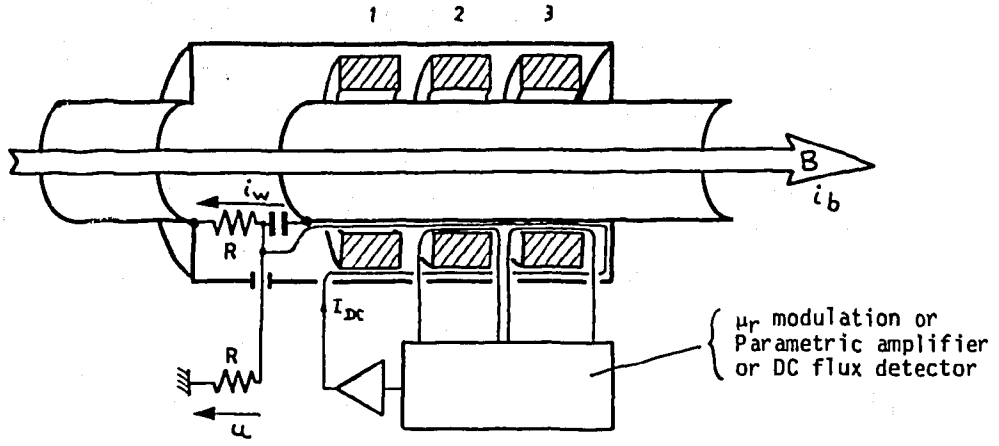

$I_{DC} = I_b$

$u = \frac{R}{2} \cdot i_b$ from DC to high frequency.

Ring 1 : AC coupling for mid-frequencies

Rings 2, 3 : DC detector. Ref.: 77, 32, 117, 118, 119

The technical aspects of this DC transformer are further presented in chapter 5.2

Remark:

- Such a device is quite insensitive to secondary particles.
- It is very sensitive to external magnetic fields and needs careful shielding.
- It is a low impedance device.

1.4.2 Transverse response

The magnetic transformers or monitors are also used to measure the azimuthal wall current density distribution. They are also used for position measurement.

Loop monitors:

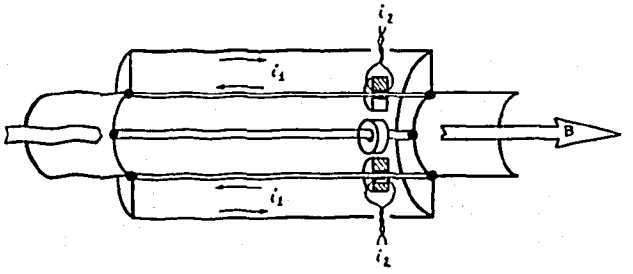

Four rods with
current transformers

$i_2 = i_1/n$ n = turns ratio

$i_1 \tilde{=} i_b/4$ to $i_b \cdot \frac{W}{2\pi R}$ W = width of rod or strip

Depends on frequency Ref.: 116.

Transverse position sensitivity is like one of the strip line monitor. It has a non-linear position function.

Window frame monitor:

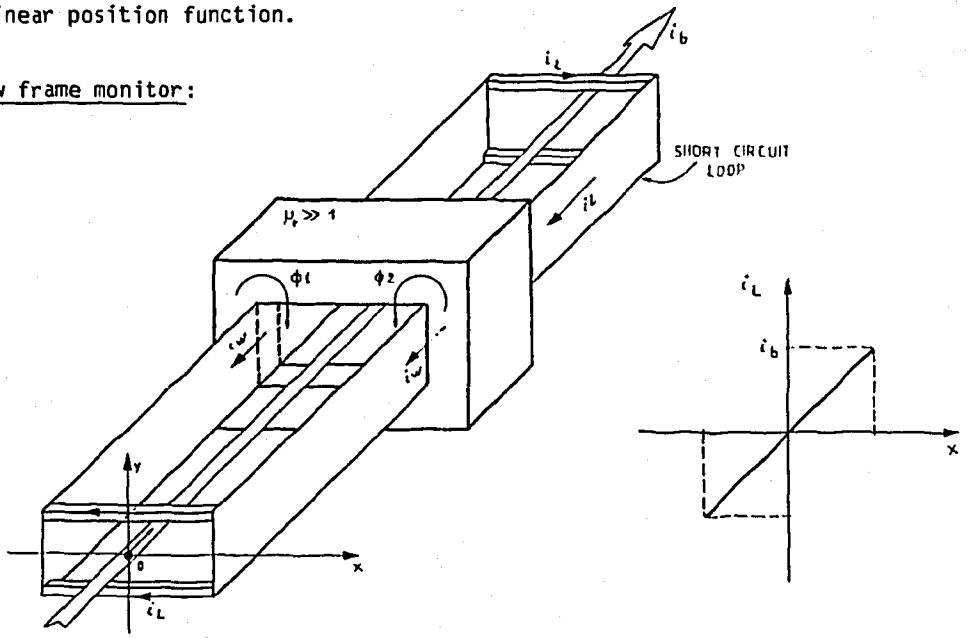

At $X = 0$ $i_L = 0 = \Delta\ i_W$

since $\Phi_1 = \Phi_2$

Such a monitor has a linear position function, for low frequencies. It is the reciprocal of the window frame magnet. Ref.: 49

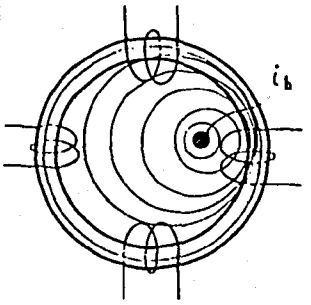

Ring core magnetic position monitor:

- Non-linear
- Difficult to shield
- Useful when secondary particles are a problem

Ref.: 22, 40, 24.

Open ring core, external LF field: Ref.: 47

1.5 Other monitors:

Slotted type:

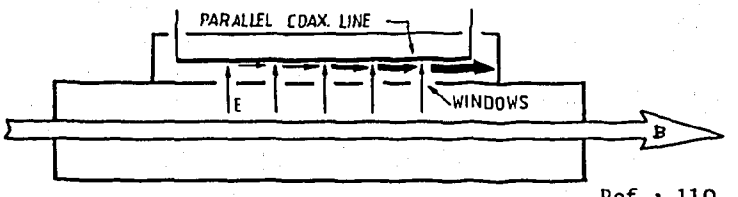

directional electric coupler

Ref.: 110, 10, 11, 12

Wave guide coupler:

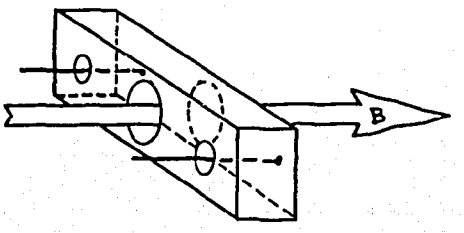

Ref.: 33

2. SIGNAL PROCESSING

2.1 Characteristics of the Beam signals:

2.1.1 Intensity

I_b = DC average current

$$= \frac{N \cdot e \cdot c}{2\pi R}$$

$$I_b = 7.6 \cdot 10^{10} \cdot \frac{N}{R}$$

e = electron charge, c = velocity of light, R = machine radius, N = nb. of particles.
If the beam is bunched it will most probably have a Gaussian bunch shape:

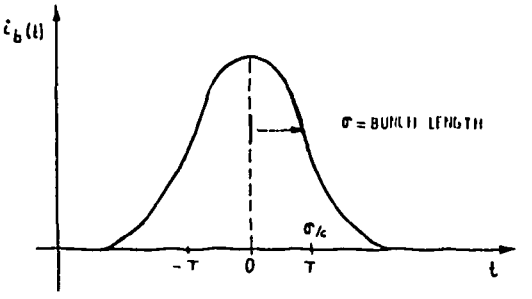

$$i_b(t) = I_b \cdot \frac{\sqrt{2\pi}R}{k_b \cdot \sigma} \cdot e^{\frac{-(ct)^2}{2\sigma^2}} \qquad k_b = \text{nb. of bunches}$$

Such a time function gives spectrum in the frequency domain of the form:

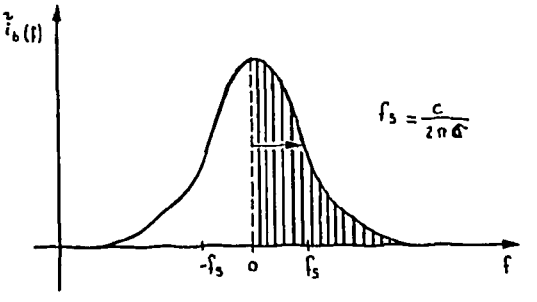

$$\tilde{i}_b(f) = \frac{I_b}{k_b \cdot f_{rev}} \cdot e^{\frac{-(2\pi f)^2\sigma^2}{2c^2}}$$

This spectrum is a line spectrum at each harmonics of the revolution frequency f_{rev} and bunch frequency $k_b \cdot f_{rev}$. Its cut-off frequency is f_s. Ref.: 2

Schottky A.C. noise signal from a non-bunched beam:

$$\tilde{i}_n^2 (f) = \frac{1}{s} \cdot I_b \cdot 2 \cdot e \qquad [A/Hz]^2$$

with spread $s = h\,|\eta|\frac{\Delta p}{p}$

It is a power density spectrum once multiplied by Z_{CO}. Ref.: 98.

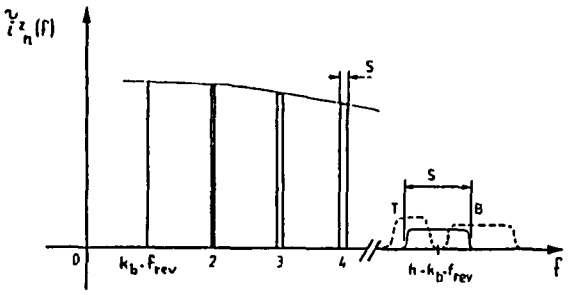

2.1.2 Transverse motion:

It is due to:

a) Position or orbit distorsion

b) β dipole oscillation

From the signal point of view it coresponds to an amplitude modulation with ratio:

$$\frac{A_\beta}{\text{aperture}}$$

c) multipole motions

For the measurement of the transverse position (case a)) the mean intensity information I_b is used.

For β dipole motion measurement or detection, the modulation information of $i_b(t)$ or $i_b(f)$ is used.

For Schottky β dipole motion measurement, the $i_n^{-2}(f)$ is used (debunched beam). See also Chapter 4. Ref.: 98, 2.

2.1.3 Dual Beams

If a machine has colliding beams: $p \leftrightarrow \bar{p}$, $e^- \leftrightarrow e^+$

it requires: - polarity sensitive monitors, or

- direction sensitive monitors

Ref.: 38,2.

2.2 Connection to the monitor

2.2.1 High impendance for voltage sources:

a) electrostatic monitor case:

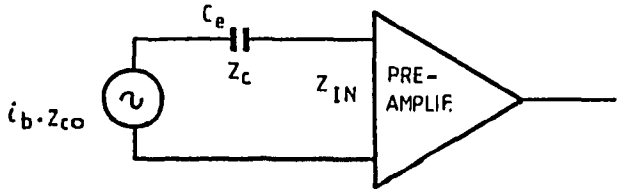

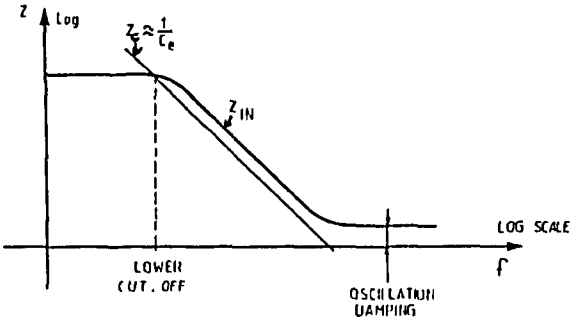

Necessary condition:
$Z_{IN} > Z_c$
with
$Z_c = \frac{1}{jwCe}$

Ref.: 76

In accelerators it is often desirable to damp electrode reactive oscillations for beam stability reasons. This is achieved by making the amplifier input impedance resistive above the frequency domain of interest.

b) tuned cavity or electrode case:

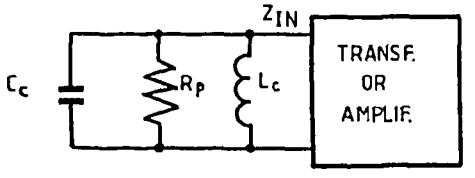

$Z_{IN} = R_p$

For the tuned electrode case an external inductor is added which resonates with the electrode capacity.

2.2.2 Low impedance for matching, or maximum power output

a) Coupler case: $Z_0 = Z_{cable}$
b) Electrostatic monitor case:

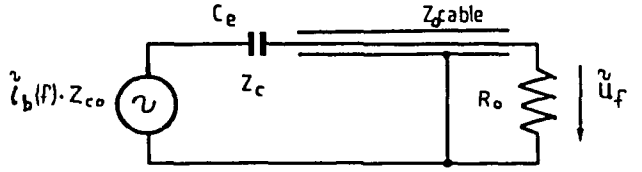

$$\tilde{u}(f) = \tilde{i}_b(f) \cdot \underbrace{\frac{Z_{co}}{1 + \frac{1}{j2\pi f R_0 C_e}}}_{Z(f)}$$

$$f_c = \frac{1}{2\pi R_0 C_e}$$

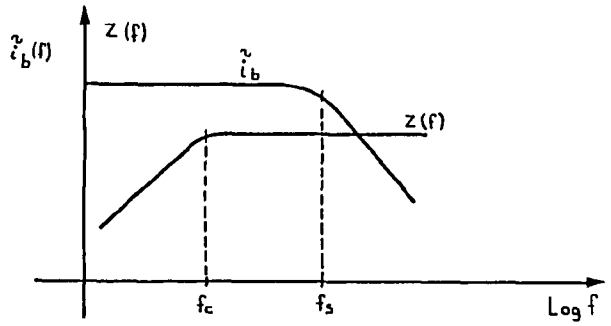

In most of the cases the cable impedance Z_0 and the electrode capacity C_e are given. The lower cut-off frequency of the coupling impedance is then f_c. The resulting $\tilde{u}(f)$ is limited by f_c and f_s which is the upper 3dβ limit of the beam signal spectrum.

2.2.3 Very low impedance for current sources

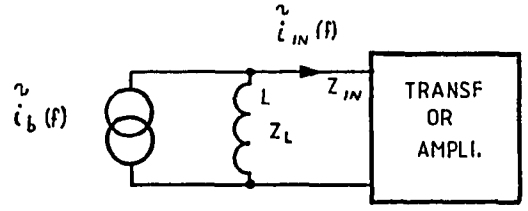

$$Z_{IN} < Z_L$$

$$f_c = \frac{R_{IN}}{2\pi L}$$

For magnetic and gap monitors

Ref.: 116, 24

2.2.4 Long Distance Analog Transmission

The different aspects of such transmission can be described in four points:

2.2.4.1 Attenuation

Very often the monitor signal has to be transmitted by long cables. The transfer function is similar to a low-pass filter with an attentuation being a function of the cable length:

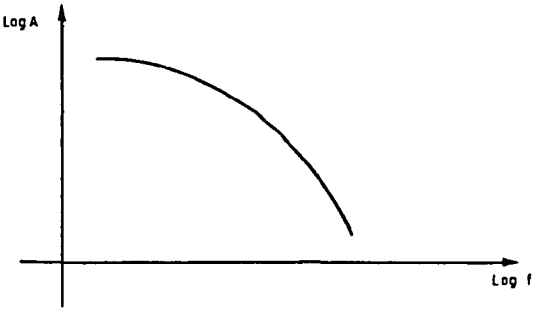

Example of an evaluation:

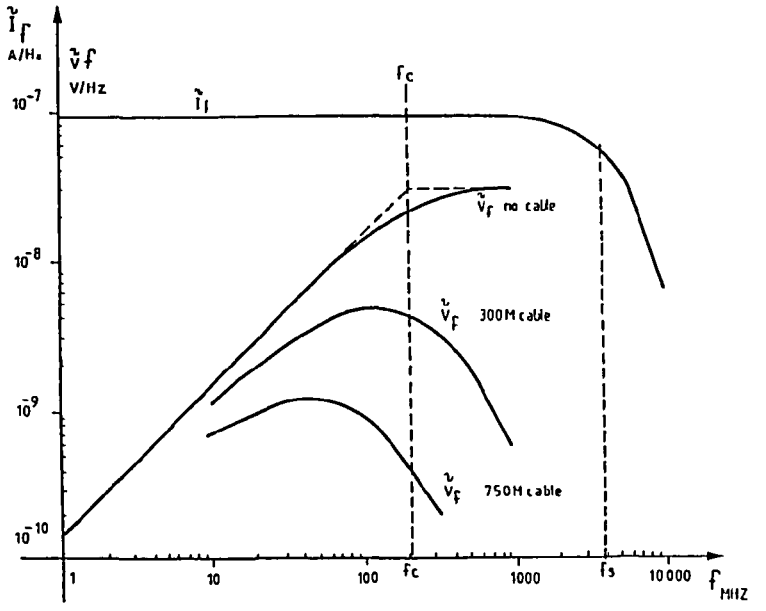

Current spectrum $\tilde{I}$ (f) and voltage spectrum $\tilde{V}(f)$ of the button signal for a single bunch with $5.56 \cdot 10^{11}$ particles (I_0 = I mA) with Z_{CO} = 0.3 Ω, C_e = 15 pF and different length of CK50 cable. Ref.: 2

The beam current spectrum $\tilde{I}(f)$ is multiplied by the cupling impedance Z_{CO} (curve $\tilde{V}(f)$ with no cable atten.) and then by the cable attentuation function (as function of the length). The resulting $\tilde{V}(f)$ is then integrated over the bandwidth of the amplifier chain and compared with the input equivalent noise voltage. This gives an evaluation of the system resolution.

2.2.4.2 Isolation from External Noises

This is major problem in accelerator instrumentation design. There are no absolute recipes to solve this problem but the most frequently used means are:

- good screening
- grounding scheme
- balanced lines
- galvanic separation
- narrow band-width of the system and/or
- time windows
- etc.

2.2.4.3 Direct, Δ-Σ and Time Multiplexed Transmissions

Among the usual modes of analog transmission the following can be named:

- Direct:

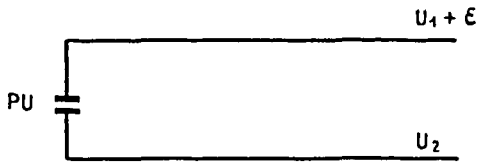

If ε = error in transmission with $\varepsilon \ll 1$

The position is given by: $\frac{\Delta}{\Sigma} = \frac{U_1 - U_2}{U_1 + U_2}$ resulting in $\frac{\varepsilon}{\Sigma}$ = error in position or position offset.

- Δ and Σ:

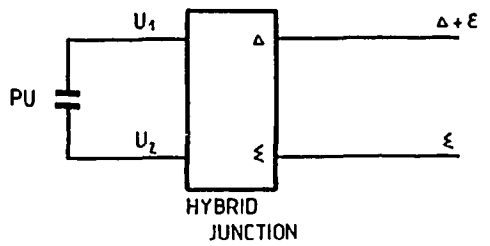

In this case the error in transmission results in $(\Delta/\Sigma)\cdot(1 + \varepsilon)$ = error in scale, and not in offset which is more critical.

- Time multiplexing:

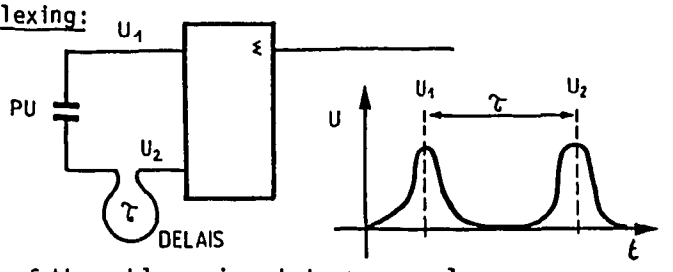

Ideal because of the cable saving, but more complex.

2.2.4.4 Band-Width of The Analog Transmission And its Uses

Wide bandwidth:

for - time domain signal processing
- fast signal processing
- maximum power from the monitor

Narrow bandwidth:

for - tuned devices, maximum sensitivity
- ringing filter and synchronous demodulation
- good noise rejection
- phase modulation and demodulation for large dynamic range (auto normalization)

2.2.5 Coupling to the beam and instabilities

A stability criteria for the beam must also be considered:

	Uses:	
Large $I_b \rightarrow Z_{co}$ low	Accelerators	for longitudinal and transversal couplings
Small $I_b \rightarrow Z_{co}$ high	Cooling	

2.2.6 Front-end signal to noise ratio and resolution

Last, but not least, the monitor resolution.
Definitions:

- Precision: mostly means the absolute precision of a measurement, intensity or position.
- Resolution: mostly means the smallest detectable change in magnitude or position. It also refers to a useful signal to noise signal ratio of one.

The problem of precision is related to the mechanical precision of the device and to the gain balance of the processing chain (see also § 2.2.4.3 and 2.4.2). The problem of resolution can only be solved by either increasing the monitor sensitivity, Z_{co} and transverse sensitivity, or by diminishing the processing chain front end noise figure. Picked-up external noise signals can also be a non-negligible factor since most monitor signals have quite a low level. This difficulty is evidently solved by front-end amplification and optimised screening. Ref.: 2.

2.3 Signal Detection

2.3.1 Wide-band case

Three types of detectors are used in this case:

- Sample-Hold or Track-Hold:

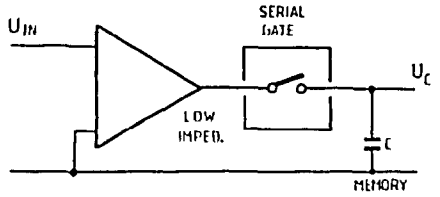

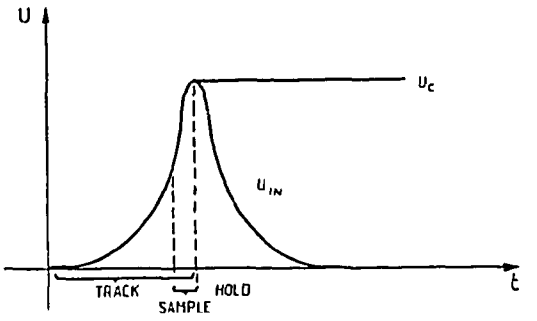

- Peak-Hold:

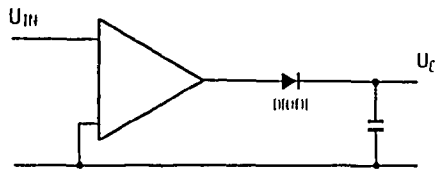

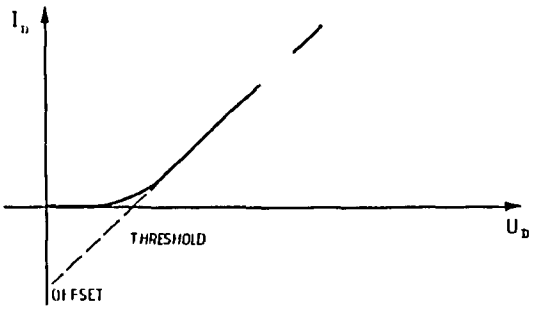

It has a non-linear characteristic.

- Clamp:

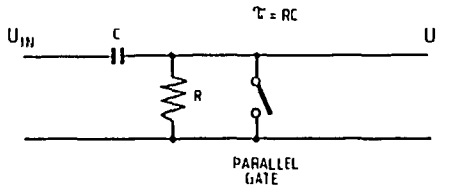

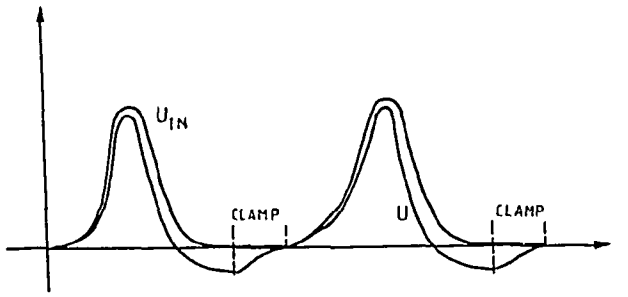

The clamp circuit is a DC restorer or a synchronous detector similar to the sample-hold circuit since both parallel and serial gates must be synchronously driven relative to the beam signal. Ref.: 2,21, 76

2.3.2 Narrow-band case

Three types of demodulators are used in this case:

- Synchronous detector:

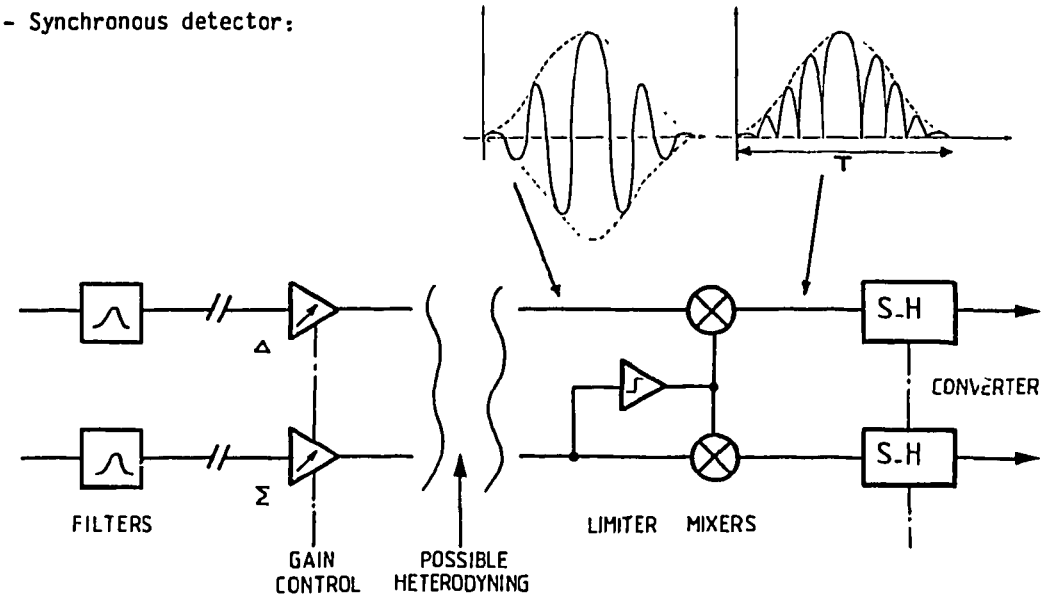

Its main advantage is insensitivity to external noise. But the duration T of the burst can be a problem if the repetition rate of the bunch signal is high.

Ref.: 2, 4, 7, 38, 39

- Phase modulator-demodulator:

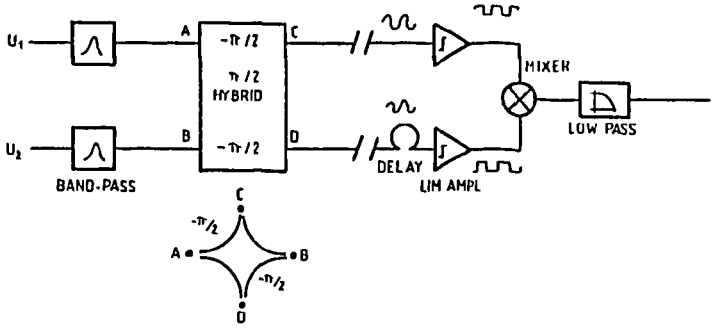

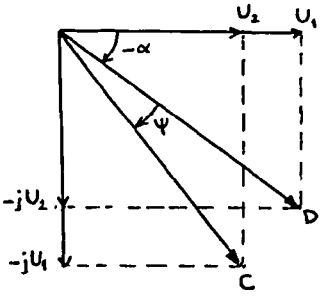

$$\alpha = \frac{1}{2}\left(\Psi + \frac{\Pi}{2}\right)$$

Position information :

$$x \text{ or } y = \frac{\Delta}{\Sigma} = \frac{U_2 - U_1}{U_2 + U_1} = \tan\frac{\Psi}{2}$$

Phase modulation :

$$\Psi = 2\,\text{Arctan}\left(\frac{U_2}{U_1}\right) - \frac{\Pi}{2}$$

Its main advantage is its wide dynamic range since the intensity information is normalized. But this can be a drawback if the intensity information is needed.

Ref.: 5, 25, 27, 28

- Analog multiplexing and Network analyser:

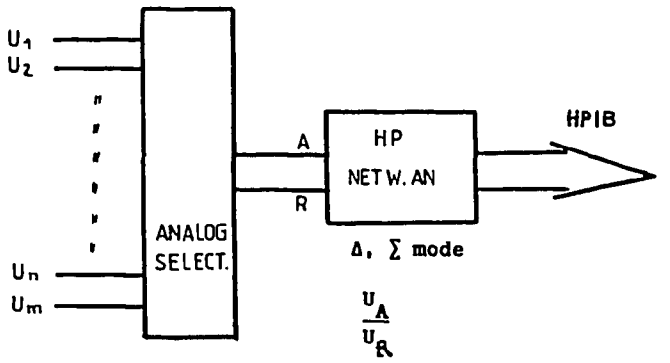

Ref.: 17

2.4 Digital Acquisition and Processing

2.4.1 A - D conversion

One usually finds two approaches: AD converters close to the monitor. This is characterised by:

- Long time storage by the ADC and simpler S-H
- Large numbers of ADC's
- Long distance digital transmission

AD converters centralised. This is characterised by:

- Longer time storage in analog form for the S-H
- Possibility of multiplexing prior to conversion
- Long distance analog transmission

The most frequently used system is the 12 bits conversion corresponding to 1/4000 resolution.

2.4.2 Position Calculation

A calibration procedure is usually used to improve the system's precision. With a test signal the offsets and balance coefficients are recorded for subsequent application to the raw data from the monitors. The position calculation is then:

$$X \text{ or } Y = K_S \frac{(U_1-U_{01}) - K_0\,(U_2-U_{02})}{(U_1-U_{01}) - K_0\,(U_2-U_{02})}$$

With U_{0n} = offset voltages

K_0 = balance coefficient

K_S = scaling factor from the monitor lab test.

This formula is used for linear monitors (Ref.: 21). The resolution of the measurement system is defined as a ratio of the system's equivalent input noise and the minimum measureable displacement. The resolutions are usually in the range of 0,1 mm to 0.01 mm. The precision, or absolute precision of the position is usually 3 mm to 0.3 mm.

2.4.3 System modes

Most of the orbit acquisition systems have at least two modes of operation:

- Single shot or first turn orbit corresponding to the mode in transfer lines
- Average or closed orbit which is the mean over n turns to eliminate the betatron motion information

The single shot mode over many turns is also used to obtain the betatron displacement around the mean orbit. This information is used to optimize the injection into an accelerator and to analyse the optic functions. Ref.: 21

2.4.4 System Test and Trigger

- A testing facility, i.e. beam simulation, is not only necessary for calibration purposes but also to test the proper operation of the system under conditions as close as possible to those with beam (Running-In, Maintenance).
- The fast timing of the system-detectors, S-H, ADC, should be beam self triggered for operational reliability reasons. Ref.: 2, 21

SUMMARY TABLE

MONITORS TYPES	CONDITION		DIAGNOSTICS									ACTIVE SYSTEM	
			Beam current				Function		Machine Paremeters				
	Radiation Secondary Particles	$p-\bar{p}$ e^-e^+	high	low	bunch	un-bunch	Intens	Position	B	Working line	Coupling	Feed-back	Cooling
Electrost. P.U.			X		X		X	X	X		X	X	
Idem reson.	X		X	X	X	X	X	X		X	X		
Gap	X		X	X	X	X	X	(X)		X			X
Cavity reson.	X			X			X			X			
DC transf.	X		X	X	X	X	X			X			
Dir. Coupler	X	X	X		X			X				X	
Idem, 1 plane, high coupling	X	X	X	X		X	X	X				X	X
Magn. Posit. Mon	X		X					X					
Slotted Coupler	X		X			X		X					X
Buttons	X	X	X		X			X	X			X	

From ref. 21 an example of beam position acquisition systems is given:

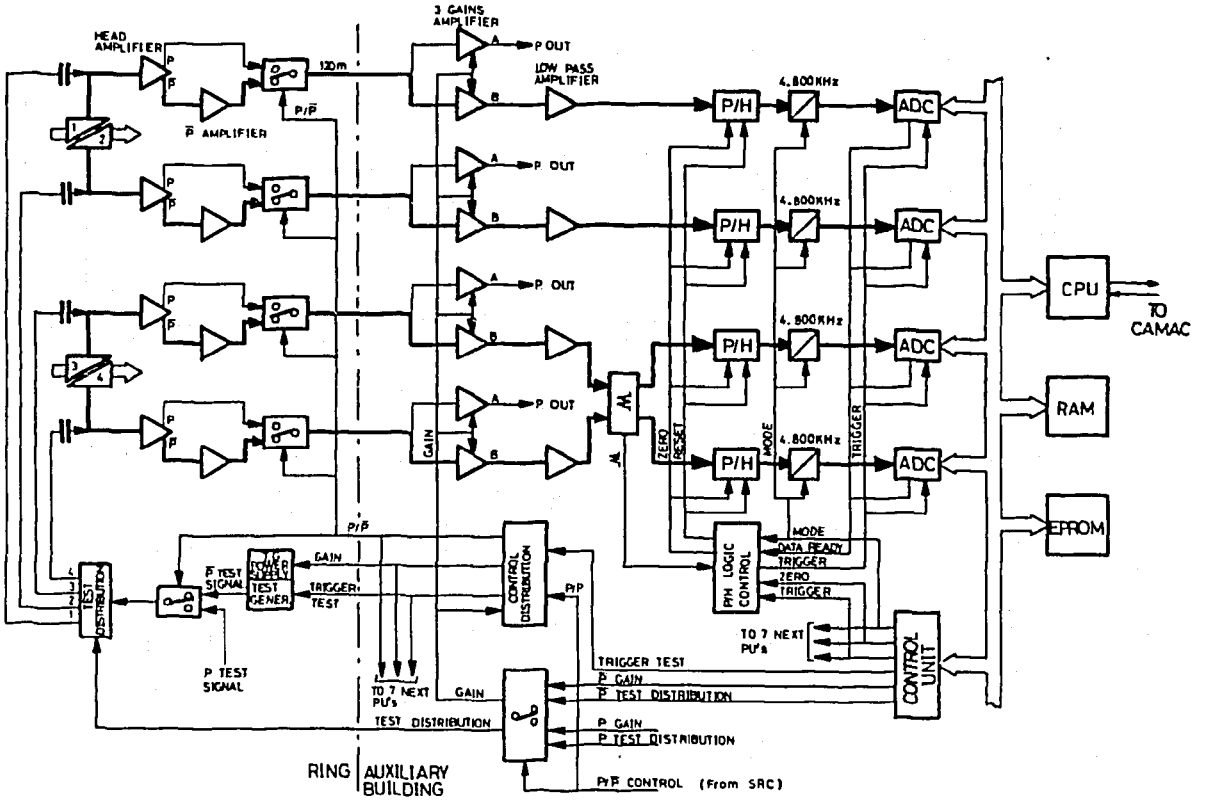

ISR P̄ PICK_UP__ BLOCK DIAGRAM

B_ISR_1321/7

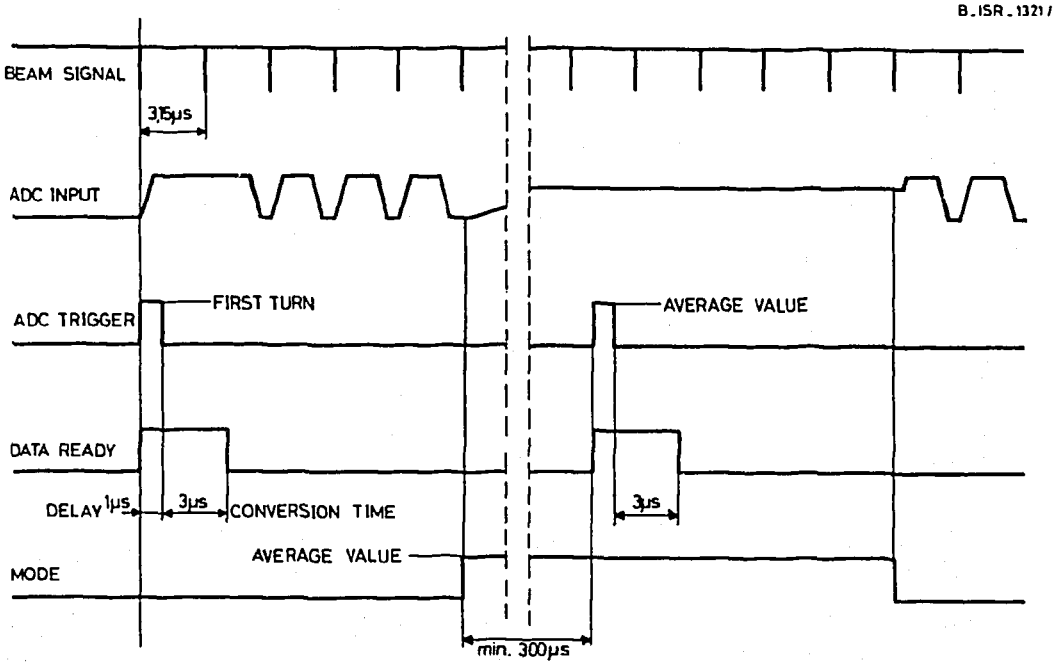

ISR P̄ PICK_UP__ TYPICAL SEQUENCES

B_ISR_1321/10

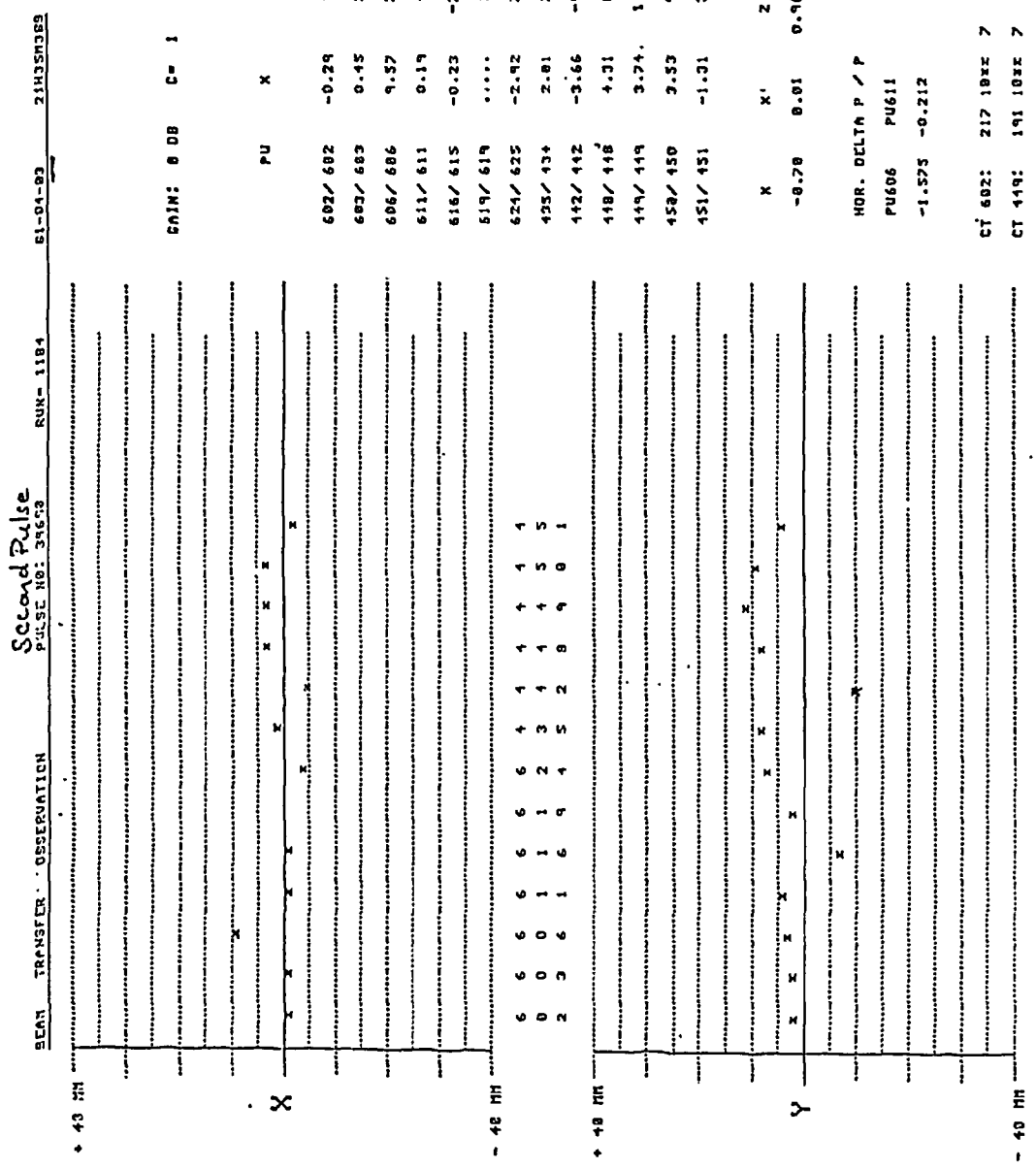

Example of a trajectory measured in a transfer line
(line TT1 and TT2 toward the ISR, with antiprotons)

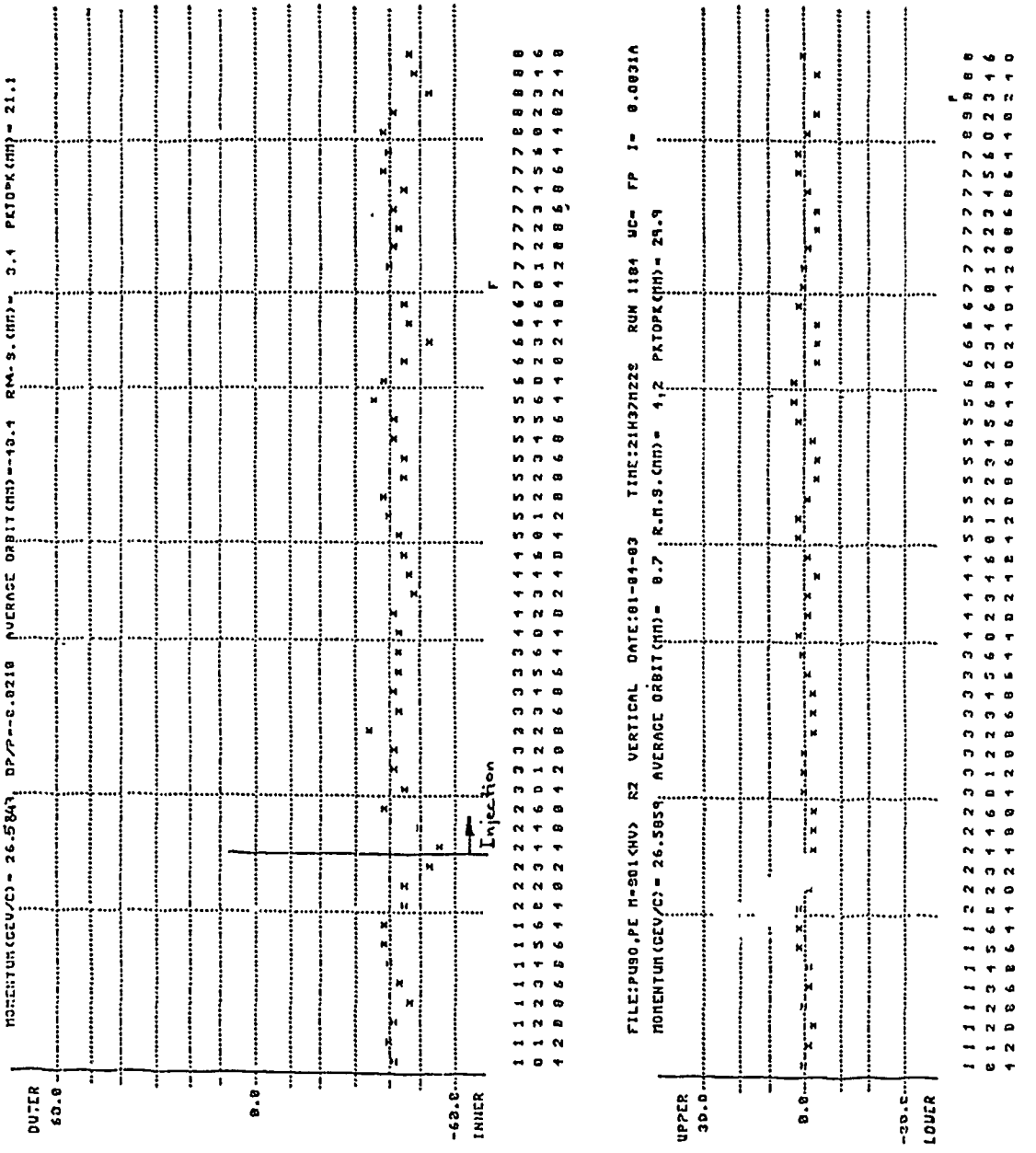

Example of a first turn orbit measured in the ISR Ring
with antiprotons, intensity $2 \cdot 10^9$ particles.

3. OTHER MONITOR DESIGN ASPECTS OR PARAMETERS

Other considerations, which are not covered here but are of the utmost importance in the practical design and choices, are namely:

- Vacuum, metal of the chamber
- Space, dimensions
- External fields (magnetic)
- Radiation, secondary particles
- Particle velocity < c, etc.

4. SCHOTTKY AND BEAM TRANSFER FUNCTION INSTRUMENTATION

Ref. : 81 to 113.

4.1. Introduction and theoretical background

This beam monitoring system gives access to both the incoherent and coherent motions of coasting beams in storage rings.

4.1.1 Schottky signals

The first aspect is called Schottky beam induced noise since it corresponds to the shot noise of free charges in an electrical current. A single revolving proton passing a monitor produces dirac pulses in time domain which corresponds in the frequency domain to a spectrum of lines at all harmonics of the revolution frequency. The combined response of a large but finite number of particles randomly distributed around the accelerator circumference produces the so-called longitudinal Schottky spectrum.

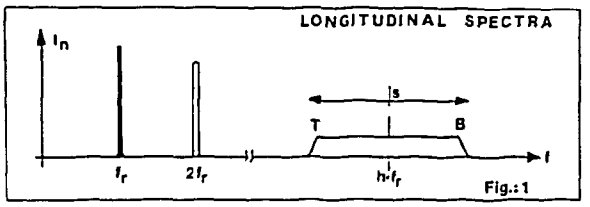

Fig.:1

The noise current In per instrumentation bandwidth Δf is : $I_n^2 = 1/S.2e\ I_{DC}\ \Delta f$ I_{DC} = N nb. of protons and spread $S = h|\eta|\Delta p/p$ at the harmonic h. The squared longitudinal spectrum is therefore an image of the N or current density as function of the momentum or radial position.

If, in addition, a particle has a transverse betatron motion, the signal obtained from a position sensitive monitor will be an amplitude modulated dirac pulse train. Averaging over all particles one obtains sidebands corresponding to the so-called transverse Schottky scans related to the betatron distribution $F(\omega)$. The frequency f_β of the transverse spectrum are related to the 'working line' or tune diagram $Q(\Delta p/p)$. The magnitude or dipole density $D_{rms}(f_\beta)$ is:

$$D_{rms}(f_\beta) = \frac{\sqrt{e/2}}{2\pi R} \cdot A(f_\beta) \sqrt{N(f_\beta) df_\beta}$$

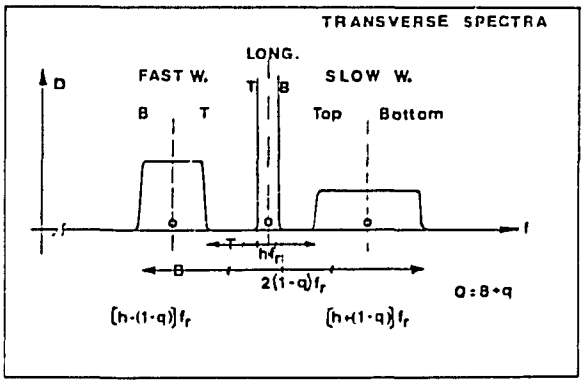

where $N(f_\beta)$ is the number of particles per unit interval of betatron frequency, $f_\beta = (h \pm Q)f_r$ and $A(f_\beta)$ their individual rms transverse motion amplitude which is proportional to the beam emittance.

It should be underlined, from the instrumental point of view, that such incoherent Schottky noise signals are: proportional to $\sqrt{N}$ as well as $\sqrt{\Delta f}$, very small, i.e. in the μV range and that the transverse sidebands are about 1/100 of the longitudinal spectra for ISR conditions.

4.1.2 The beam transfer function

The second aspect is the beam transfer function (BTF) as obtained from an exciter and a position monitor. Only the transverse case will be treated here because it is the most important one for the ISR from the stability point of view.

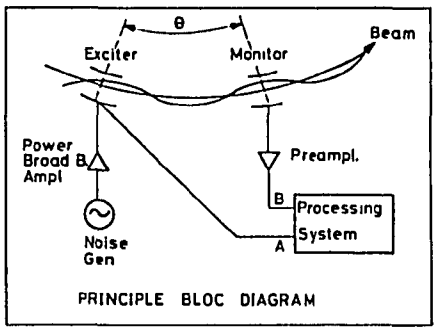

Coming back to the single revolving particle, this will respond when the exciting signal frequency corresponds to its betatron frequency. If the monitor signal is related to the exciter signal the transfer function obtained is, at each resonance, equivalent to the response of a high Q tuned circuit with a phase rotation from - 90° to + 90°. But, since particles in the beam have a betatron distribution $F(\omega)$, their transfer function is that of a system with a continuous distribution of resonators (Fig. 4). For frequencies below that of all the resonators the relative phase is + 90°. For frequencies above, the phase is - 90°, resulting in a smooth phase change of 180° across the sidebands. Such BTF is calculated from the displacement x of single particles with an excitation g and then averaged over the betatron distribution $F(\omega)$. It has been shown to be the inverse of the dispersion integral:

$$+/- \; ID' = +/- \frac{-1}{2 Q_0 \Omega_0 N} \int \frac{F(\omega)\, d\omega}{\omega - \omega_e} = +/- \frac{1}{2 Q_0 \Omega_0 S} ID$$

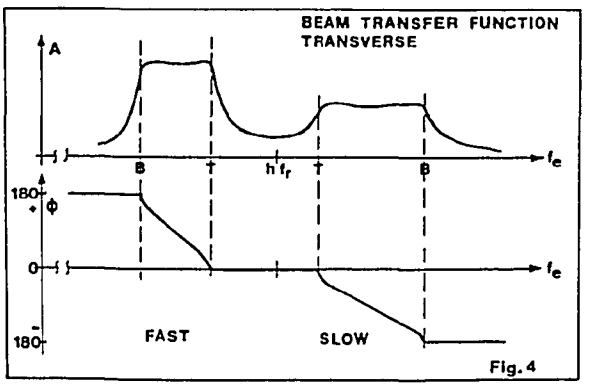

with: slow wave: - sign and $\omega_e = (h-Q)$, fast wave: + sign and $\omega_e = (h+Q)$. $\Omega = 2\pi f_r$ index '0' at centre of distribution. The so-called dispersion integral ID is well known and has been calculated for different $F(\omega)$ (Fig. 7).

The effect of image fields (transverse wall impedance) effect on the beam has to be included and can be described as a feed-back through a passive network (Fig. 5):

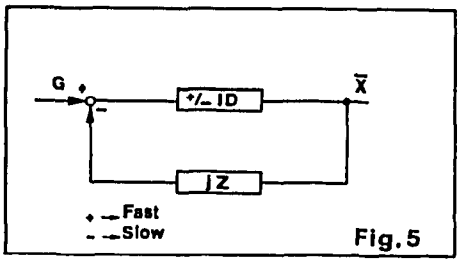

Fig.5

$$Z = \frac{eIZ_T}{2\pi R\gamma m_o} \quad \text{and} \quad G = G_0 + Z\bar{X}/j$$

The resulting total BTF is then:

$$\frac{\bar{X}}{G_0} = +/- \frac{ID'}{1 \pm jID'Z}$$

From Nyquist, the stability criterion of the beam system is that:

$$Z < - j/ID' \quad \text{slow wave}$$
$$Z < + j/ID' \quad \text{fast wave}$$

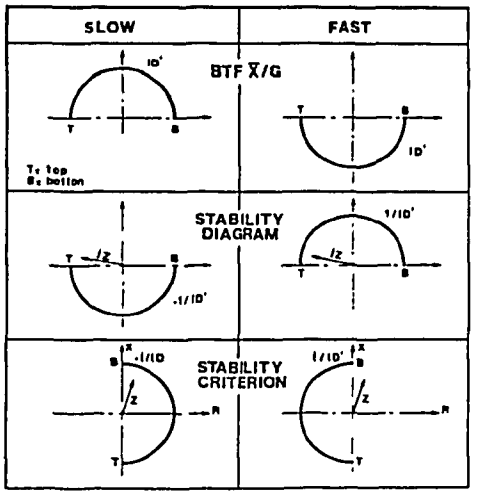

Fig.6

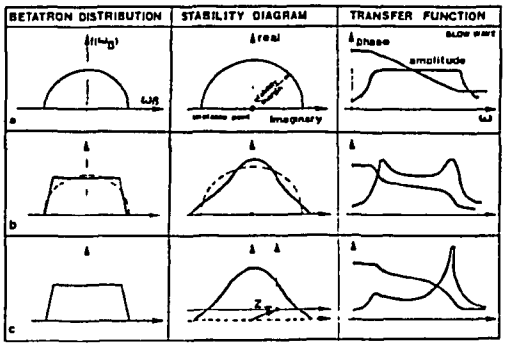

Fig.7

Fig. 6 gives an example for a circular distribution $F(\omega)$. The reactive and resistive parts are positive in the ISR. Negative values for the resistive part can only be obtained with active feedback. Only the slow wave is prone to instabilities and this at the bottom of the stack (high revolution and betatron frequencies). The influence of $F(\omega)$ is also very important for the stability margin (Fig. 7).

To summarize the BTF contains information on the stability margin under real operating conditions, the Z_T wall transverse impedance and active feedback negative impedance, and the betatron distribution from which the tune diagram or working line can be derived. From the instrumentational point of view, it should be underlined that the beam response and hence the monitor signal is proportional to N and is the coherent response of the beam centre of mass even if the exciter signal is noise with a constant power spectrum. This fact allows the treatment of signals much higher than the Schottky beam and amplifier noise; even so, the disturbing signal to individual particles remains very small since it is proportional to 1/N. Hence this measurement technique does not produce any visible beam disturbance. This approach is only valid if the system is linear, which is true as long as the beam transverse motion remains small and the distributions are not modified.

4.2 Instrumentation description

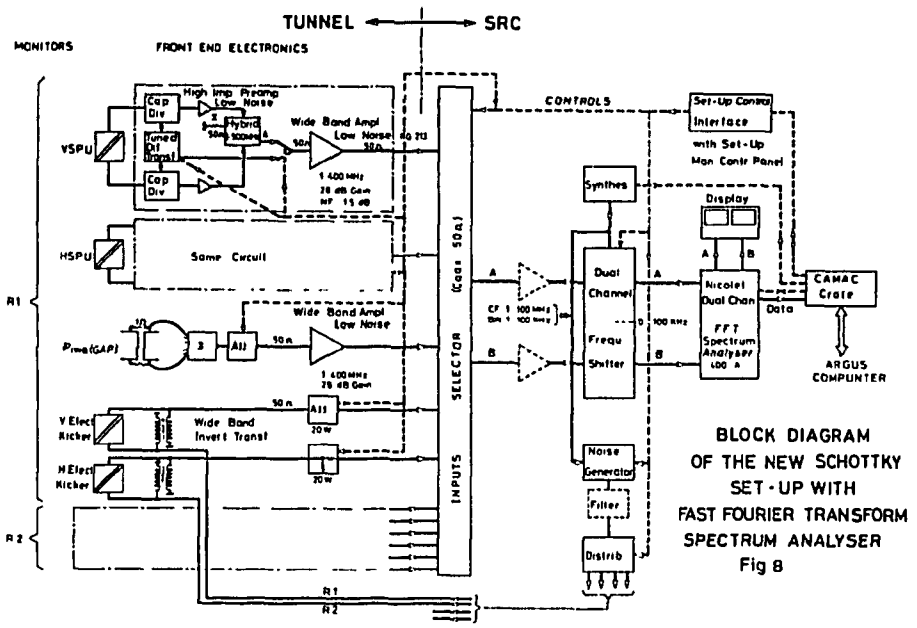

BLOCK DIAGRAM OF THE NEW SCHOTTKY SET-UP WITH FAST FOURIER TRANSFORM SPECTRUM ANALYSER
Fig 8

The first Schottky spectra observation system was implemented with a swept spectrum analyzer. The high speed of present digital processing allows the on-line calculation of the fast Fourier transform of time domain samples. In comparison with a swept spectrum analyzer of the same IF bandwidth or resolution, an FFT instrument with N frequency channels represents N filters in parallel and the time needed for the average of noise spectra is reduced by N. With a dual channel instrument, the transfer function is calculated in amplitude and phase. This instrument having a bandwidth of 0-100 kHz and the Schottky signals of interest being situated in a frequency range of 30 kHz to 100 MHz, a dual channel frequency shifter was developed and built. Its amplitude and phase characteristics must be constant across the band-pass and identical for both channels. One tenth of the FFT bandwidth has to be allowed for a steep attenuation (high-pass) in order to avoid frequency fold-over around 0 Hz. The frequency shifter block diagram and characteristics are given in Fig. 9. An input selector connects the desired signals from the preamplifiers to the inputs of the frequency shifter, whose central frequency setting is controlled by a synthesizer. The same signal controls also the central frequency of a tracking noise source of constant spectrum across 300 kHz, which is used for BTF measurements.

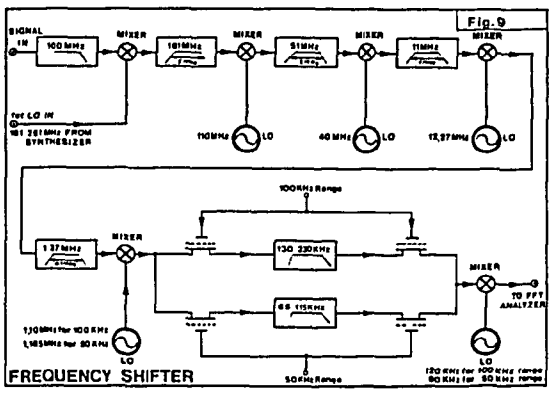

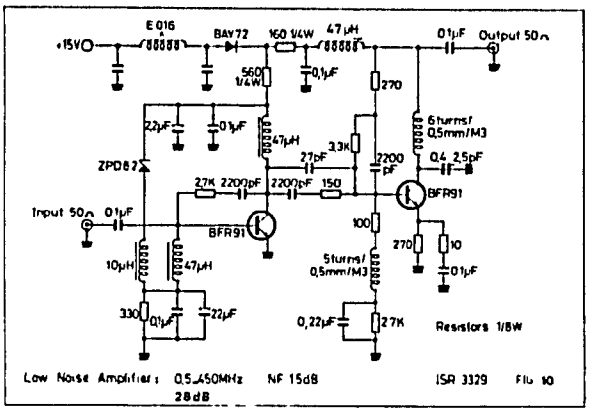

A very low noise broad band amplifier with good linearity has been developed for this equipment and its circuit is given in Fig. 10. It uses UHF silicon bipolar transistors and shunt feed-back to obtain an 'electronically cooled' input 50 Ω active impedance corresponding to a resistor at 70 °K. This amplifier is used throughout the system as wideband amplifier. For transverse Schottky signal observation a 300 kHz bandwidth FET amplifier, with a differential tuned input circuit resonating with the monitor electrode capacitance at 10.8 MHz (h=34), is necessary to obtain good S/N ratio with such low signals.

The horizontal and vertical monitors as well as exciters are of the diagonally split electrostatic type. They are used both for transverse Schottky spectra and BTF measurements. A gap, or coaxial transformer monitor is used for the longitudinal Schottky scans.

Numerous practical problems had to be solved to ensure proper and reliable operational characteristics. The system did allow for automated BTF measurement from 2 to 80 MHz, for longitudinal Schottky spectra at 52 MHz and transverse ones at 10.75 MHz and this for ISR currents ranging from 10 mA (single pulse) to 60 A (stack).

4.3 Data acquisition and processing

The system was connected to the ARGUS computer via a CAMAC crate containing a local processor (Ferranti ACC100) for hardware control. Schottky scan programs controlled the settings of the instrumentation, transferred the data and normalized them for presentation on display. They also calculated radial position and current density of the stack from longitudinal Schottky spectra and the Q value of the two stack edges from the transverse Schottky spectra whose magnitude is proportional to the local stack emittance.

BTF programs controlled the system settings, transferred the data and presented them on the display. Its magnitude is a direct indication of the stability margin. Another program corrected the BTF data and calculated the stability diagram, the transverse impedance and the measured dispersion integral from which the transverse distribution $F(\omega)$ and the tune diagram or working line was derived.

4.3.1 Resistive part of Z

As seen in the introduction

$$ID = PV - j\pi F$$

where

$$PV = \int_{\omega_1}^{\omega_2} \frac{F(\omega)\,d\omega}{\omega - \omega_e}$$

ω_1, ω_2 being the edges of the distribution. For ω_e close to ω_1, PV will be positive, while for ω_e close to ω_2, PV will be negative. This means that ID describes an angle of π radians in the polar diagram since $F(\omega_1) = F(\omega_2) = 0$ at the edges. This is equally the case for 1/ID. The inverse response however will describe an angle different from π and this is caused by the resistive part of Z. Fig. 6.

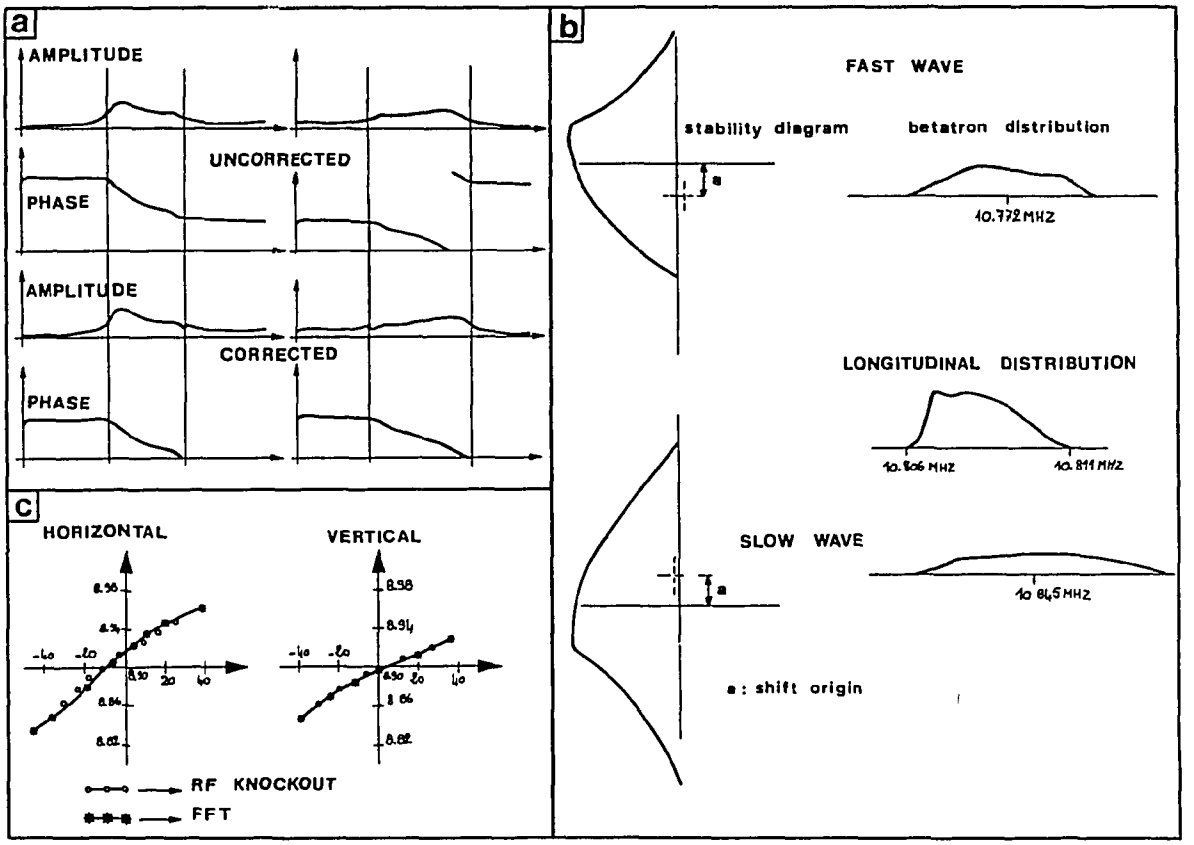

Fig.11 a : signals from FFT; b : calculated betatron distributions and stability diagram; c : working line measurement.

4.3.2 Reactive part of Z

The reactive part of Z shifts the origin of the inverse diagram along the ordinate. Suppose that this shift is known.

Consider the case where the influence of the environment on the response of an excited beam is negligible, in other words Z = 0. The resistive response gives the particle betatron distribution function for a fast and a slow wave. The two total integrals over each wave must be equal since they concern the same particles. Partial integrals which start from the low momentum side and which are equal, cover the same particles, i.e. the other boundary identifies the same particles in the stack (Fig. 12).

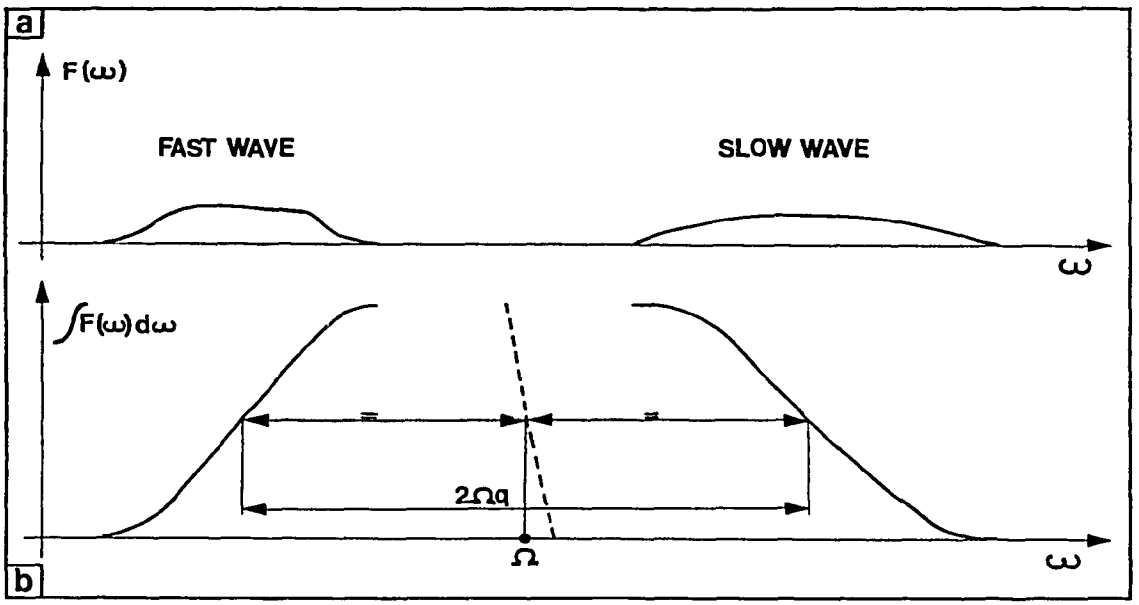

Fig. 12: Principle of working line measurement

This method can be used and for every momentum (radial position) in the stack, one can calculate Q(q). From the betatron distribution and the correlated momenta, one can calculate a corresponding longitudinal distribution. However this distribution could also be directly measured in the ISR and could be compared with the longitudinal distribution computed from the beam transfer function. Different origins in the inverse diagram can be tried out and the resultant longitudinal distribution compared with the measured one. The origin which yields the best match is a measure for the reactive part of the impedance. It has been pointed out that the measurement of the longitudinal distribution may be influenced as well by the corresponding longitudinal impedance. Experiments in the ISR have shown that the margin of longitudinal stability is extremely large and hence the influence on the density measurement may be neglected.

The search for the value of the reactive part of Z_T uses an iterative algorithm.

The results can be split in two groups, i.e. tune measurements and transverse impedance measurements. Figure 11c gives an example of a working line measurement on a stack. A good correspondance has been found with the measurements performed with RF knock-out.

Measurements of Z_T at 10 MHz on a number of stacks have been done as well. For the horizontal plane we notice much smaller values of the reactive part than in the vertical plane, i.e. less than 1 MΩ/m in the vertical plane. This is explained by the fact that the chamber cross section is elliptic with the longer axis in the horizontal plane. The resistive part of Z_T has been found to be a few tenths MΩ/m.

4.4 Operational Applications

The evident application of the BTF is to monitor the stability margin and to control the betatron distribution by modulating the chromaticity in order to compensate for the reactive part of Z_T and optimize the stability. This accurate method is a step forward relative to the simplified stability criterion previously used: $I/\Delta Q < k(F\gamma/|Z_T|)$ with Q' constant.

Figure 13(a) shows an actual beam transfer function, where the influence of the reactive wall impedance is clearly preponderant over the influence of the betatron distribution. Transverse stability optimization will thus be achieved by compensation of the inductive wall impedance.

The frequency spectrum of the disturbances being a priori unknown, the best stability diagram that can be aimed at is a semi-circle, i.e. a constant amplitude transfer function. To meet this criterion, two possibilities are open:

- either to provide a reactive feedback system, which, within its frequency range, compensates Z_T,
- or to choose a betatron distribution such that the stability diagram will be as close as possible to a semi-circle; such a compensation is valid for all collective modes.

The modification of the betatron distribution for a given longitudinal distribution may be performed by controlling the variation of the chromaticity over the energy aperture (Fig. 14): $f(\omega_\beta) \sim 1/Q'(\Delta p/p)$.

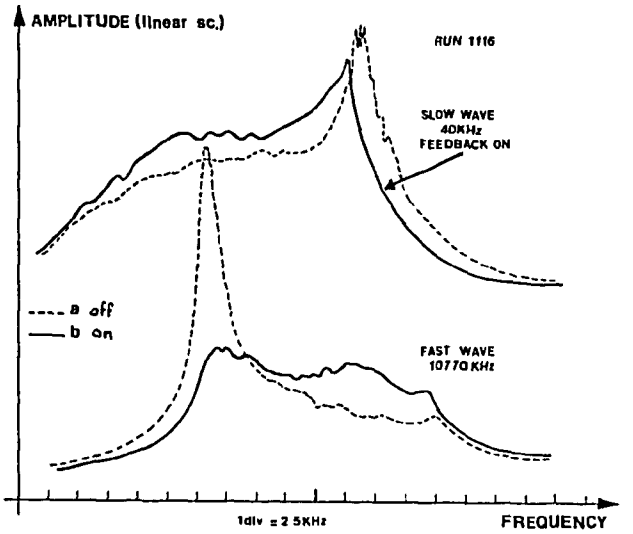

Fig. 13 : Beam transfer function of an ISR beam

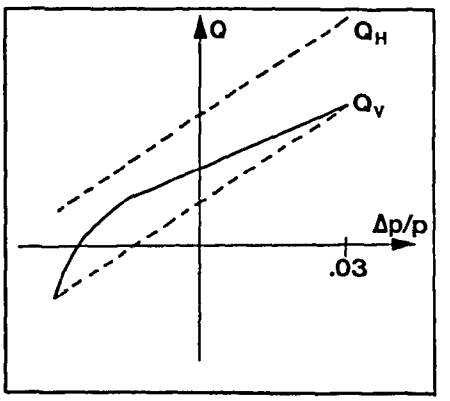

Fig. 14: Tune diagram

In a simple approach the chromaticity at the bottom of the stack is increased in steps whilst the tune and chromaticity over the rest of the stack is modified to keep the tune and tune spread constant; the process is repeated until the optimum stability criterion is fulfilled.

In a more systematic approach a specific skew trapezoidal betatron distribution was found to compensate almost ideally the effect of the reactive wall impedance (Fig. 15); for an initially linear (Q,Δp/p) relationship, the ratio of this ideal betatron distribution to the measured one gives simple the correction factor to be applied to Q'(Δp/p), and, by integration, the ideal tune diagram.

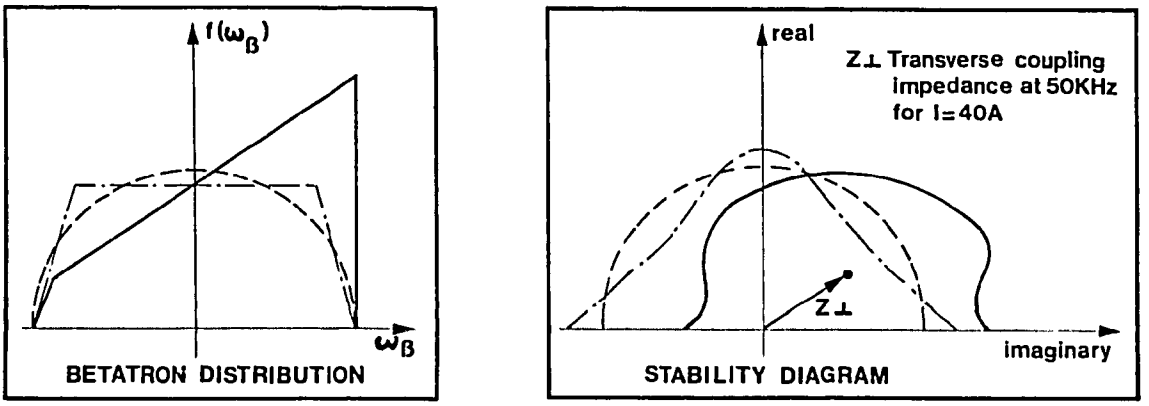

Fig. 15

The BTF was also used to optimize the phase angle of the low frequency (20 kHz to 1 MHz transverse feedback system.

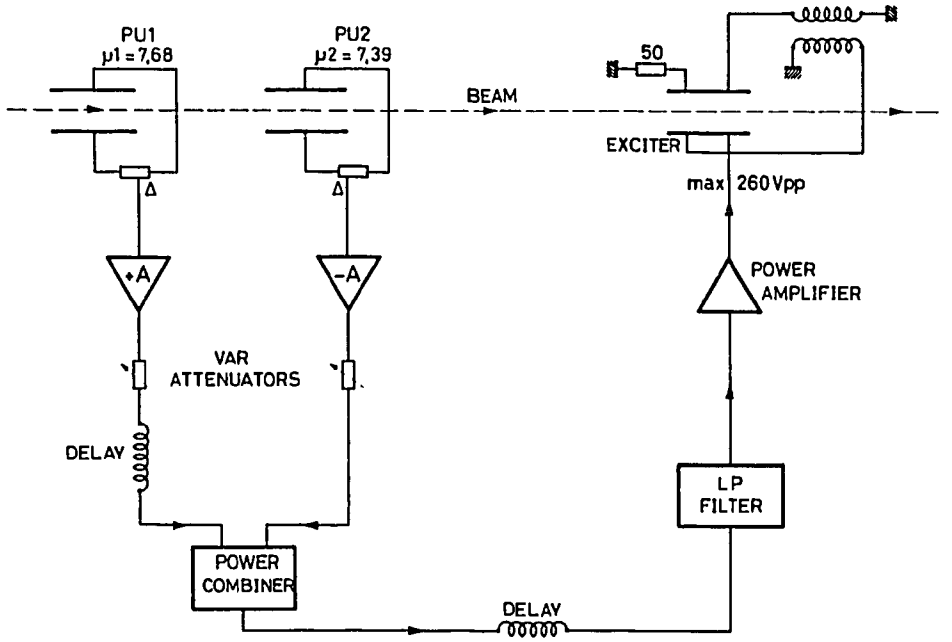

Simplified block diagram of the transverse feedback system with adjustable inductive compensation.

Fig. 16

For compensation of the resistive part of the wall impedance the distance between pick-up and kicker is chosen to be an odd number of betatron wavelengths. Figure 13 shows BTF without and with transverse feedback.

However, the stability margin can be further increased by compensating for not only the resistive part but also for the inductive part of the wall impedance. The phase angle of the compensation can be changed by changing the distance between the pick-up and the kicker of the feedback system.

In the ISR $Im(Z_T)/Re(Z_T) = 1.24$ for the lowest mode. The optimum value of μ is then

$$\mu_{opt} = (0.871 + n/2)\ 2\pi$$

where n is an even integer for positive A_e and an odd integer for negative A_e.

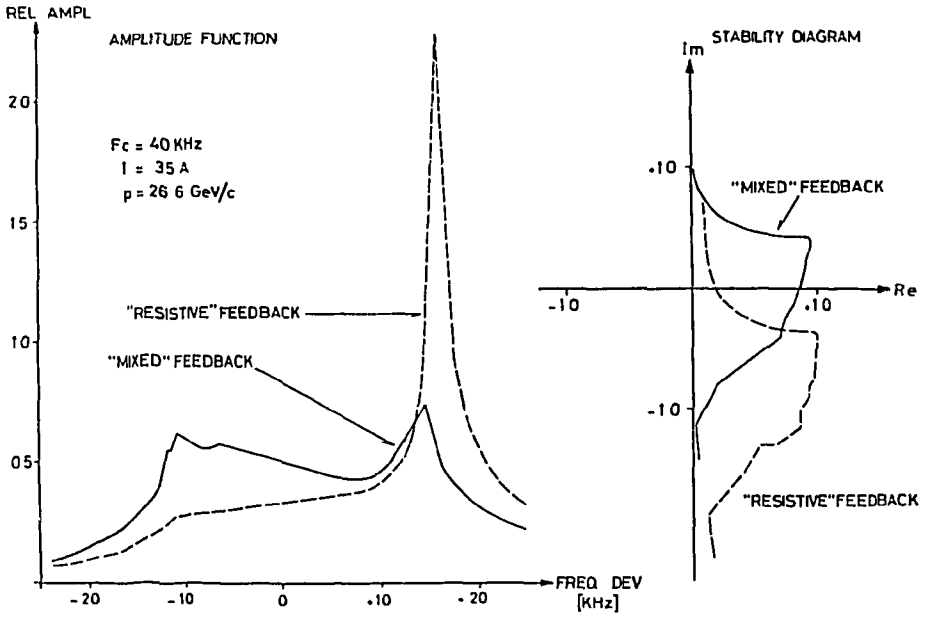

Fig. 17

In practice it is hardly possible to obtain the correct value of μ with a single pick-up as the angle of the feedback will change with the average tune value. Therefore another approach had been taken in the ISR (see Fig. 16). Two pick-ups are used, PU 1 with $\mu_1 = 7.676$ and PU 2 with $\mu_2 = 7.388$ (for an average tune value of 8.882). The signals from the two pick-ups are added in a power combiner. By adjusting the attenuators (the total gain is kept constant) the phase of the feedback is then adjustable from $+27^o$ to -50^o.

The system had been tested on a high density stack of 35 A (Fig. 17) with BTF's measured at the lowest transverse sideband. With the feedback system the stack is very close to the stability limit [the average Q-value of this stack was rather low ($Q_{AV} = 8.865$) so the system increased slightly the inductive impedance). The electronic gain was kept constant. From the stability diagram it is seen that the stability margin has been increased by a factor of 3.

At higher frequencies the transverse impedance becomes more inductive but the total impedance decreases as the skin effect falls off. Therefore, a total compensation of the transverse coupling impedance at the lowest sideband will cause overcompensation at higher frequencies and the stability margin kept large all over the frequency range of the feedback system.

An inductive compensation of the (n-Q) term will give a similar compensation of the (n+Q) term provided that the electronic delay of the feedback system equals the time of flight of the particles between pick-up and kicker.

4.5 *Monitoring system uses for other applications*

Transfer functions can be measured in the longitudinal mode with a gap exciter and for the horizontal-vertical β coupling. The β coupling transfer function has been found to be a very efficient means of measuring the coupling factor and to minimize it.

The coupling transfer function is obtained by correlating a horizontal transverse perturbation imposed on a beam to the resulting vertical coherent motion (Fig. 18). The set-up used is the same as for beam transfer function measurement . The transfer function obtained (Fig. 19) reflects the general properties of coupled oscillators; its detailed behaviour is related to the distance from the linear coupling resonance and to the machine coupling vector.

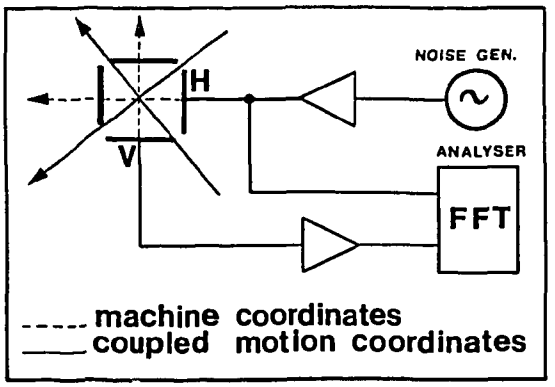

Fig. 18

A coupling transfer function:

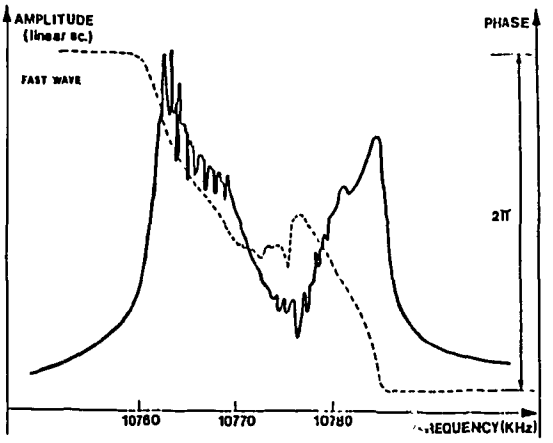

Fig. 19

The transfer function of a distribution $f(\omega_\beta)$ of particles is found by integration; the calculation is done, e.g. in the fast wave approximation ($\omega = (n + Q)\Omega$):

$$\frac{\langle X_0 \rangle}{G_{H_{FW}}} = \frac{e^{-in\theta}c}{4Q_0} \{ \underbrace{\frac{1}{\Delta\omega_\beta} \left[\frac{f(\omega_\beta)d\omega_\beta}{\omega - \omega_\beta} - \frac{f(\omega_\beta)d\omega_\beta}{\omega - \omega_\beta - \Delta\omega_\beta} \right]}_{I_{ZZ}} \}$$

with $\omega_\beta = \Omega(n + Q_z)$; $\Delta\omega_\beta = \Omega(Q_x - Q_z) = \Omega\Delta$; Δ is taken to be constant for all particles.

The coupling transfer function is thus simply proportional to the complex coupling coefficient c whilst its dependence on Δ (or $\Delta\omega_\beta$) is more elaborate.

The term I_{ZZ} in brackets is a finite difference of the vertical dispersion integral; qualitatively, it explains the reason why the beam response is large for frequencies corresponding to the distribution edges whilst it is low for the middle (Fig. 19), for a nearly flat distribution.

Coherent oscillations give rise to electromagnetic fields which, through the transverse wall impedances introduce an additional perturbing acceleration; this effect however does not alter the proportionality between the coupling vector and the transfer function.

The complete expression for the transfer function becomes:

$$\frac{\langle X_0 \rangle}{G_{H_{FW}}} = \frac{ce^{-in\theta}}{4Q_0} I_{zz} [1 - i2S\Omega Z_H ID_H]^{-1} \left[1 + i \frac{S\Omega}{2Q_0} \frac{Z_V I_{zz}}{1 - i2S\Omega Z_H ID_H}\right]^{-1}$$

with I_{zz} = bracketed expression in preceding equation; Z_H, Z_V: transverse wall impedances; ID_H horizontal dispersion integral; S frequency spread. Its complexity excludes a direct absolute measurement of c!

The measured beam transfer function is expressed as a set of pairs amplitude/phase $[A[\omega); \phi(\omega)]$.

According to the model:

$$A(\omega) \sim \sqrt{c_r^2 + c_i^2} \; ; \quad \text{this is equally true for } \int A(\omega)\, d\omega$$

$$\phi(\omega) = \text{Arc tg} \frac{c_i}{c_r} + \phi(I_{zz}) - n\theta$$

For an excitation frequency outside of the beam's natural frequencies, the phase rotation introduced by the distribution $\phi[I_{zz}]$ is either 0 or 2π; θ can be measured or calculated; hence c_i/c_r can be evaluated from a single measurement.

The proportionality factor relating the amplitude to the coupling modulus can be measured if a known coupling increment is added via skew quadrupoles. The linearity of this relationship was found to be good (Fig. 20). In practice, the proportionality factor does not vary significantly from one beam to another. As can be seen in Fig. 20, the accuracy of the measurement is better than 10% on a realistic range of the c values. The sensitivity is large, allowing coupling compensation to $\sim 10^{-4}$.

The method described was used operationally to minimize the residual coupling which did vary from run to run.

Fine coupling compensation is most efficient in reducing the hourly luminosity decay and the "background" measured by the physics detectors (Fig. 21).

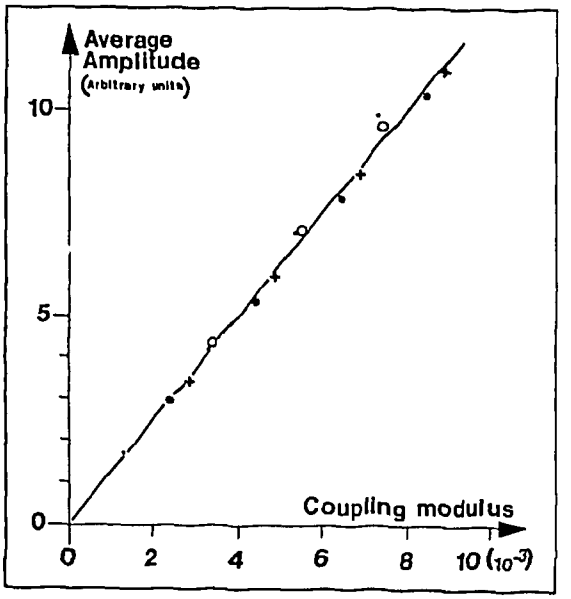

Fig. 20

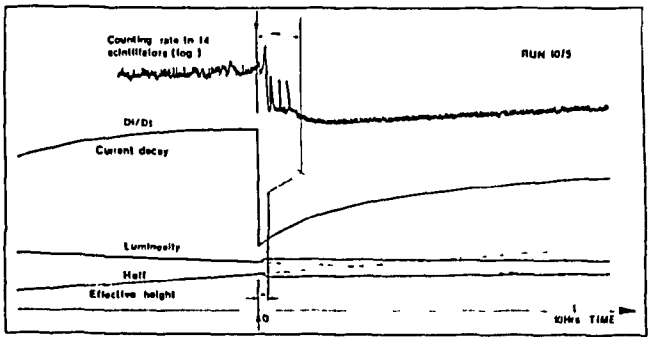

Fig. 21

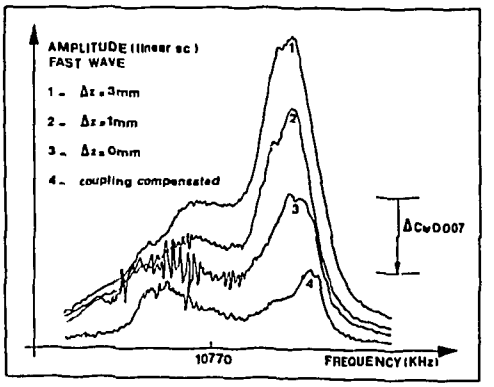

Fig.22

Coupling measurement has been used to study the effect of vertical bumps (Fig. 22) and of localized axial fields.

4.6 Instrumentation for bunched beams

Ref. : 81, 91, 93, 96, 107

The problem with a bunched beam signal is that the coherent signals due to the bunch "centre of mass" have a much larger amplitude than the one of the individual particles. The practical solution is to use as high as possible a harmonic number since the bunch signal spectrum decreases much more rapidly than the one of the Schottky signal. In addition narrow band filtering is necessary to avoid intermodulation in the following amplifier. A tuned cavity for the longitudinal Schottky signal and a movable tuned electrostatic monitor for the transverse Schottky signal have also been used successfully.

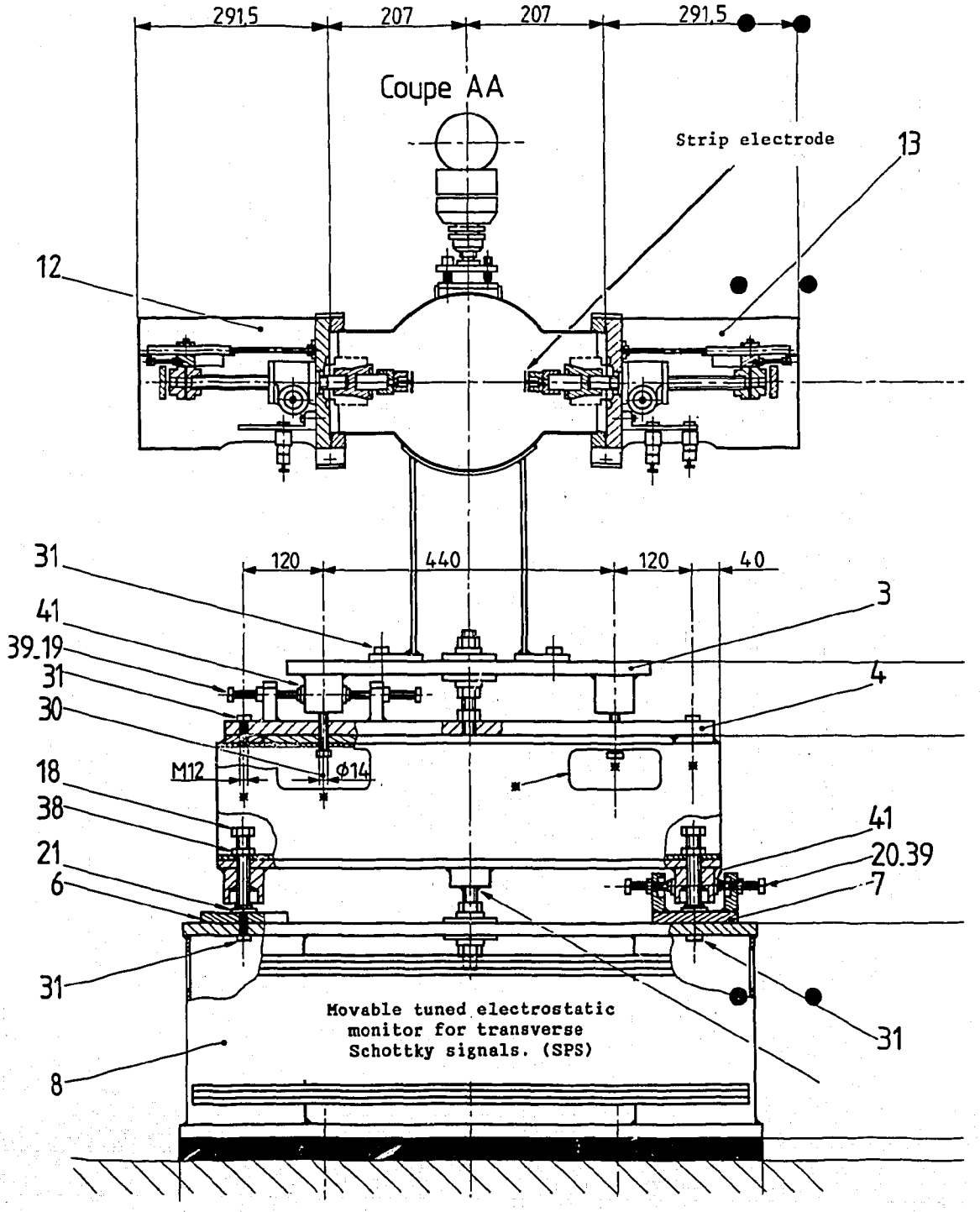

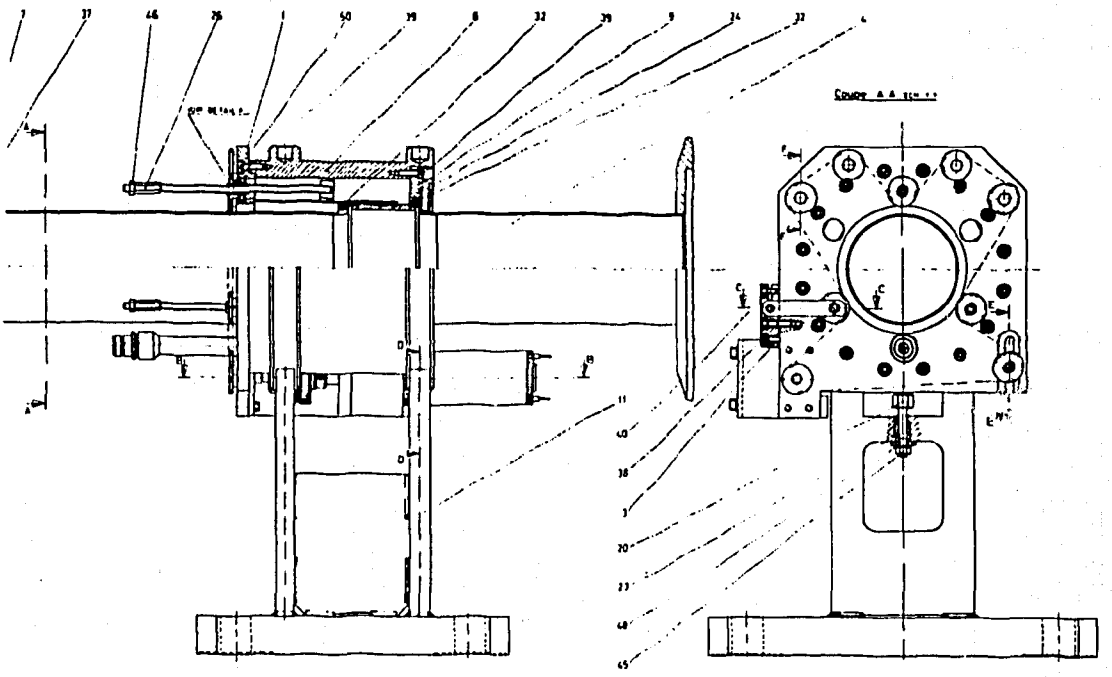

Tuned cavity for longitudinal Schottky signals of bunched beams. (SPS)

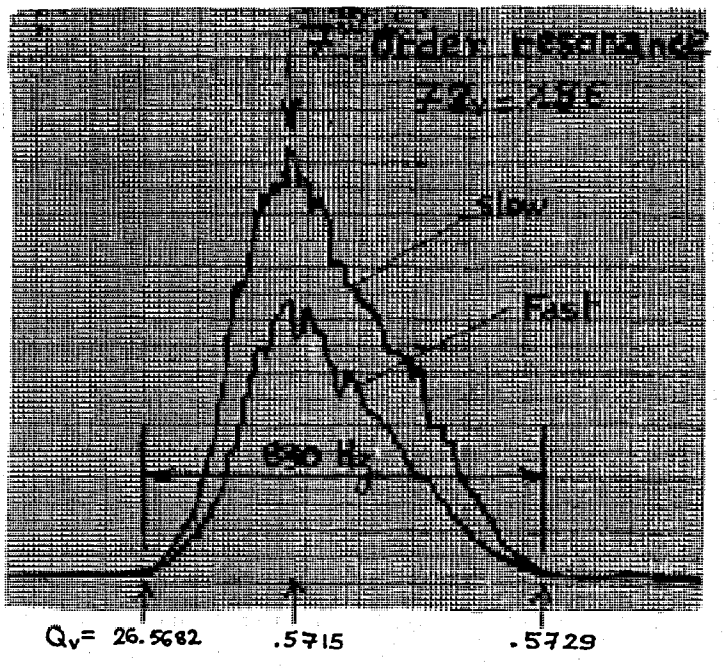

Fast and slow vertical Schottky signals, superimposed. (SPS)

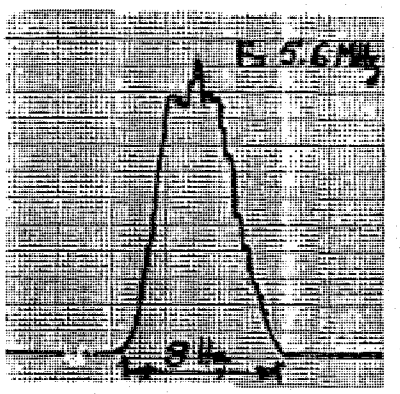

Longitudinal Schottky line.

4.7 Historical note

The BTF for monitoring the beam characteristics under real operating conditions was first implemented at the CERN ISR. Its history is interesting in many ways. It is another example of how theoretical concepts can be combined with instrumentation and experimental knowledge to provide a powerful tool that neither the theoreticians nor the experimenters can forsee. It also shows how the combined contributions of a very large number of people are needed. The progress steps from Landau damping, through the Schottky spectra measurement, to the stability diagram. The names of most of the contributors are given in Fig. 23. This BTF non-perturbing diagnostic instrumentation has made it possible to improve ISR operating conditions tremendously and to give a boost in its performance.

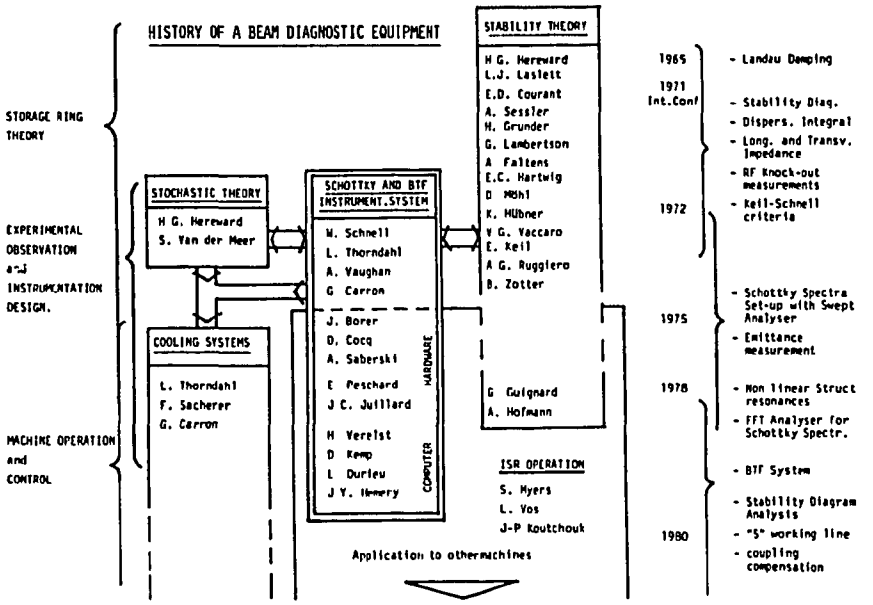

Fig. 23

5 CURRENT TRANSFORMERS

These instruments use the magnetic field induced by the beam to evaluate the instantaneous beam current $\hat{I}$. Therefore, it is possible to deduce the charge Q or the number of particles N in a beam pulse:

$$Q = \int \hat{I} dt = \hat{I}\tau \quad \text{if } \hat{I} = \text{constant along the pulse and } \tau = \text{pulse length}$$
$$N = Q/q \qquad q = \text{charge of particle}$$

For a circular machine of length l or average radius R, τ is taken equal to the revolution period:

$$\tau = T_{rev} = \frac{l}{\beta c} = \frac{2\pi R}{\beta c}$$

Two categories of current transformers will be considered.

5.1 Pulsed current transformers

This type of monitor is essentially used in the transfer channels connecting various accelerators. The bunches to be monitored have widths varying from 10ns to approximately 100ns, which results in most of the energy being concentrated below 100 MHz.

The simplest monitor is outlined below:

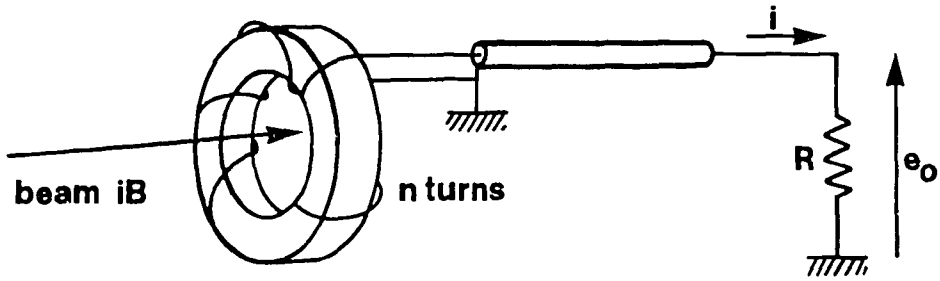

The beam passes through a toroid of magnetic material of relative permeability μ_r. Around the toroid is a winding consisting of n regularly spaced turns. This winding is connected through a coaxial cable to a load resistor R across which a voltage e_o is observed. Using Ampère's and Faraday's laws, and assuming that the load resistor R is equal to the characteristic impedance R_c of the cable, the transfer function of the monitor is shown to be:

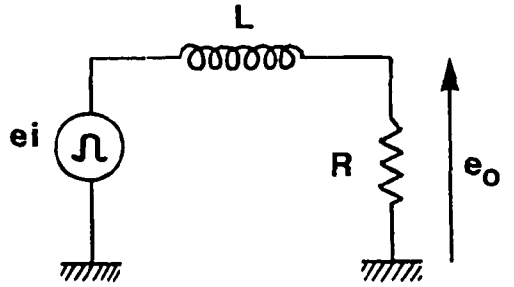

$$\frac{e_o}{iB} = -\frac{R}{n}\,\frac{1}{1+\frac{R}{L}\frac{1}{p}}$$

At frequencies where $2\pi fL >> R_c$, this expression is approximated by:

$$\frac{e_o}{i_B} = -\frac{R}{n} \text{ or } i = -\frac{i_B}{n}$$

The low pass limit is characterised by a droop time constant:

$$\tau_p = \frac{L}{R}$$

In order to increase τ_p, i.e. to decrease the low-pass limit, L has to be increased. As $L = \mu n^2 \frac{s}{l}$, s being the cross section and l the average circumference of the toroid, this means that μ and n have to be taken as large as possible. But increasing n decreases the sensitivity of the monitor as 1/n, which means that a compromise has to be found between the sensitivity and the low-pass cut-off. To maximise μ, high permeability metallic alloys are preferred to ferrite cores. The curves and table below (Ref.117) give a comparison of various materials.

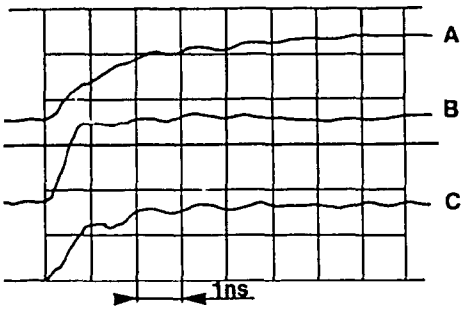

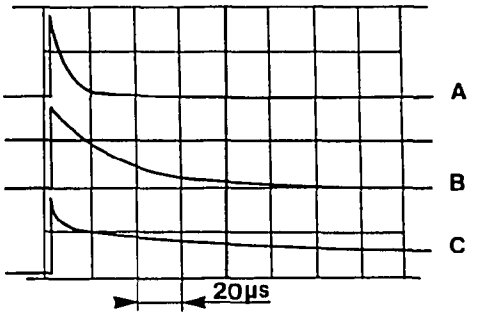

Core	A	B	C
Material	Ferrite	Ultraperm 10*	Ultraperm 10*
lamination		10 µm	50 µm
µr	2,800	24,000	80,000

* Trademark of Vacuumschmelze

The high frequency cut-off is mainly determined by the magnetic material and to a lesser extent by the stray capacitance of the windings if n is kept small.

To keep the Foucault currents small, thin laminations of magnetic material are chosen. The thickness is again a compromise, in this case between µr, the reliability of the insulation, the filling factor and the losses through Foucault currents.

The simple model which has been used until now has to be improved to be usable in an accelerator environment. In most cases, the beam circulates in a vacuum pipe and hence the image currents flowing in that pipe have to be channelled around the toroid in order not to cancel the beam induced field. This is done by breaking the vacuum chamber by a ceramic gap and by providing a by-pass of minimum impedance around the core. In order to decrease the noise induced in the windings, electrostatic and magnetic shieldings are provided. For the same reason, the winding is divided into two identical windings wound symmetrically as shown below around the toroid in order to translate in a common mode signal any signal which does not originate from the beam's magnetic field. If a coaxial cable is used, a transition from the symmetric transformer winding to the asymmetric cable has to be incorporated also (Ref. 118).

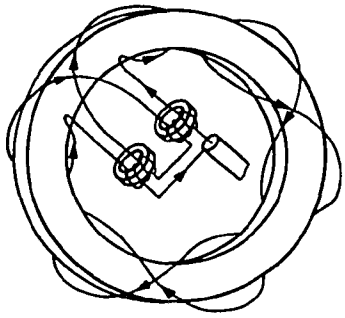

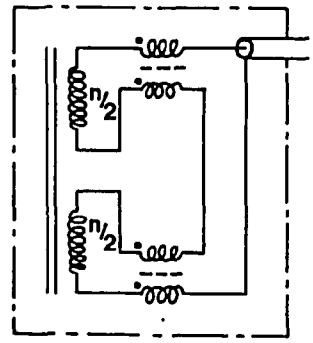

In order to derive the charge contained in the pulse, the current has to be integrated over the pulse duration. The dynamic range of the integrator will limit the range of the instrument. Below is an example of such a transformer which has been implemented in the transfer channels between AA and PS and between PS and ISR.

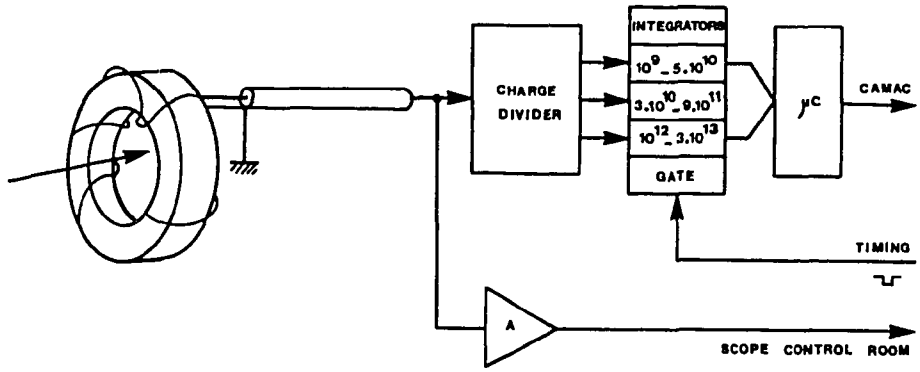

The charge divider matches the coaxial cable and divides the signal between three channels of a commercial gated charge-to-digital converter. A microcomputer reads out the converters, decides which measurement is the most relevant, translates the measurement in number of particles and transmits this information to the control system.

The performance of this monitor is as follows:

Range 10^9 to 3×10^{13} "without" range switching
Resolution 4×10^7
Noise 4×10^8 (measured in situ)
Accuracy ±1% of reading.

Whereas a relative calibration of these monitors along the same beam line is quite feasible, a relative calibration between instruments monitoring beams of different harmonic content or an absolute calibration is more difficult if precisions better than 1% are to be achieved.

For the transformers monitoring the beams transported between circular machines, a good solution is to check the calibration of these monitors with respect to the DC circulating monitors of the two machines.

5.2 DC current transformers

To lower the low-frequency cut-off of the previous transformer without decreasing it's sensitivity, the load resistor is incorporated in the feedback loop of an operational amplifier, leading to the so-called "Hereward transformer":

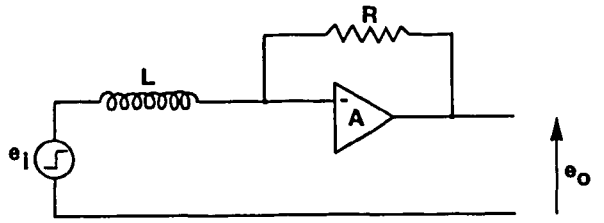

If A>>1, the transfer function of the circuit is now:

$$\frac{e_o}{i_B} = \frac{R}{n} \frac{1}{1+\frac{R}{AL}\frac{1}{p}}$$

which is approximated as before at mid-frequencies by:

$$\frac{e_o}{i_B} = \frac{R}{n}$$

The droop time constant is now $\tau_H = \frac{AL}{R} = A\tau_p$.

In reality the transformer winding has a resistance r which becomes not negligeable with respect to R/A. To avoid feeding the signal mostly into this resistance, the monitor is modified as shown below.

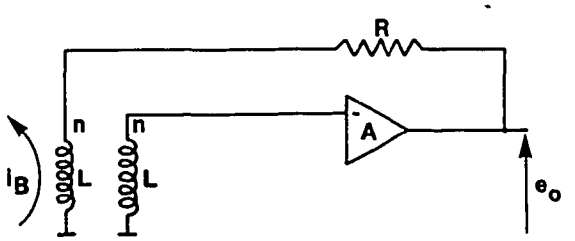

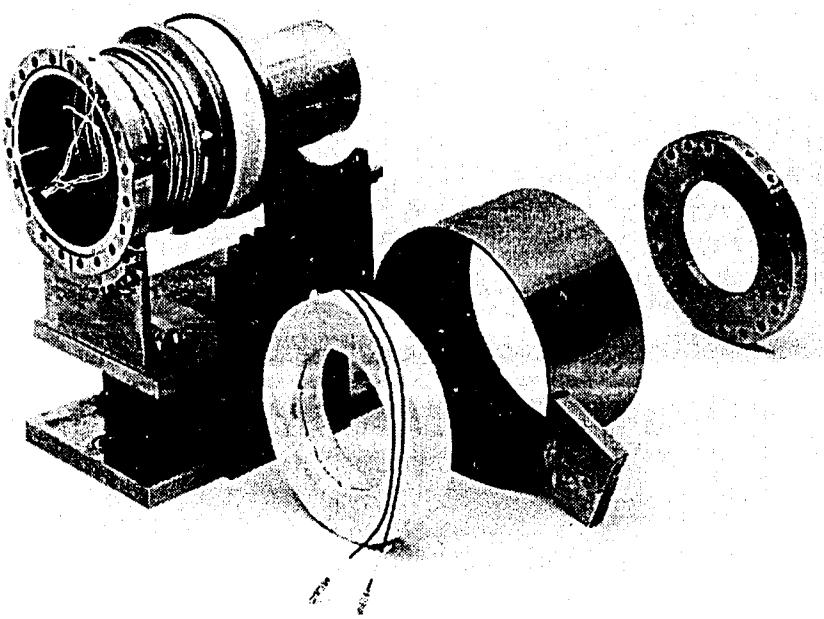

Pulsed current transformer for beam transfer line (Ref. : 118).

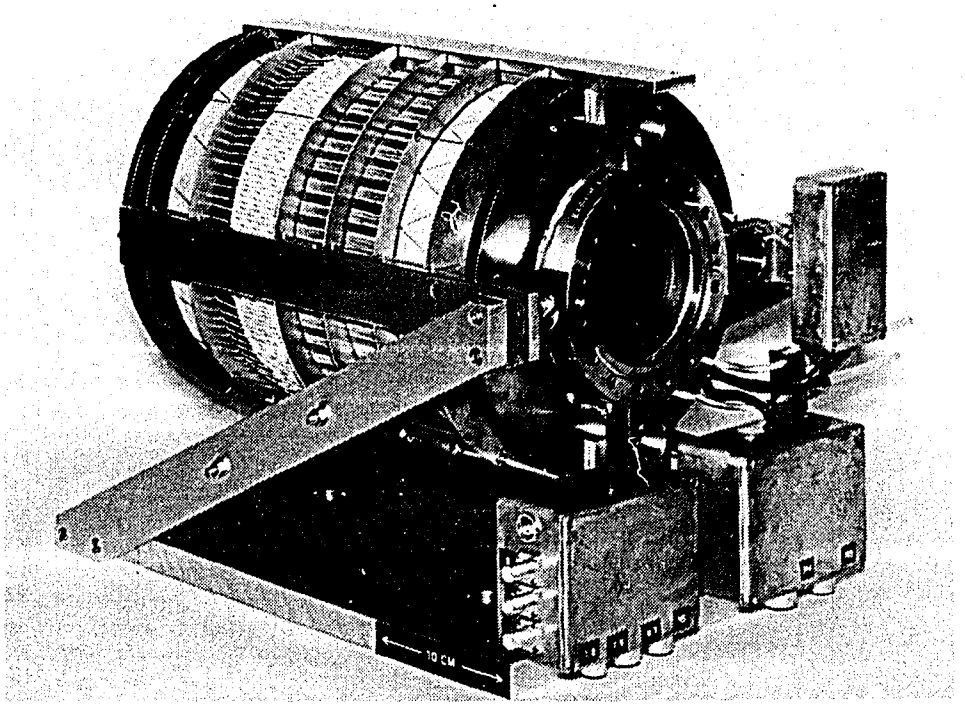

DC Current transformer for AA (Ref. : 119).

The feedback loop is now closed via the two tightly coupled identical secondary windings. It is easy to show that the transfer function is the same as the one obtained before.

Time constants of seconds and greater can be obtained with this method, however, the monitor cannot be considered as a DC one, nor is it DC stable.

In order to go to DC, which was first needed for the ISR, a DC "off-setting" has been added to the "Hereward transformer" by a magnetic modulator-demodulator system.

The block diagram of the resulting "Unser transformer" is given below (Ref.117, 119).

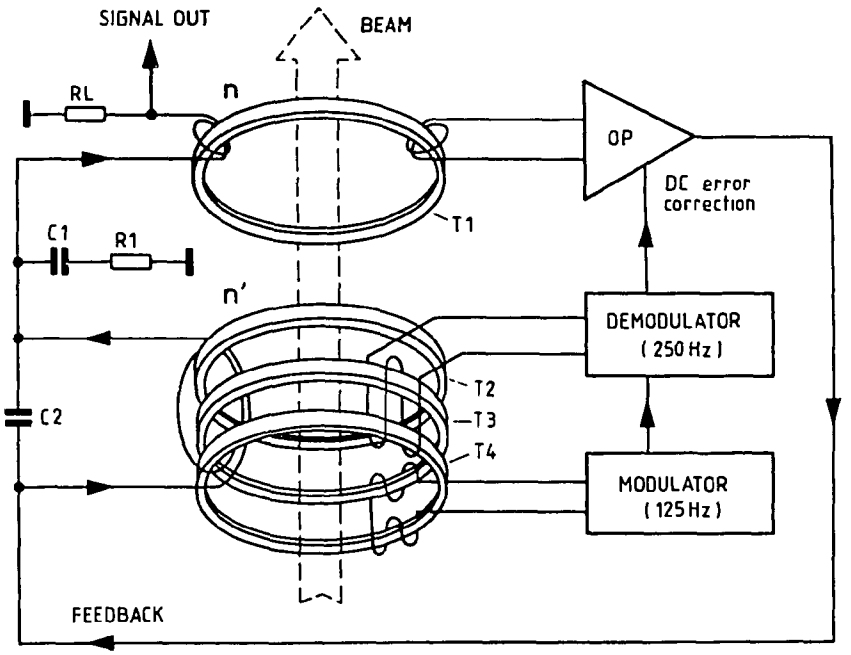

The modulator, working at frequency f (125 Hz here) drives, in opposite directions, two cores well into saturation. The demodulator senses in a common winding the flux difference. Any asymmetry will create even harmonics. The second harmonic is extracted by a synchronous detector working at 2f (250 Hz here) and produces a DC correction current in the main loop, which compensates the DC beam induced flux. The principle of this measurement is shown in the simple diagram below.

Core T2 acts as a leakage inductance to reduce the modulator induced noise in the feedback loop.

The DC correction current induces a voltage drop across the load Resistor RL which is used to read out the beam current and whose value is no longer critical. The integration period of the measuring instrument provides an additional noise rejection.

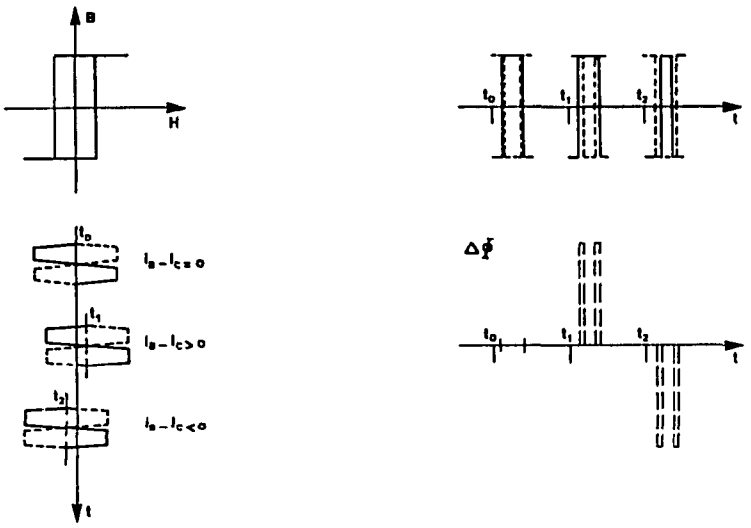

The monitor being based on an asymmetry detection, any differences in the modulator-demodulator circuit have to be avoided. Great care has to be taken in the winding of the cores and in the monitoring of the excitation signal. The greatest care has to be applied to the magnetic cores. As already mentioned before, laminations of high μ_r material are taken. Characteristics of laminations of various thickness and quality are indicated in the curves below (Ref. 118).

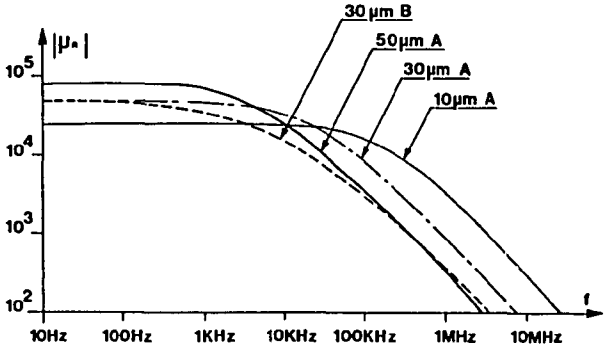

To obtain the ultimate performance of the monitor a core matching procedure is executed by measuring each core from the same manufacturing batch with a computer controlled test set-up, the results of which are shown below for one core.

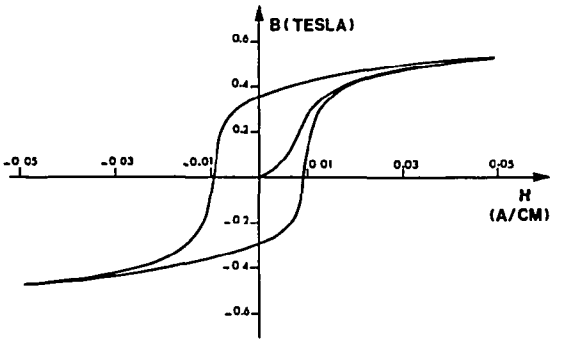

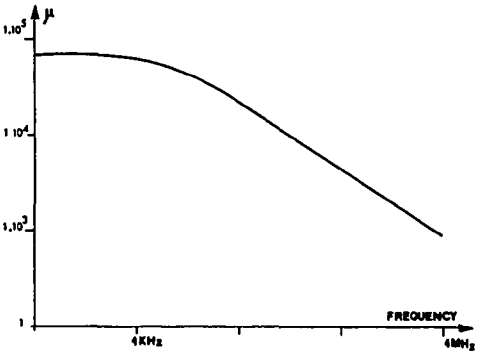

For the AA transformer, an extra feedback loop (T5-OP2) has been added to reduce further the modulator noise. In order to decouple the two loops the load resistor has been put in the return loop of OP3 (Ref. 119).

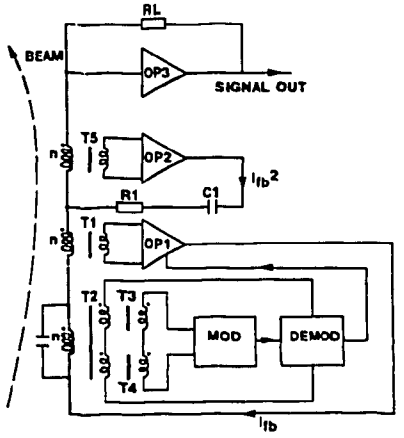

Performance	
Range	-500mA to +500 mA
Resolution	1μA with a 200 ms integration period
Zero drift	±3μA for 24h
Stability	±5ppm ±zero drift (full scale)
Linearity	±10 ppm
Frequency range	DC - 50kHz

6 SYNCHROTRON LIGHT MONITOR

This type of monitor is widely used in electron synchrotrons and storage rings. It is only recently that it was realised that it could be used under certain conditions with protons (Ref. 120, 121). This lead to the development of the proton profile monitor in the SPS (Ref. 122) which makes use of the rapid variation of the magnetic field at the edges of the bending magnets to enhance the emitted spectrum in the visible region. This enhancement was not enough for the lower intensity antiproton beams and an undulator magnet was installed.

6.1 Monitor using the fringe field of the main dipoles

A quantitative description of the synchrotron light emitted in a bending magnet can be found in Ref. 123 and 124. In the following section, a qualitative description of the phenomena is given.

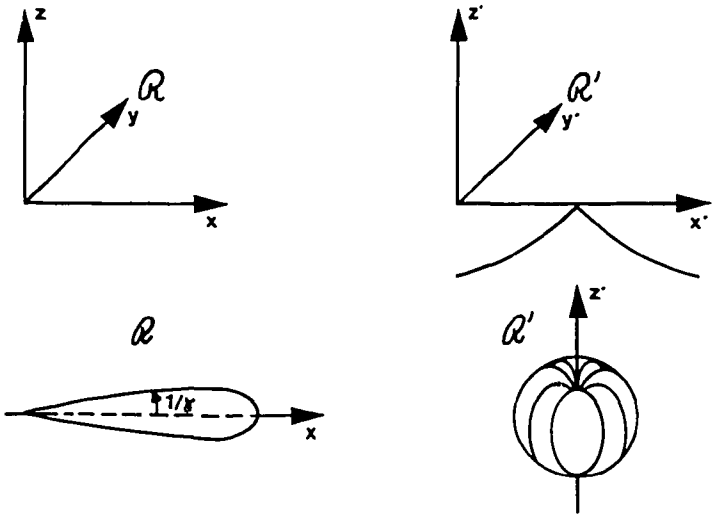

Let R be the laboratory reference frame and R' be a frame in translation with respect to R, moving with the particle and tangent to the particle's trajectory in a bending magnet. In R', the particle has a trajectory as sketched above and hence radiates a dipole-like pattern. Going back to the laboratory frame R, a strongly forward peaked radiation pattern is obtained. This pattern has a typical opening angle $1/\gamma$.

The radiation is strongly polarised in the bending plane. For an observer in R, this radiation pattern will result in a light pulse of duration $\tau \sim \rho / c\gamma^3$, resulting in a spectrum characterised by the critical wavelength λc

$$\lambda_c = \frac{2}{3} \frac{\rho}{\gamma^3}$$

which is at the 50% partition of the power spectrum.

The normalised power spectrum (ref. 125) is given below,

$P_o = \frac{2}{3} \frac{\iota_o c^3 e^2 B^2 E^2}{(m_o c)^3}$ being the total power radiated by one particle

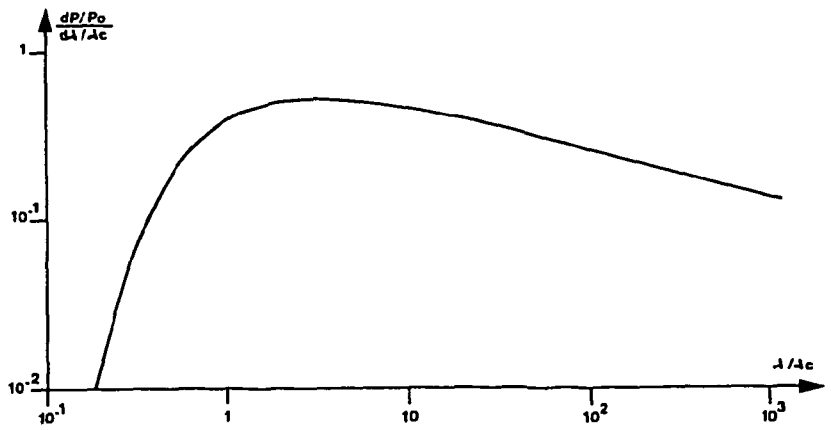

For the SPS at 270 GeV, $\lambda_c \sim 20{,}000$nm. This results in very little power emitted in the visible spectrum (400 to 700nm) for which the usual detectors are designed. To enhance the light emitted in the visible spectrum the edge effect at the bending magnets was first used. The rise and fall-times in the case of a magnetic field variation from 0 to Bo over a short distance L is τ_d, equivalent to a wavelength (Ref.122)

$$\lambda_d = c\,\tau_d \sim \frac{L}{2\gamma^2}$$

equal, in the considered case where L = 10cm, to λ_d = 600nm. The resulting power spectrum can be seen later on.

6.2 Monitor using a dedicated undulator

The properties of the radiation emitted in an undulator have first been studied for electrons (ref. 126). A full description can be found in ref. 127. The monitor built at the SPS (ref. 128, 129) uses a weak undulator having the following structure:

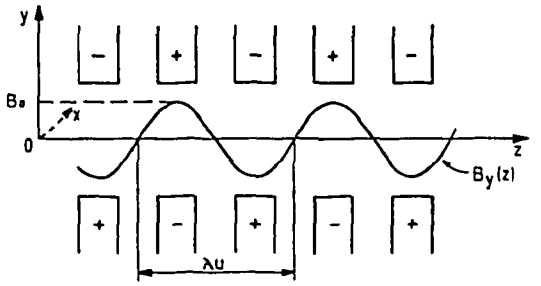

$$B_y(z) = B_o \sin \frac{2\pi z}{\lambda u}$$

$B_o = .32T$

five periods λ_u

The deflection angle ψ_o is much smaller than $1/\gamma$, i.e. $K = \psi_o \gamma << 1$. Considering again the frame R' defined previously, the particle executes a harmonic oscillation in R' with frequency $f' = c/\lambda'_u$, λ'_u being the Lorentz contraction of λ_u in R'. The dipole pattern obtained is again Lorentz transformed into R. The emitted wavelength is now:

$$\lambda \sim \frac{\lambda_u}{2\gamma^2} \left(1 + \frac{K^2}{2} + \gamma^2\theta^2\right) \sim \frac{\lambda_u}{2\gamma^2} \left(1 + \gamma^2\theta^2\right)$$

θ being the angle of observation wrt Oz.

The total power emitted is identical to the value given previously, but is concentrated around λ.

In the case of the SPS monitor, E = 270 GeV, λ_u = 88mm, and λ = 531nm which is in the visible part of the spectrum. The finite length of the undulator results in a broadening of the previous spectral line, given by (Ref. 127) $\Delta\lambda / \lambda \sim 1/n$, i.e. $\Delta\lambda \sim$ 100 nm. This finite length accounts also for the wiggles on the spectral response.

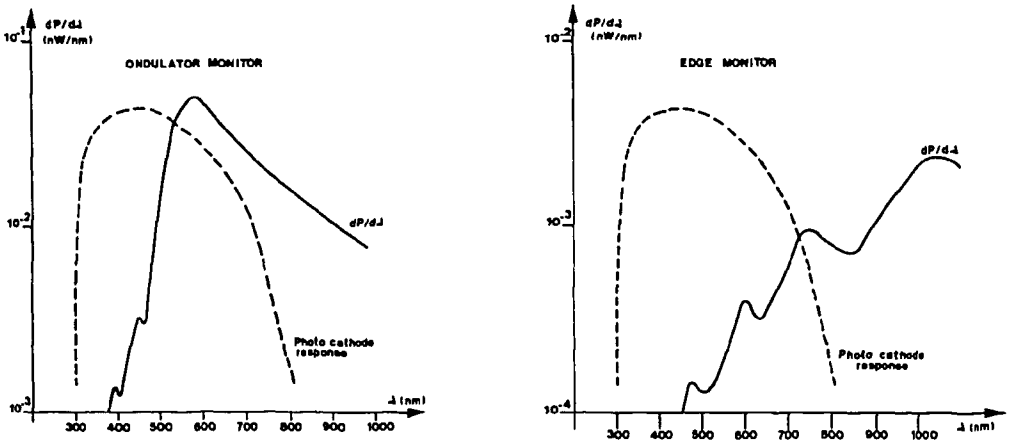

The monitor installed in the SPS is fully described in Ref. 128 and 129, and sketched below.

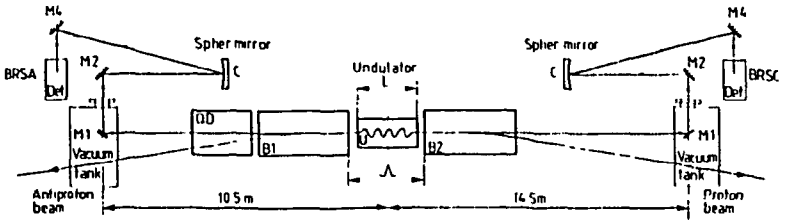

The beams are imaged on the detectors with a Herschel type telescope having a demagnification of 4.

The detector consists of a microchannel image intensifier, acting also as an electronic shutter for gating out individual bunches, followed by a SIT (Silicon Intensified Target) Vidicon for the proton beam and an ISIT (Intensified SIT) Vidicon for the antiproton beam. Given below are the profiles of the three proton and antiproton bunches together with the estimated luminosity curve. The evolution of this curve is the same as the one obtained from the scintillator telescope.

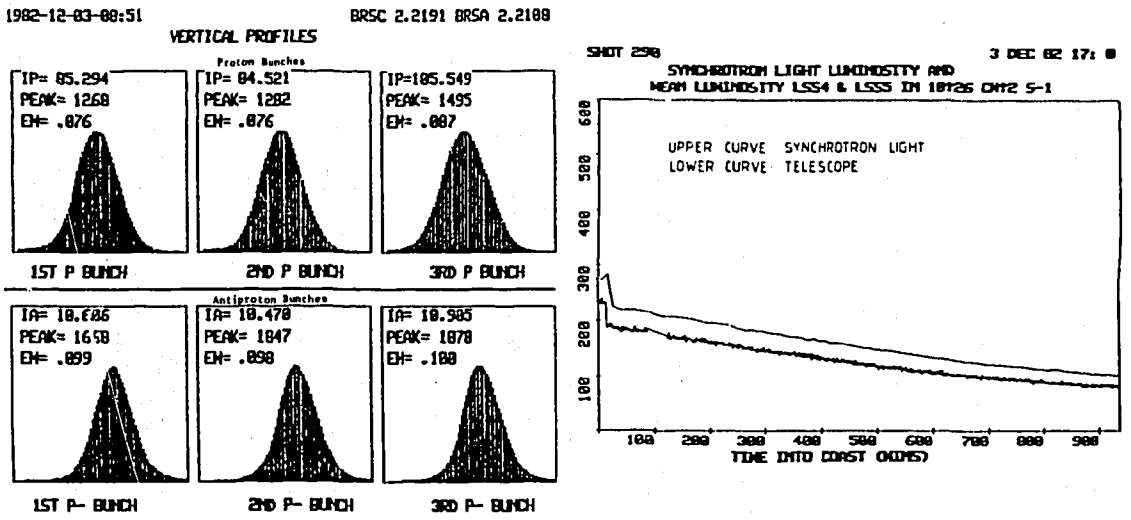

7 SODIUM CURTAIN MONITOR

Before closing the subject on non-intercepting profile monitors, the sodium curtain monitor installed in the ISR has to be mentioned. This monitor is used to measure the horizontal and essentially vertical profiles of the stored beams from approximately 100mA to 40A. As this monitor has not been upgraded to cope with the very low intensity antiproton beams, it is not described here due to lack of space. Its description can be found in Ref. 130 and 131. Since then, a digital signal processing has been added to the monitor to compute the beam height across the stacked beam.

8 BEAM INTERCEPTING MONITORS

Two general problems are associated with this type of monitor. The first problem is the beam energy loss dE/dx of which the exact formula can be found in ref. 132 and from which the curve below has been taken.

The consequences which have to be considered are the energy change of the beam, which is, of course, most important at low energy, and the heating up of the monitor.

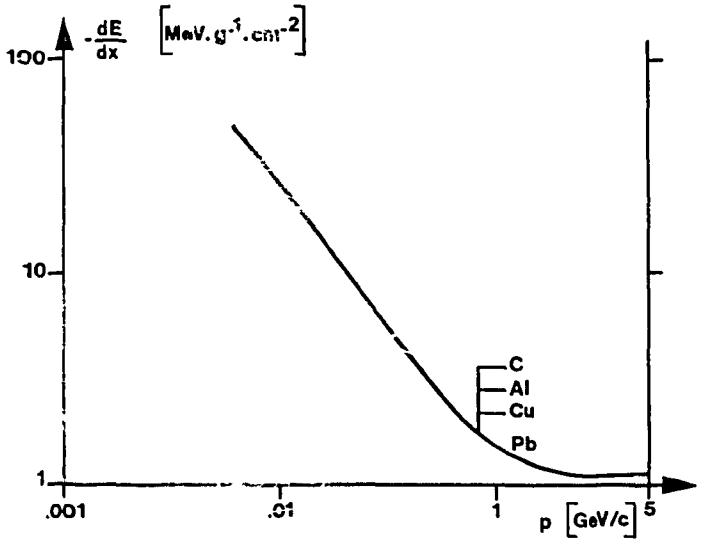

The second problem is the beam blow-up through multiple scattering. Using a gaussian approximation, the projected angular distribution of the scattered beam can be characterised by (ref.132)

$$\theta^{\text{rms}}_{\text{plane}} = \frac{14.1}{p_{\text{MeV/c}}\,\beta}\sqrt{\frac{L}{L_{\text{rad}}}}\;\left(1 + \frac{1}{9}\log\frac{L}{L_{\text{rad}}}\right)\ \text{rad}$$

L being the thickness of the scatterer and L_{rad} its radiation length. Given below are the data for the most commonly used materials. More data will be found in ref. 132 and 133.

Material	L_{rad}(cm)	Material	L_{rad}(cm)
Be	35	Fe	1.76
C	19	Pb	.56
Al	8.9	Ta	.41
Ti	3.6	W	.35

The effects are in general acceptable for a single passage of the beam in a monitor as in the transfer channels or in the single turn operation of the circular machines. They are in most cases unacceptable for circulating beams.

8.1 Secondary emmission profile monitors (SEM Grids)

When a beam passes through a material, low energy electrons, amounting to a few per cent of the traversing beam, are emitted from the superficial layers. The production efficiency decreases from low energy (ref.134) to high energy as summarised below:

Beam Energy E	5 MeV	200 MeV	GeV's
SEM efficiency	~20%	~7%	~5%

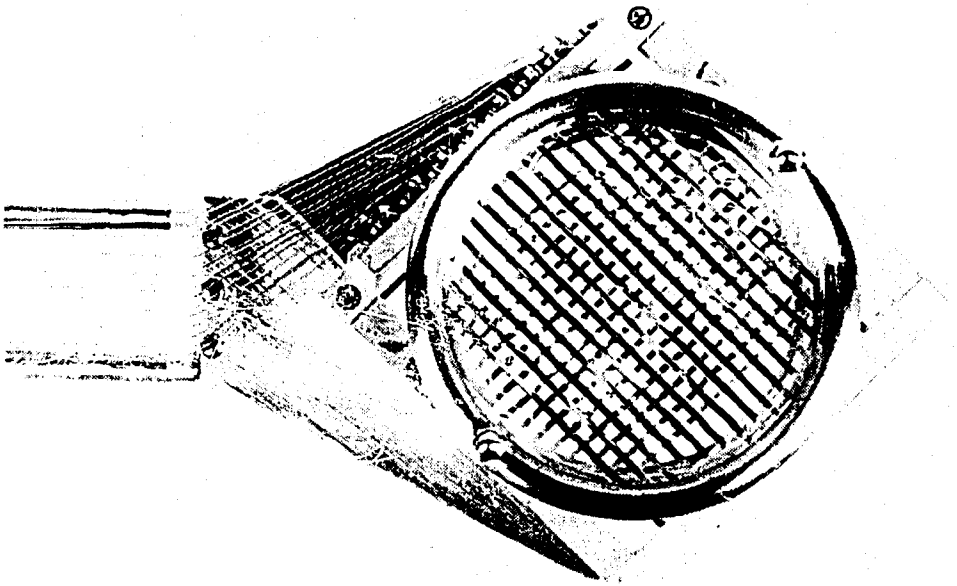

Beam transfer channel SEM profil monitor (Ref. : 135).

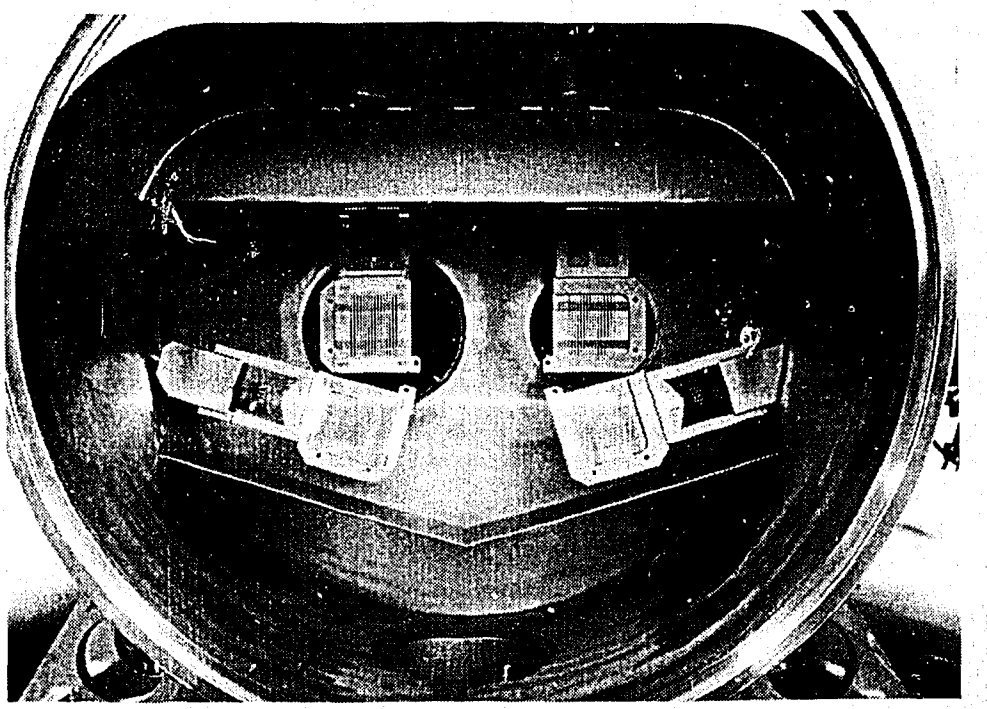

Ring and injection line SEM profile monitors for LEAR (Ref. : 136).

Some problems encountered with this type of monitor are listed below :

- energy loss in the case of low energy beams (Linac, LEAR)
- beam blow-up
- collection of unwanted charges
- small signals (pC) with a high source impedance (G Ω)
- finite resolution

The first two points are taken care off by using low density materials, in general aluminium or titanium. To counter the collection of unwanted charges, the monitor has to be used in "clean" conditions and/or surrounded by clearing electrodes with voltages ranging from ~ 100 to 400 V. To cope with the fourth problem, high insulation material (Ref. 135) and high quality local electronics (Ref. 136) have to be used. Finally, to overcome the finite resolution of the monitor, it is possible to tilt the SEM head with respect to the beam to decrease the apparent step size. The practical limit is around 30° (Ref. 134).

A good example of this type of monitor is the one developed for LEAR (Ref. 136). It consists of a titanium foil of 8μm ($0.2.10^{-3}$ Lrad) in which 15 strips of 1.5 mm or 3.5 mm, separated by .5 mm, have been etched. At both ends of the structure are two large strips to detect possible tails. The local electronics given below have an input noise equivalent to .3pC and feed a 12 bit digitizer. A measured beam profile is also represented.

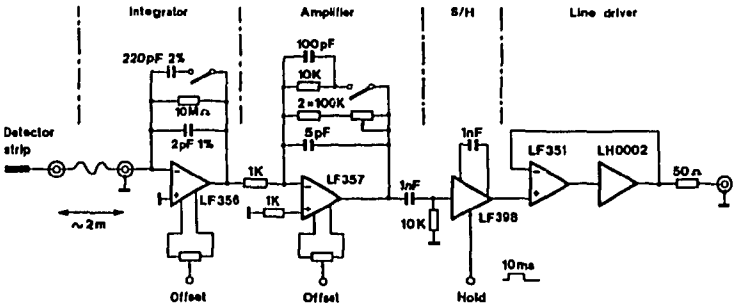


```
SEMGRID-FAST  14-DEC-82 17:00:59
ZONE:E4  LOC:11        HORIZONTAL
+**********+**********+**********+**********+
+                                 + TSAMPLING=
21-+++                            +       8μs
 +++++++++++++++                  +
14-++++++++++++++++++++++++       +HWGAIN=8 100
 +++++++++++++++++++++++++++      +SWGAIN=4 80
 7-++++++++++++++++++++++++       +
 +++++++++++++++++++++            +
 0-++++++++                       0-PARTIAL=
  -++                             -  100.0 %
  7                               +
  -                               -  MEAN=
 14                               +   9.5 mm
  -                               -  SIGMA=
 21                               +   5.8 mm
  -                               -
 OR                               0-RESIDUAL=
 +----------+----------+----------+    0.0 %
STATUS: O.K.                      0-TOTAL=100%
```

These monitors are used to measure beam profiles and eventually position and charge. From the profile measurements in three locations, it is possible to deduce the beam emittance. The most common strategy is to place the central monitor at a beam waist and the adjacent monitors 120° apart (Refs. 137, 138) in the normalized phase-space (Ref. 139). The matching is

another parameter which can be deduced from a string of SEM monitors in the following way. Let's consider the normalized phase space (η, η') where the beam is represented by a circle. If a focussing error, ie a mismatch, occurs, the beam circle is transformed into an ellipse which will tumble down the beam line resulting in a modulation of the beam envelope. The detection and measurement of this superimposed modulation will determine the mismatch of the beam line.

8.2 Fast Wire Scanner

This monitor (Ref. 140) was introduced in the SPS to overcome the problems mentioned earlier for SEM grids with a circulating beam when an independent measurement of counterstreaming proton and antiproton beam profiles was sought.

The monitor consists of a thin 23 μm carbon wire passing at 4 m/s through the beam. The wire is held in a fork rotating through 120° and driven by a DC motor which is included with its position transducer in a servo loop fed by a function generator. Care has to be taken to achieve a constant travelling speed through the beam and a smooth acceleration and deceleration.

The emittance blow-up per scan is given by (Ref. 140):

$$\frac{dE}{dn} = \frac{1.12\ 10^{-4}}{p^2}\ \beta_y \frac{d^2}{v}\ \frac{f_{rev}}{L_{rad}}\ \pi \text{ m.rad/scan}$$

For the SPS monitor: p = 270 GeV/c, β_y = 50 m, f_{rev} = 44 kHz, hence dE/dn = 2.3 10^{-6} π mm mrad, which is negligible.

The distinction between p and p^- bunches could have been obtained when using the monitor in the SEM mode by a fast gating circuit. Instead the particles produced by the interaction of the beam with the wire are

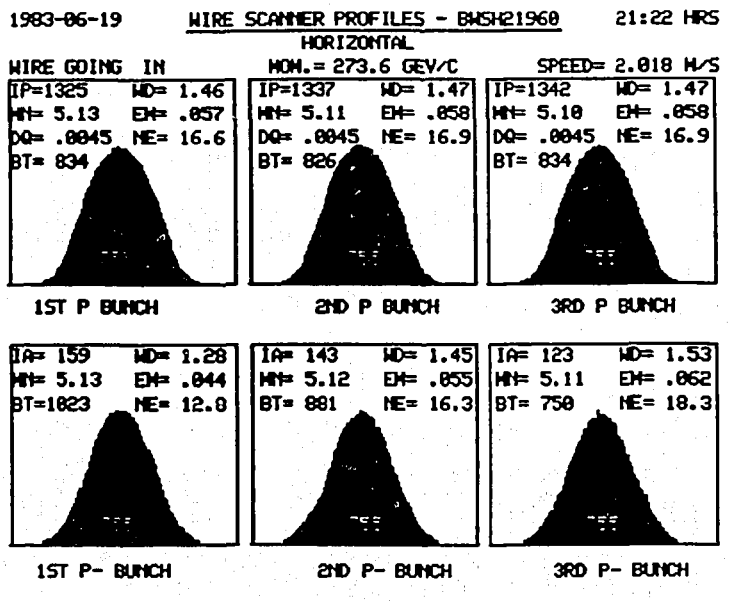

observed with scintillators placed above and below the beam pipe and coupled to 6-stage photomultipliers.

The distinction between p and p^- bunches is obtained in this set-up by the strongly forward peaked particle distribution. It is better than 10^4. The photomultiplier signal is processed by a low-pass filter before being fed to a Sample-and-Hold, which gates out the individual bunches, and a fast Analog-to-Digital Converter. Given above are typical profiles measured with this monitor. An important use of this monitor is the cross-check of the profiles obtained with the synchrotron light monitor.

8.3 Scrapers

Scrapers are scatterers which can be used in conjunction with an absorber (located at $(2k+1)\,\pi/2$ from the scraper) and an intensity monitor to define the beam envelope (Ref.143). Next to this destructive profile monitoring, they are also used to calibrate precisely beam orbit bumps (Ref. 141). Their main use is often halo clean-ups.

8.4 Luminescent screens

Luminescent screens are installed in all machines. They are mainly used during running-in and when machine problems occur shedding some doubt on the more sophisticated monitors. A typical monitor (Ref. 142) is depicted below.

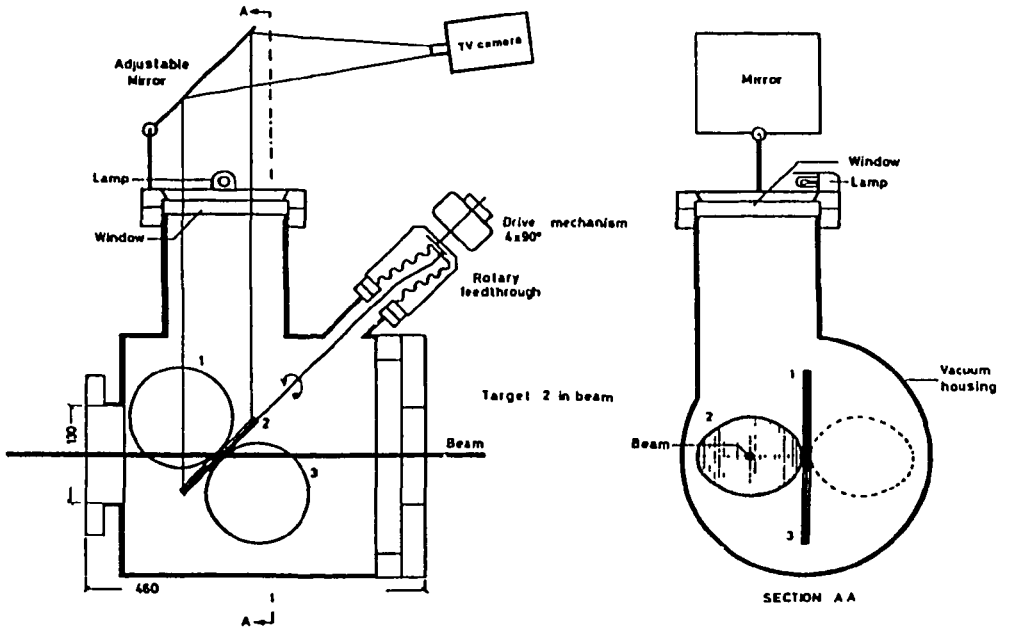

The monitor consists of one or more scintillating screens which are moved in and out of the beam. The screens, inclined at 45° wrt beam, are observed through a window with a TV camera. In order to locate the beam, a reference grid is deposited on the screen and the screen is illuminated by an external lamp. Cerium activated lithium glass scintillating in the blue and chromium activated alumina scintillating in the red part of the

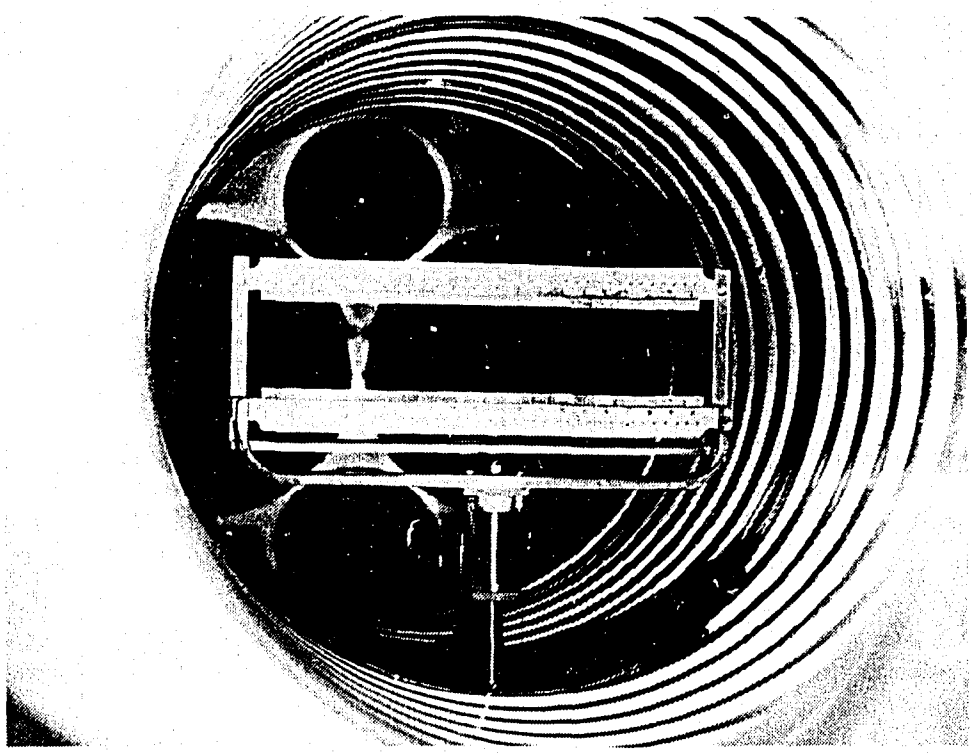

Intersection scraper for ISR (Ref. : 141).

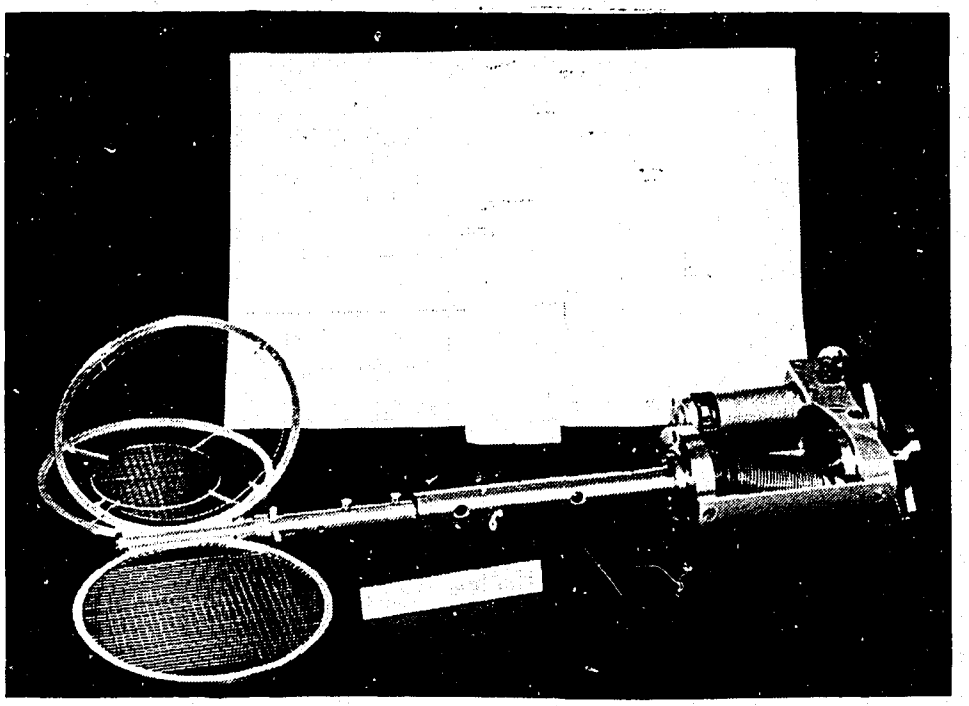

Luminescent screen mechanism (Ref. : 142).

spectrum are widely used for the screens located in high vacuum. The sensitivity of the first material is around 2.10^{10} p/cm^2 (Ref. 142) for a 1 mm plate when using a normal vidicon. The second material emits ten times more light. If more sensitivity is needed, SIT or ISIT cameras are used. The main problems with these monitors are the beam scattering (Lrad ~13 cm) and the radiation resistance of the scintillator and the TV cameras. At the end of the extracted beam channels where very high sensitivities are needed, CsI scintillators having a sensitivity of 10^4 p/cm^2 are used (Ref. 143). In single shot experiments such as p^- transfers, the TV cameras are connected to video recorders.

9 MISCELLANEOUS MONITORS

In this chapter, an additional two monitoring devices used with the pp^- operations are mentioned. Several monitors, like ionisation chambers (Ref. 144) for beam loss localisation, multiwire proportional chambers for extracted beam profile acquisition (Ref. 143), etc. will not be decribed due to lack of space.

9.1 Luminosity and Background Monitors

These monitors have been installed around the collision points of the ISR and the SPS. In the case of the ISR (Ref. 145), eight scintillator-photomultiplier assemblies are placed around the eight intersections as sketched below.

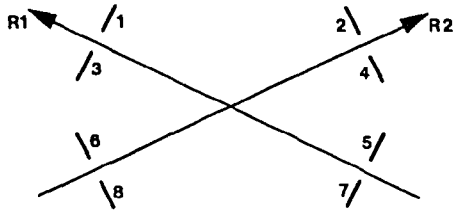

The various quantities of interest are defined as follows:

Beam-beam = (1.2) + (3.4) - Accidentals

Ring 1 upstream background = 5+7

Ring 1 downstream background = 1+3

and the same for R2.

In the SPS (Ref. 146) two monitors have been installed around LSS4 and LSS5. They consist of two planes of 10 or 12 scintillators placed at 6.25 or 10.3 m around the intersection points. As previously beam-beam and beam-gas interaction rates are obtained, the number of requested multiplicities varying from 1 to 4.

These monitors give an absolute luminosity if a monitor calibration is available, like the Van der Meer method (Ref. 147) in the ISR. If not, they give a relative beam-beam rate. The other essential parameter given by these monitors is the background in each collision point, which permits its control to optimise the data taking conditions.

Important factors of the background are not only the average level but also the "spikes" and "structure" superimposed on it.

The signals are processed digitally for computing the luminosity or the average background and the analogue way to present on chart recorders and bargraph displays the transient behaviour.

9.2 Transient Recorders

Transient recorders sample an analogue input signal, digitize it and store the data continuously in a fixed length digital memory. This process is interrupted on receipt of an external or internal trigger signal. The frozen data will be comprised of data acquired before and/or after the trigger, depending on the choices made and the size of the memory. The sampling period may be chosen between 10 ns and 10s. The memory size is normally a few thousand data points of 8 to 10 bits. The data can be read out digitally to a computer or as a slow analogue signal to an X-Y monitor or plotter. The block diagram of such an instrument is given below.

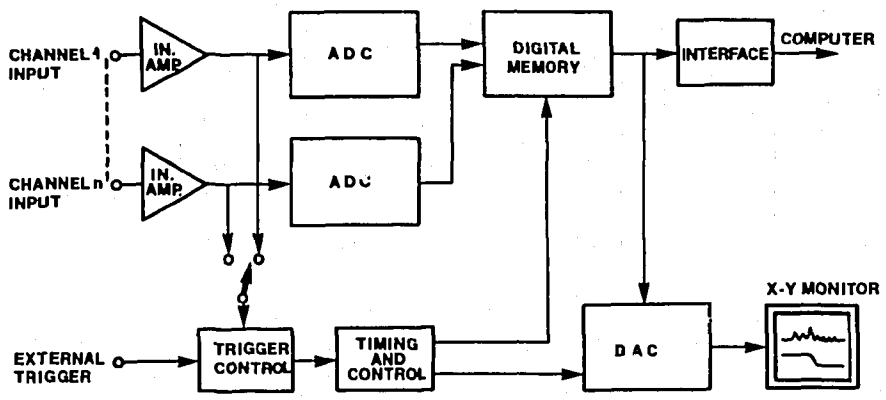

These instruments are used in all machines (Ref. 148) to catch transient phenomena on the stored beam or single shot data during antiproton transfers for post-mortem analysis.

Given below is an output showing the sum signal of the ISR injection kicker pulse and of an injected p^- "pilot" pulse of 1.6 10^9 p^-, as picked up by a scintillator.

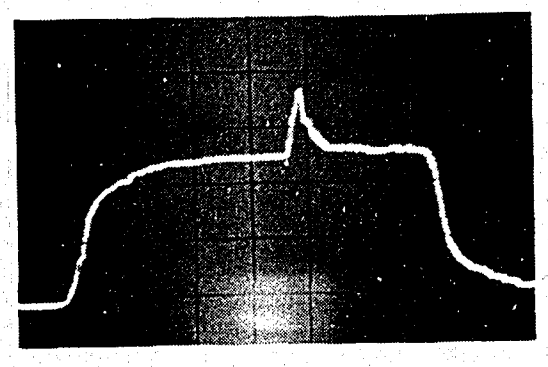

Recorder settings: sampling period 10ns
amplitude 5V FS

Display : 350ns/div

References

NON INTERACTING MONITORS AND ORBIT MEASUREMENTS

1. G. Schneider, Antiproton Beam Transfer Instrumentation, CERN-PS-BT/83.4

2. J. Borer et al., Beam Orbit Measurement for Correction in LEP, LEP Note 437, 4.2.1983.

3. J. Borer and C. Bovet, Calculated Response of Four P.U. Buttons in an Elliptical Vacuum Chamber, LEP Note 461, 28.7.83.

4. L. Burnod, "Single Bunch" Position Measurement in the SPS, SPS-ABM/83-190/0094G, 26.5.1983.

5. J. Bosser, L. Burnod and G. Ferioli, Beam Position Measurements by Use of 90° Hybrids (Proposal for LEP), SPS/ABM/83.01/0058G, 10.1.1983.

6. Edward F. Higgins, Beam Signal Processing for the Fermilab Longitudinal and Transverse Beam Damping Systems, FNAL.

7. R. Bossart, J.P. Papis and V. Rossi, Synchronous Receiver for Closed Orbit Measurement of Single Bunches, SPS/ABM/83-103/0086G, 28.3.1983.

8. J. Durand, Transmission et simulation des signaux de Pick-Ups électrostatiques large bande au PS, PS/PSR/Note 83-7, 24.6.1983.

9. T. Teiri, H. Ishii, Y. Mitzumachi, A. Ogata, J.L. Pellegrin and M. Tejima, Beam Diagnostics of the Tristan Accumulation Ring, IEEE Transactions on Nuclear Science, Vol. NS-30, No. 4, August 1983.

10. G.R. Lambertson, K.J. Kim and F.V. Voelker, The Slotted Coax as a Beam Electrode, IEEE Transactions on Nuclear Science, Vol. NS-30, August 1983.

11. F. Voelker, T. Henderson and J. Johnson, An Array of 1 to 2 GHz Electrodes for Stochastic Cooling, IEEE Transactions on Nuclear Science, Vol. NS-30, No. 4, August 1983.

12. J.D. Simpson, S.L. Kramer, D. Suddeth and R. Konecny, Slot Coupled Beam Signal Pickup Development at Argonne National Laboratory, IEEE Transactions on Nuclear Science, Vol. NS-30, No. 4, August 1983.

13. J. Simpson, R. Konecny, S.L. Kramer and D. Suddeth, Test Facility for Relativistic Beam Pickups, IEEE Transactions on Nuclear Science, Vol. NS-30, No. 4, August 1983.

14. D. Rice, G. Aharonian, K. Adams, M. Billing, G. Decker, C. Dunnam, M. Giannella, G. Jackson, R. Littauer, B. McDaniel, D. Morse, S. Peck, L. Sakazaki, J. Seeman, R. Siemann and R. Talman, Beam Diagnostic Instrumentation at CESR, IEEE Transactions on Nuclear Science, Vol. NS-30, No. 4, August 1983.

15. Y. Yin, Beam Diagnostics for Hesyrl, the 800 MeG Synchrotron Radiation Facility in Hefei, IEEE Transactions on Nuclear Science, Vol. NS-30, No. 4, August 1983.

16. J.C. Denard, G. Oxoby, J.L. Pellegrin and S. Williams, Monitoring of the Stanford Linac Microbunches Position, IEEE Transactions on Nuclear Science, Vol. NS-30, No. 4, August 1983.

17. L. Bernard, C. Dutriat, J. Gabardo, M. Le Gras, U. Taligren, P. Têtu and D.J. Williams, Wide Dynamic Range (7 Decades) Beam Position and Profile Measurement for the CERN LEAR, CERN/PS/LEAR/83-15, March 1983.

18. G. Cyvogt, B. Frammery, A. Krusche, R. Maccaferri, M. Ruette, G.C. Schneider and E. Schulte, Single Pass Antiproton Beam Diagnostics of the CERN PS Accelerator Complex, IEEE Transactions on Nuclear Science, Vol. NS-30, No. 4, August 1983.

19. J.D. Gilpatric, B.A. Sherwood, J. Hahn and D.D. Chamberlin, Wide-Bandwidth Test Fixture for Electromagnetic Beam Sensors, IEEE Transactions on Nuclear Science, Vol. NS-30, No. 4, August 1983.

20. Q.A. Kerns, G.H. Biallas, F. Turkot, R.C. Webber and A. Wehman, An RF Device for Precision Location of the Beam Position Detectors in the Energy Saver, IEEE Transactions on Nuclear Science, Vol. NS-30, No. 4, August 1983.

21. J. Borer, D. Cocq, H. Kropf, C. Paillard and P. Tranchant, Système de Mesure de Trajectoires en TT6-TT1 et d'Orbites en R2 pour les Antiprotons aux ISR, CERN/ISR-RF/82-08, avril 1982.

22. V. Agoritsas, G. Gelato, M. Van Rooij, E. Schulte and P. Têtu, Inventaire de l'instrumentation "Faisceaux" au PS, PS/DL/Note 82-2.

23. E. Schulte, Détecteurs, PS, 12.11.1982.

24. W. Radloff, The New Beam Position Measurement System for the DESY Synchrotron, IEEE Transactions on Nuclear Science, Vol. NS-28, No. 3, juin 1981.

25. E.F. Higgins and F.D. Wells, A Beam Position Monitor System for the Proton Storage Ring at LAMPF, IEEE Transactions on Nuclear Science, Vol. NS-28, No. 3, juin 1981.

26. R.E. Schafer, R.C. Webber and T.H. Nicol, Fermilab Energy Doubler Beam Position Detector, IEEE Transactions on Nuclear Science, Vol. NS-28, No. 3, juin 1981.

27. S.P. Jachim, R.C. Webber and R.E. Shafer, An RF Beam Position Measurement Module for the Fermilab Energy Doubler, IEEE Transactions on Nuclear Science, Vol. NS-28, No. 3, juin 1981.

28. C.R. Yu, A Radial Signal Process Method for the BPS Booster LLRF Control System, IEEE Transactions on Nuclear Science, Vol. NS-28, No. 3, juin 1981.

29. K.C.D. Chan, R.T.F. Bird, M.F. Coulas, J. McKeown and Y.M. Shin, Experiments with Beam Position Sensors, IEEE Transactions on Nuclear Science, Vol. NS-28, No. 3, juin 1981.

30. T. Katsura, H. Nakagawa and S. Shibata, Beam Diagnostic Instrumentation in the Photon Factory Storage Ring, IEEE Transactions on Nuclear Science, Vol. NS-28, No. 3, juin 1981.

31. M. Le Gras, Performance du Module Normalisateur pour la mesure de la position du faisceau au AA, PS/BR/Note 81-4.

32. G. Gelato, H. Koziol, M. Le Gras and D.J. Williams, The Closed Orbit Observation System of the CERN Antiproton Accumulator, IEEE Transactions on Nuclear Science, Vol. NS-28, No. 3, juin 1981.

33. F.B. Kroes, A. Masskant, T. Sluyt and J.B. Spelt, Non Intercepting High Resolution Beam Monitors, IEEE Transactions on Nuclear Science, Vol. NS-28, No. 3, juin 1981.

34. A.V. Rauchas, F.R. Brumwell, Y.C. Cho and W.S. Czys, Beam Position Measurement System at the Argonne Rapid Cycling Synchrotron, IEEE Transactions on Nuclear Science, Vol. NS-28, No. 3, juin 1981.

35. A.T. Brousseau and D.D. Chamberlin, FMIT Direct-Current Beam Monitor, IEEE Transactions on Nuclear Science, Vol. NS-28, No. 3, juin 1981.

36. J.S. Fraser, Developments in Non-Destructive Beam Diagnostics, IEEE Transactions on Nuclear Science, Vol. NS-28, No. 3, juin 1981.

37. R. Melen, The PEP Instrumentation and Control System, SLAC-PUB-2553, June 1980.

38. R. Bossart, A. Chapman-Hatchett, E. d'Amico, J.P. Papis, H. Rossi and V. Rossi, Beam Position Measurement for Proton-Antiproton Operation in the SPS, SPS/ABM/RB/Report 80-12, 7.7.1980.

39. J.L. Pellegrin, Synchronous Detection of Beam Induced Pulses, SLAC-PUB-2359, PEP Note 312, July 1979.

40. W. Radloff, The Intensity Monitor Device for PETRA, IEEE Transactions on Nuclear Science, Vol. NS-26, No. 3, June 1979.

41. H. Nakagawa, H. Ishimaru and S. Shibita, Beam Diagnostics with Wall Current Monitor, IEEE Transactions on Nuclear Science, Vol. NS-26, No. 3, June 1979.

42. K. Satoh, New Wall Current Beam Position Monitor, IEEE Transactions on Nuclear Science, Vol. NS-26, No. 3, June 1979.

43. T.P.R. Linnecar, The High Frequency Longitudinal and Transverse Pick-Ups in the CERN SPS Accelerator, IEEE Transactions on Nuclear Science, Vol. NS-26, No. 3, June 1979.

44. R. Bossart, B. Bouchet, J.P. Papis and V. Rossi, Beam Test with Directional Coupler, SPS/ABM/RB/Report 79-14, 6.12.1979.

45. R. Bossart, Beam Position Monitors for Antiprotons, SPS/ABM/RB/Report 78-8, 18.9.1978.

46. T. Linnecar, The High Frequency Longitudinal and Transverse Pick-Ups used in the SPS, CERN SPS/ARF/78-17, August 1978.

47. K. Brand and J.P. Gourber, A Magnetic Beam Position Detector, CERN-ISR-BOM/77-3, March 1977.

48. J. Gardenas and J.C. Denard, Mesure de Position et d'Intensité, NI/9-75, 21.4.75.

49. J. Claus, A Magnetic Beam Position Monitor, 1973 Particle Acc. Conf., IEEE Transactions on Nuclear Science, June 1983.

50. R. Bossart, L. Burnod, T. d'Amico, H. Jakob, N. Morgan, J.P. Papis, H. Rossi and V. Rossi, Results of the Beam Test in the PS on 25.6.75, LAB II-CO/BM/Int. Note/RB75-28, 17.7.1975.

51. R. Bossart, Coaxial Cavity as Position Monitor of Ultrahigh Frequency Beams, 26.2.1975.

52. R. Bossart, Analysis and Performance of the Wall Current Monitor for the SPS, LAB II-CO/Int./BM75.2, 20.1.1975.

53. G. Gelato and L. Magnani, Improved Radial Pick-Up Electronics for Use over a Wide Dynamic Range, MPS/Int.Br/75.8, 16.6.1975.

54. G.C. Schneider, Signal Transmission Theory of the Low Energy UHF Wide Band Pick-Up Station for the New Linac, MPS/AE/Note 74.6.

55. R. Bossart, Possible Beam Position Monitors for the Enlarged Straight Section, LAB II CO/BM/Int. Note/RB74.3, 12.2.1974.

56. R. Bossart, L. Burnod, H. Jakob, N. Morgan, J.P. Papis and H. Rossi, SPS Beam Position Monitor Experimental Results achieved on the PS on 20th and 21st December, 1973, LAB II-CO/Int/BM74.1, 15.1.1974.

57. R. Bossart and H. Rossi, Test of Beam Position Monitors at Daresbury Nuclear Physics Laboratory on 11/12.6.73, LAB II-CO/RB/73.48, 27.11.1873.

58. G.C. Schneider, Proposal for a Resistive Non-Destructive UHF Wide-Band Pick-Up Station with Beam Position Measurement, MPS/SR/Note 73.32, 20.8.1973.

59. J.P. Gourber and C. Wyss, ISR Performance report runs 317 and 320 - 22 and 25 June 1973 Ring 1-15 and 26 GeV/c, 2.7.1973.

60. J.P. Gourber, ISR Performance Report, Device for Measuring the Beam Position in the SFM, ISR.MA/JPG/rh, 7.2.1973.

61. J.H. Cupérus, A Beam Transformer System for Measuring Fast Ejection Efficiencies, PS/FES/72-6, 13.11.1972.

62. R. Colchester, S. Turner and K. Unser, Beam Current Transformers for the ISR and West Hall Beam Transfer System, CERN-ISR-OP/72-2, August 1972.

63. R.K. Cooper and V.K. Neil, Resistor Beam Bugs - Scientific Explanation, UCID 16057, 12.6.1972.

64. G. Nassibian, The Basic Limits to the Measurements of the charge Distribution in a Cylindrical Beam by Means of Electrostatic Induction Electrodes, SI/Note EL/71-2, 19.4.1971.

65. G. Schneider, Messwerterfassung und -Übertragung zur Strahllage-bestimmung beim 28 GeV-Protonen-Synchrotron von CERN, Dissertation, Technischen Universität Hannover, 1971.

66. G. Nassibian, The Measurements of the Multipole Coefficients of a Cylindrical Charge Distribution, SI/Note EL/70.13, 30.12.1970.

67. G. Gelato, PSB Wide Band Observation System Survey of Options and Proposed Solution, SI/Note EL/70-5, 31.8.1970.

68. T.J. Fessenden, B.W. Stallard and G.G. Berg, Beam Current and Position Monitor for the ASTRON Accelerator.

69. R.T. Avery, A. Faltens and E.C. Hartwig, Non-Intercepting Monitor of Beam Current and Position, UCRL 20166.

70. G. Gelato, Options concerning the Wide Band Beam Observation System, SI/Note EL/70-5, 25.6.1970.

71. J. Cupérus, The FES Beam-Diagnostic System, PS/FES/TN-137, 25.2.1970.

72. H.H. Umstätter, The New Wide-Band Pick-Up Station of the PS, CERN/MPS/SR 70.1, 11.5.1970.

73. Yu.D. Bol'shakow, K.F. Gertsev, Yu.S. Ivanov, A.A. Kuz'min, S.M. Rubchpting and Y.A. Uvarov, Système d'Observation du Faisceau du Synchrotron a Protons de 70 GeV, Rapport NTD 6827, octobre 1969.

74. J. Cupérus, Preliminary Report on the FES Beam Profile Monitors, PS/FES/TN-101, 27.10.1969.

75. M. Rabany and L. Sjögren, Pick-Up Electrodes and Current Work, SI/Note EL/69.1, 24.2.1969.

76. J. Borer and R. Scholl, The ISR Beam Monitoring System, CERN-ISR-CO-RF/69.55.

77. K. Unser, The Circulating Beam Current Monitor, MPS/CO Electronique 68-1, 5.3.1968.

78. R. Rohbach and S. Mango, An Inductive Beam Monitor for the Extracted Proton Beam of the CERN Synchro-Cyclotron, CERN 67.9.

79. L.L. Gol'din, Investigation of a Beam of Charged Particles by Means of Pick-Up Electrodes (CERN/Trans. 66.6) October 1966.

80. G. Schneider, The New Pick-Up Electrodes for the CPS, MPS/Int./RF 65.9, 8.7.1965.

MONITORING SYSTEMS USING "SCHOTTKY NOISE" AND BEAM TRANSFER FUNCTION

81. T. Linnecar and W. Scandale, Continuous Tune Measurements Using the Schottky Detector, IEEE Transaction on Nuclear Science, Vol. NS-30, No. 4, August 1983.

82. G. Carron, R. Johnson, S. van der Meer, C. Taylor and L. Thorndahl, Recent Experience with Antiproton Cooling, IEEE Transaction on Nuclear Science, Vol. NS-30, No. 4, August 1983.

83. G. Carron, R. Johnson, S. van der Meer, C. Taylor and L. Thorndahl, Recent Experience with Antiproton Cooling, CERN/PS/AA/83-10, March 1983.

84. J. Borer, A. Hofmann, J.P. Koutchouk, T. Risselada and B. Zotter, Measurements of Betatron Phase Advance and Beta Function in the ISR, CERN/LEP/ISR/83.12, March 1983.

85. E. Peschardt and M. Studer, ISR Performance Report, The Momentum Cooling System, 28.9.1982.

86. J. Borer and A. Hofmann, Measurement of Beta Function and Betatron Phase Advance by Means of the Beam Transfer Function, ISR-RF-TH/JB/AH/ps, 24.2.1982.

87. E. Peschardt, The Antiproton Vertical Betatron Cooling System on the FP Working Line, 17th November 1981.

88. E. Peschardt, ISR Performance Report, The Status of the Antiproton Cooling System, 30 June 1981.

89. S. van der Meer, Stochastic Cooling in the CERN Accumulator, CERN/PS/AA/81.21, March 1981.

90. C. Carter, J. Donnat, G. Gelato, M. Le Gras, H. Schönauer and D.J. Williams, The Transverse Feedback System for the CERN PS Booster, IEEE Transcations on Nuclear Science, Vol. NS-28, June 1981.

91. T. Linnecar and W. Scandale, A Transverse Schottky Noise Detection for Bunched Proton Beams, IEEE Transactions on Nuclear Science, Vol. NS-28, No. 3, June 1981.

92. F. Tazzioli, Investigations on Beam Longitudinal Transfer Function and Coupling Impedance in Adone, RM-23, 8.5.1981.

93. T. Linnecar and W. Scandale, A Transverse Schottky Noise Detector for Bunched Proton Beams, CERN SPS/81-5 (DI), February 1981.

94. J.P. Koutchouk, Linear Betatron Coupling Measurement and Compensation in the ISR, CERN ISR-OP/80-27, July 1980.

95. J.Y. Hemmery and L. Vos, A Procedure for Obtaining Transverse Wall Impedance and Working Line from Transfer Functions Measurements, CERN ISR-CO/80-32, July 1980.

96. D. Boussard, L. Evans, J. Gareyte, C. Graziani, R. Lauckner, T. Linnecar, W. Scandale and D. Thomas, Single Bunch Storage with the Low-Noise Phase Loop, SPS Improvement Report No. 175, 15.02.1980.

97. S. van der Meer, A Different Formulation for the Longitudinal and Transverse Beam Response, CERN/PS/AA/80.4, 25.1.1980.

98. J. Borer et al., ISR Beam Monitoring System using "Schottky Noise" and Transfer Function, CERN-ISR-RF/80-30.

99. A. Hofmann, Diagnostics and Cures for Beam Instabilities, CERN/ISR/TH/80-35, July 1980.

100. D. Kemp, E. Peschardt and A. Vaughan, On-Line Q Measurement During Phase Displacement Accelerator in the CERN ISR, IEEE Transactions on Nuclear Science, Vol. NS-26, No. 3, June 1979.

101. M.A. Allen, M. Cornacchia and A. Millich, A Longitudinal Feedback System for PEP, IEEE Transactions on Nuclear Science, Vol. NS-26, No. 3, June 1979.

102. R. Bossart, L. Burnod, J. Gareyte, B. de Raad and V. Rossi, The Damper for the Transverse Instabilities of the SPS, IEEE Transactions on Nuclear Science, Vol. NS-26, No. 3, June 1979.

103. K. Wille, Damping of Coherent Transverse Oscillations in PETRA, IEEE Transactions on Nuclear Science, Vol. NS-26, No. 3, June 1979.

104. E. Peschardt, Compensation of the Resistive and Reactive Transverse Wall Impedance in the ISR with a Feedback System, CERN-ISR-RF/80.31, July 1980.

105. J. Borer, G. Guignard, A. Hofmann, E. Peschardt, F. Sacherer and B. Zotter, Information from Beam Response to Longitudinal and Transverse Excitation, CERN-ISR-RF-TH-BOM/79.20, March 1979.

106. D. Boussard, L. Evans, J. Gareyte, C. Graziani, R. Lauckner, T. Linnecar, W. Scandale and D. Thomas, Long Storage of Short Single Bunches Transverse Schottky Scans of Continuous Beams, SPS Improvement Report No. 167, 20.11.1979.

107. D. Boussard, R. Bossart, L. Evans, J. Gareyte, T. Linnecar, W. Mills, W. Scandale, and D. Thomas, Storage of a Continuous Beam at 240 GeV/c Longitudinal and Transverse Schottky Scans, Emittance Growth, Improvement Report No. 163, 24.8.1979.

108. D. Möhl, G. Petrucci, L. Thorndahl and S. van der Meer, Physics and Technique of Stochastic Cooling, CERN/PS/AA 79-23, 23 July 1979.

109. J. Borer, G. Guignard, A. Hofmann, E. Peschardt, F. Sacherer and B. Zotter, Information from Beam Response to Longitudinal and Transverse Excitation, IEEE Transactions on Nuclear Science, Vol. NS-26, No. 3, June 1979.

110. L. Faltin, Slot-Type Pick-Up and Kicker for Stochastic Beam Cooling, CERN-ISR-RF/77-47, July 1977.

111. L. Faltin, Stochastic Acceleration and Vertical Betatron Cooling with the Improved Cooling Pick-Up, ISR-RF/LF/ps, ISR Performance Report.

112. G. Carron, L. Faltin, W. Schnell and L. Thorndahl, Experiments with Stochastic Cooling in the ISR, CERN-ISR-RF/77-17, March 1977.

113. H.G. Hereward, F. Sacherer, W. Schnell and B. Zotter, CERN Yellow Report 77-13, 19.7.77, Theoretical Aspects of the Behaviour of Beams in Accelerators and Storage Rings, Proceedings of the First Course of the International School of Particle Accelerators at Erice, November 1976.

114. D. Boussard and L. Burnod, Choix du type de détecteurs de position pour le SPS, CERN LAB II-CO/BM/72-6.

115. F. Gardiol, Electromagnétisme, Volume III, Traité d'électricité, Ecole Polytechnique Fédérale de Lausanne, Edition Georgi.

116. J. Borer and K. Unser, Transfer Beam Position Monitoring System (with Inductive Loop Monitors), Technical Note ISR-R/JB/ps, 21 June 1976.

CURRENT TRANSFORMERS

117. K. Unser, Beam Current Transformer with DC to 200 MHz Range, IEEE Transactions on Nuclear Science, Vol. NS-16, No. 3, June 1969.

118. R. Colchester, S. Turner, K. Unser, Beam current transformers for the ISR and West Hall beam transfer system, CERN-ISR-OP/72-2, August 1972.

119. K. Unser, A Toroidal D.C. Beam Current Transformer with High Resolution, IEEE Transactions on Nuclear Science, Vol. NS-28, No. 3, June 1981.

SYNCHROTRON LIGHT MONITOR

120. R. Coïsson, On Synchrotron Radiation in Non-Uniform Magnetic fields, Optics Communications, Vol. 22, No. 2, August 1977.

121. R. Coisson, Narrow Band Visible Synchrotron Radiation from High Energy Proton Beams, Nucl. Instrum. and Methods 143 (1977), 241-243.

122. R. Bossart et al., Observation of Visible Synchrotron Radiation Emitted by a High Energy Proton Beam at the Edge of a Magnetic Field, Nucl. Instrum. and Methods 164 (1979) 375-380.

123. J.D. Jackson, Classical electrodynamics, 2nd edition, (J. Wiley, New York, 1975).

124. A.A. Sokolov and J.M. Ternov, Synchrotron Radiation (Akademie-Verlag, Berlin, 1968).

125. A. Hofmann, Electron and Proton Beam Diagnostics with Synchrotron Radiation, IEEE Transactions on Nuclear Science, Vol. NS-28, No. 3, June 1981.

126. H. Motz, Applications of the Radiation from Fast Electron Beam, J. Appl. Phys., Vol. 22, No. 5 (1951), 527.

127. A. Hofman, Quasi-Monochromatic Synchrotron Radiation from Undulators, Nucl. Instrum. and Methods 152 (1978) 17-21.

128. F. Méot, Mesure de profil par rayonnement ondulateur des faisceaux de protons et d'antiprotons, Thesis INP Grenoble and CERN/SPS/81-21 (ABM), October 1981.

129. J. Bosser et al., Single Bunch Profile Measurement using Synchrotron Light from an Undulator, IEEE Transactions on Nuclear Science, Vol. NS-30, No. 4, August 1983.

SODIUM CURTAIN MONITOR

130. B. Vosicki and K. Zankel, The Sodium Curtain Beam Profile Monitor of the ISR, IEEE Transactions on Nuclear Science, Vol. NS-22, No. 3, 1975.

131. K. Zankel and B. Vosicki, Generator of a Dense Atomic Gas Curtain, Journal of Physics E, Scientific Instruments, Vol. 8, 1975.

BEAM INTERCEPTING MONITORS

132. Particle data group, Review of particle properties, Physics letters, Vol. 111B, 22nd April, 1982.

133. Yung-Su Tsai, Pair Production and Bremsstrahlung of Charged Leptons, Rev. Mod. Physics, Vol. 46, No. 4, Oct. 1974.

134. P.Tétu, CERN-PS, private communication.

135. D.A.G. Neet, Beam Profile Monitors for Fast and Slow Extracted Proton Beams, IEEE Transactions on Nuclear Science, Vol. NS-16, No. 3, 1969.

136. L. Bernard et al., Wide Dynamic (7 decades) Beam Position and Profile Measurement for the CERN LEAR, IEEE Transactions on Nuclear Science, Vol. NS-30, No. 4, August 1983.

137. C. Metzger, Mesures des emittances et du centrage des faisceaux dans la ligne de mesure 800 MeV du PSB, CERN/SI/Int.DL/69-10.

138. Accelerator technology program, January-March 1978, LA-8218-PR, Los Alamos Scientific Laboratory.

139. C. Bovet et al., A Selection of Formulae and Data useful for the Design of A.G. Synchrotrons, CERN/MPS-SI/Int.DL/70/4, April 1970.

140. H. Barisy et al., A Transverse Beam Profile Monitor for p-p^- Studies in the CERN SPS, IEEE Transactions on Nuclear Science, Vol. NS-28, No. 3, June 1981.

141. K. Potter and S. Turner, High Precision Scrapers for ISR Luminosity Measurements, IEEE Transactions on Nuclear Science, Vol. NS-22, No. 3, June 1975.

142. D.A.G. Neet, Beam Observation in the Transfer Channels of the Intersecting Storage Rings, CERN/ISR-CO/68-47, October 1968.

143. P. Lefèvre, CERN-LEAR, private communication.

MISCALLANEOUS MONITORS

144. A.K. Barlow, R.J. Colchester, H. Kropf and S. Turner, The ISR Beam Loss Detection and Location System, CERN-ISR-OP 74-6, January 1974.

145. J.-Y. Hémery, F. Lemeilleur, R. Olsen and K. Potter, Background and Luminosity Monitoring at the CERN ISR, IEEE Transactions on Nuclear Science, Vol. NS-28, No. 3, June 1981.

146. E. Rossa and G. von Holtey, Compteur de Luminosité, CERN-SPS/ELE/Note 82-9, 11.5.1982.

147. S. van der Meer, Calibration of the Effective Beam Height in the ISR, CERN-ISR-PO/68-31, 18.6.1968.

148. T. Dorenbos, Treatment and Display of Transient Signals in the CERN Antiproton Accumulator, CERN/PS-AA/83-41, September 1983.